DTIC FILE COPY

(2)

AD-A223 173

COMPRESSIVE BEHAVIOUR OF PBZ FIBRES

DEPARTMENT OF THE AIR FORCE - UMIST

TIC
ELECTE
JUN 19 1990
D
D

Final Technical Report

Results of work undertaken
March 1988 - February 1990

R.J. Young and P.P. Ang

Polymer Science and Technology Group
Manchester Materials Science Centre
UMIST, PO BOX 88,
Manchester, M60 1QD, UK.

Contract Number AFOSR-88-0148

The research reported in this document was made possible through the support and sponsorship of the US Government through its European Office of Aerospace Research and Development. This report is intended only for internal management use of the Contractor and the US Government.

DISTRIBUTION STATEMENT A
Approved for public release
Distribution Unlimited

90 06 18 291

EOARD-TR-90-08

This report has been reviewed by EOARD and is releasable to the National Technical Information Service (NTIS). At NTIS it will be releasable to the general public, including foreign nations.

This technical report has been reviewed and is approved for publication.

JAMES G.R. HANSEN, Lt Col, USAF
Chief, Structures/Struc Materials

FRED T. GILLIAM, Lt Col, USAF
Chief Scientist

UNCLASSIFIED

SECURITY CLASSIFICATION OF THIS PAGE

REPORT DOCUMENTATION PAGE

1a REPORT SECURITY CLASSIFICATION UNCLASSIFIED	1b. RESTRICTIVE MARKINGS
2a. SECURITY CLASSIFICATION AUTHORITY	3. DISTRIBUTION/AVAILABILITY OF REPOR. Approved for p blic release; distribution unlimited.
2b DECLASSIFICATION/DOWNGRADING SCHEDULE	
4. PERFORMING ORGANIZATION REPORT NUMBER(S)	5. MONITORING ORGANIZATION REPORT NUMBER(S) EOARD-TR-90-08
6a. NAME OF PERFORMING ORGANIZATION University of Manchester Inst. of Science & Technology 6b. OFFICE SYMBOL (If applicable)	7a. NAME OF MONITORING ORGANIZATION European Office of Aerospace Research and Development (EOARD)
6c. ADDRESS (City, State, and ZIP Code) P.O. Box 88 Manchester M60 1QD United Kingdom	7b ADDRESS (City, State, and ZIP Code) Box 14 FPO NY 09510
8a. NAME OF FUNDING/SPONSORING ORGANIZATION AFWAL 8b. OFFICE SYMBOL (If applicable) MLBP	9 PROCUREMENT INSTRUMENT IDENTIFICATION NUMBER AFOSR-88-0148
8c ADDRESS (City, State, and ZIP Code) Wright-Patterson AFB, OH 45433-6533	10 SOURCE OF FUNDING NUMBERS PROGRAM ELEMENT NO. 61102F; PROJECT NO. 2301; TASK NO. D1; WORK UNIT ACCESSION NO. 005

11. TITLE (Include Security Classification)

Compressive Behaviour of PBZ Fibers in Composites

12. PERSONAL AUTHOR(S)
R. J. YOUNG AND P. P. ANG

13a. TYPE OF REPORT	13b TIME COVERED	14. DATE OF REPORT (Year, Month, Day)	15 PAGE COUNT
FINAL	FROM 3/88 TO 2/90	1990 May	148

16. SUPPLEMENTARY NOTATION

17 COSATI CODES		
FIELD	GROUP	SUB-GROUP

18 SUBJECT TERMS (Continue on reverse if necessary and identify by block number)
Composites, Rigid Rods, High Modulus Fibres, Compressive behaviour, PBZ fibres, poly(p-phenylene benzobisthiazole, poly(p-phenylene benzobisoxazole, poly(2,5(6)-benzoxazole

19 ABSTRACT (Continue on reverse if necessary and identify by block number)

This final report reviews progress over the two years of the project concerning the compressive behaviour of three types of PBZ fibres. The materials investigated were as-spun and heat-treated fibres of PBT, PBO and ABPBO. Their structure has been determined using X-ray diffraction, optical microscopy and scanning electron microscopy. The tensile properties of the fibres have been determined using tensile tests in individual filaments and their compressive deformation behaviour has been examined initially by bending individual fibres. The formation of kinkbands has been followed in detail by the compression of epoxy resin blocks containing single fibres aligned in the compression direction.

Molecular deformation in the fibres has been followed using Raman microscopy. It has been found that the bands in the Raman spectra shift to lower frequency on the application of a tensile stress or strain. The onset of kinkband formation has been monitored at the molecular level by obtaining Raman spectra from the single filaments within epoxy resin blocks subjected to axial compression. It has been found that kinkbands form at a strain of the order of 0.8%

OVER/

20. DISTRIBUTION/AVAILABILITY OF ABSTRACT	21 ABSTRACT SECURITY CLASSIFICATION
☒ UNCLASSIFIED/UNLIMITED ☐ SAME AS RPT ☐ OTIC USERS	

22a NAME OF RESPONSIBLE INDIVIDUAL	22b TELEPHONE (Include Area Code)	22c OFFICE SYMBOL
Dr Wade Adams	(513) 255-9148	MLBP

DD FORM 1473, 84 MAR 83 APR edition may be used until exhausted
All other editions are obsolete

SECURITY CLASSIFICATION OF THIS PAGE

for the three types of as-spun fibres and about 0.3% for the three types of heat-treated fibres. There is also an indication from Raman microscopy that the Young's modulus of the rigid-rod PBT and PBO fibres is lower in compression than in tension and this may be related to their tendency to undergo compressive failure by kinkband formation.

CONTENTS

	PAGE
1. INTRODUCTION	1
2. EXPERIMENTAL DETAILS	3
2.1 Characterisation of Materials	3
2.2 Effect of Deformation on the Raman Spectra	8
2.3 Continous Single Fibre Composites	9
2.4 Compression of Composites	12
2.5 Optical Microscopy	15
3. RESULTS AND DISCUSSION	16
3.1 Characterisation of Materials	16
3.1.1 Optical and Scanning electron microscopy of as-received fibres	16
3.1.2 X-ray diffraction	26
3.1.3 Mechanical Testing	32
3.2 Raman Microscopy	63
3.2.1 Raman spectra	63
3.2.2 Effect of deformation on the Raman spectra	69
3.2.3 Extension of the composites	88
3.2.4 Compression of the composites	98
3.3 Observation of Kinkband Formation	115
4. CONCLUSIONS	143

Accesion For
NTIS CRA&I
DTIC TAB
Unannounced
Justification
By
Distribution/
Availability Codes
Dist | Avail and/or Special
A-1
QUALITY INSPECTED

1 INTRODUCTION

This project has been concerned with the characterisation of the compressive behaviour of three types of PBZ fibres, PBT, PBO and ABPBO, developed under the USAF ordered polymer programme. The chemical structure of the fibres is given below:

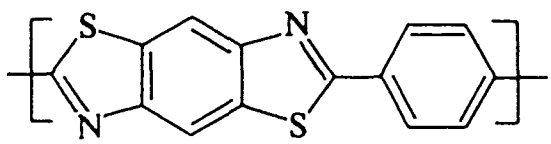

Poly(p-phenylene benzobisthiazole) -- PBT

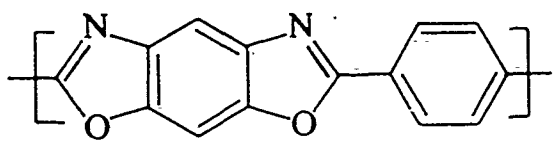

Poly(p-phenylene benzobisoxazole) -- PBO

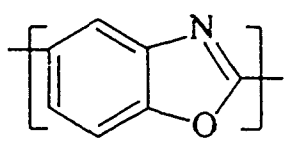

Poly(2,5(6)-benzoxazole)--ABPBO

They were supplied in both the as-spun (AS) and heat-treated forms (HT). The heat-treatment temperature were 650 °C for PBT, 600 °C for PBO and 525 °C for ABPBO.

The fibres are known to have very impressive properties in tension but their behaviour during compressive loading was thought to be relatively poor. The project has therefore been concerned with a detailed study of compressive deformation of these three types of

fibres in both the AS and HT state.

The structure of the fibres has been characterised using a combination of wide-angle X-ray diffraction, optical microscopy and scanning electron microscopy. The tensile properties have been evaluated by the tensile deformation of single fibres employing different gauge lengths to eliminate end effects. The formation of kinkbands during compressive deformation is observed in the first instance from the examination of fibres in the optical and scanning electron microscope following bending in air. This is measured quantitatively by compressing epoxy composite samples containing single PBZ fibres aligned parallel to the compression direction. The strain at which failure by kinking takes place is determined by the direct observation of kinkband formation.

Molecular deformation in the PBZ fibres has been followed using Raman microscopy. It is found that the bands in the Raman spectra of the fibres shift to lower frequency on the application of a tensile stress or strain and the rate of shift is correlated with the modulus of the fibres. The onset of kinkband formation can be determined very accurately by obtaining Raman spectra from single filaments subjected to axial compressive deformation within the epoxy resin block. In addition, it has been possible to measure the stress-strain behaviour of fibres in both tension and compression using the Raman technique.

2 EXPERIMENTAL DETAILS

2-1 Characterisation of materials

2-1-1 X-ray diffraction

Wide-angle x-ray scattering (WAXS) patterns were obtained from bundles of the AS and HT PBT, PBO and ABPBO fibres using a flat-plate transmission geometry and Ni-filtered CuKα radiation. This enabled the level of molecular orientation in the different types of fibre to be compared.

2-1-2 Scanning electron microscope

AS and HT PBT, PBO and ABPBO fibres were examined in a scanning electron microscope (SEM, Philips 505). They were cleaned with solvent and then rendered conductive by sputter coating with a thin layer of gold. The fibres were viewed in different directions to examine their perfection and deformed by bending and compressing in order to observe the kinkbands. Fibres which were fractured in an Instron model 1121 using a crosshead speed of 1mm/min were also examined.

2-1-3 Mechanical testing of single fibres

Individual fibres of AS and HT PBT, PBO and ABPBO fibres were mounted across holes on paper cards using a slow-setting, cold-curing, epoxy resin adhesive. Once the adhesive had set, the pieces of card were mounted between fibre testing grips in a Instron model 1121 and the card edges were cut. Data for stress-strain curves were collected using an HP 85 computer and also chart paper. Load ranges of between 2 and 5N were employed using a 5N capacity load cell and gauge lengths of 50, 84, 110 and 130mm were used. The fibre strain was determined from the crosshead displacement and a crosshead speed of 1mm/min was used making initial strain rates of $3.3 \times 10^{-4}s^{-1}$, $2.0 \times 10^{-4}s^{-1}$, $1.5 \times 10^{-4}s^{-1}$ and $1.3 \times 10^{-4}s^{-1}$ for the gauge lengths of 50, 84, 110 and 130mm respectively. At least 10 samples of each type of fibre and gauge length were employed. All tests were carried out at 23 $\pm$ 1°C and a relative humidity of 50 $\pm$ 5%.

2-1-4 Raman microscopy

Raman spectra were obtained from AS and HT PBT, PBO and ABPBO fibres using a Raman microscopy system (Figure 2.1). This is based upon a SPEX 1403 double monochromator connected to a modified Nikon optical microscope which was used to focus the incident beam on the fibre. A x40 objective lens with a numerical aperture of 0.65 was used for the free-standing fibres and this gave a 2 um spot on the fibre when focused. A x20 objective lens with a numerical aperature of 0.4 was used for the single fibre composites because it had a larger working distance. This enabled the laser beam to be focused on fibres below the surface of the resin and thus spectra to be obtained from the fibres

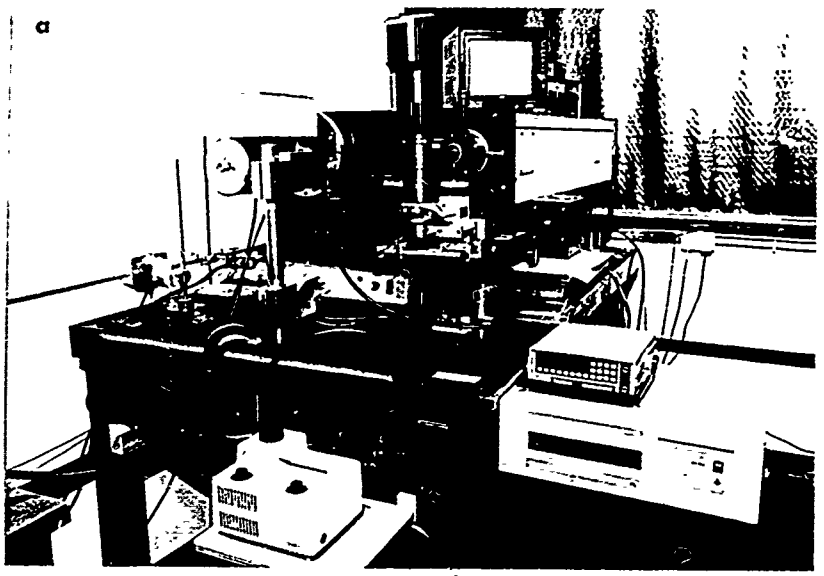

Figure 2.1(a) Raman microscope system.

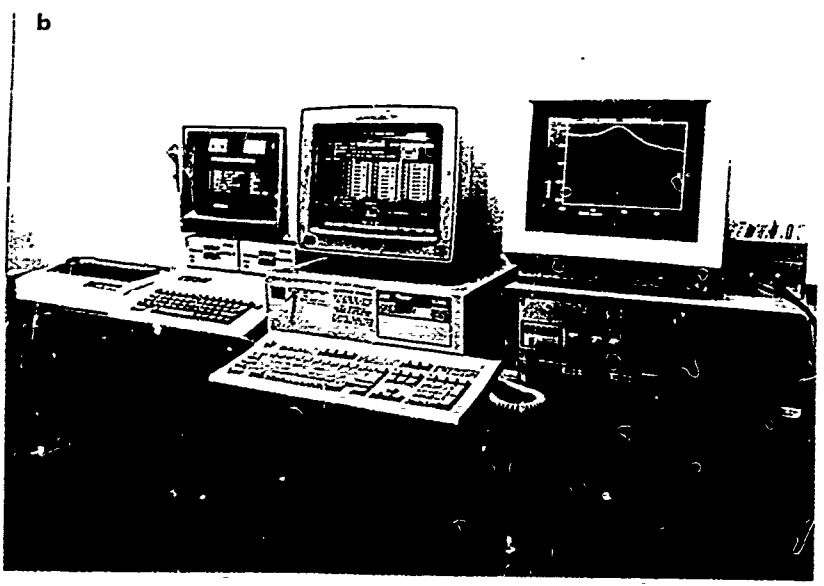

Figure 2.1(b) The computer system.

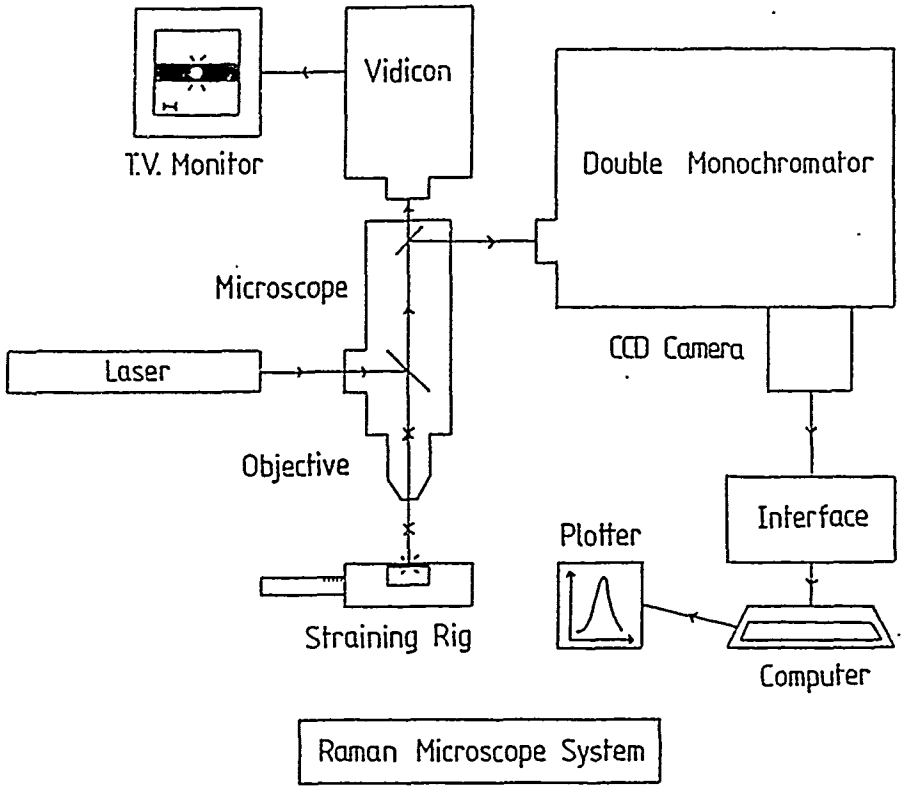

Figure 2.1(c) A schematic diagram of Raman microscope system.

inside the resin. The light was polarized parallel to the fibre and polymer chain axis. The scattered light was then collected using the 180° backscattering geometry and focused on the entrance slit of the SPEX 1403 double monochromator. Spectra were obtained at a spectral band pass of the order of $\pm 5cm^{-1}$ using the 632.8nm line of a 10mW Helium Neon (He/Ne) laser for AS PBO and AS ABPBO fibres whilst a 488.0nm line from Argon Ion (Ar/Ion) laser operating at an intensity of 5mW was used for AS and HT PBT, HT PBO and HT ABPBO fibres. The He/Ne laser was used for AS PBO and ABPBO fibres and the Ar/Ion laser was used for the rest of the fibres because it had been found that better spectra could be obtained with the particular laser. The detector used was a Wright Instrument CCD camera employed for recording the Raman spectra. The CCD camera was preferred because t was more accurate and faster than a photomultiplier. This was then interfaced to the computer where the spectra were analysed (Figure 2.1(b)).

2-2 Effect of deformation on the Raman spectra

Spectra were obtained from free-standing fibres during deformation using the small straining rig shown in Figure 2.2 which fitted directly onto the microscope stage. Individual free- standing fibres were fixed between aluminium foil tabs which were placed onto the Al blocks of the straining rig using cyanoacrylate adhesive, giving a gauge length of about 15mm, which was measured accurately using the light microscope. The fibres were deformed by displacing the blocks using a micrometer attachment which could be read to $\pm$0.005mm. This allowed a precision of the order of $\pm$0.03% for strain measurement. Raman spectra were obtained during deformation by scanning strong individual peaks between loading steps of 0.1% strain. Since it took about 20 seconds to scan a peak this corresponded to an effective strain rate of the order of $3 \times 10^{-5} s^{-1}$.

2-3 Continuous single fibre composites

Single fibre composites were prepared using Ciba-Geigy XD927 two part solvent free cold setting epoxy resin, using 100 parts (by weight) of resin to 36 parts of hardener. The epoxy resin was sufficiently transparent and free from fluorescence that Raman spectra could be measured for embedded fibres. A " dog-bone " shape PTFE mould (Figure 2.3) was filled with half of the resin/hardener mixture and allowed to set partially before the fibre and the rest of the epoxy resin were added. In this way a tensile specimen could be produced with a fibre aligned within $\pm 5^{\circ}$ to the axial direction at the centre of a 6mm thick section. In this way a long fibre was aligned along the length of the specimen. After setting for 7 days at room temperature (24 $\pm 3^{\circ}$C), thin film resistance strain gauge of gauge factor 2.06 were attached with adhesive to the surface of the specimen at the centre of the fibre (Figure 2.4). It was possible to measure matrix strain to an absolute accuracy of $\pm 0.01\%$ with a Digital voltmeter (DVM).

All the specimens were polished to give a smooth, transparent surfaces and holes were drilled at both ends to accomodate the clamps used to apply the tensile stress in the fibre direction. The tensile tester (Figure 2.5) was mounted on a micrometer slide so that the whole length of the specimen could be transversed through the incident laser beam. The tester used was a " Minimat " produced by Polymer Laboratories. The sample was then extended to about 0.5% before the fibre and the matrix start to yield so that the same sample could be used for the compression test.

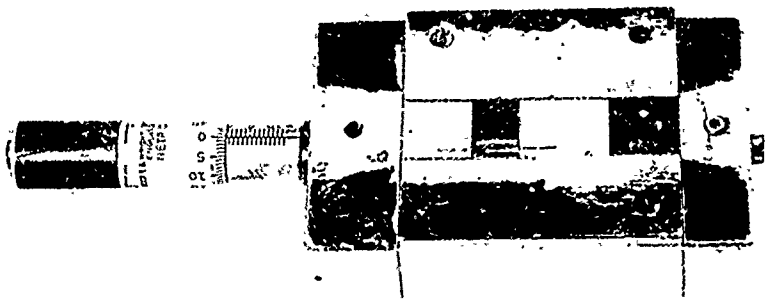

Figure 2.2 A straining rig.

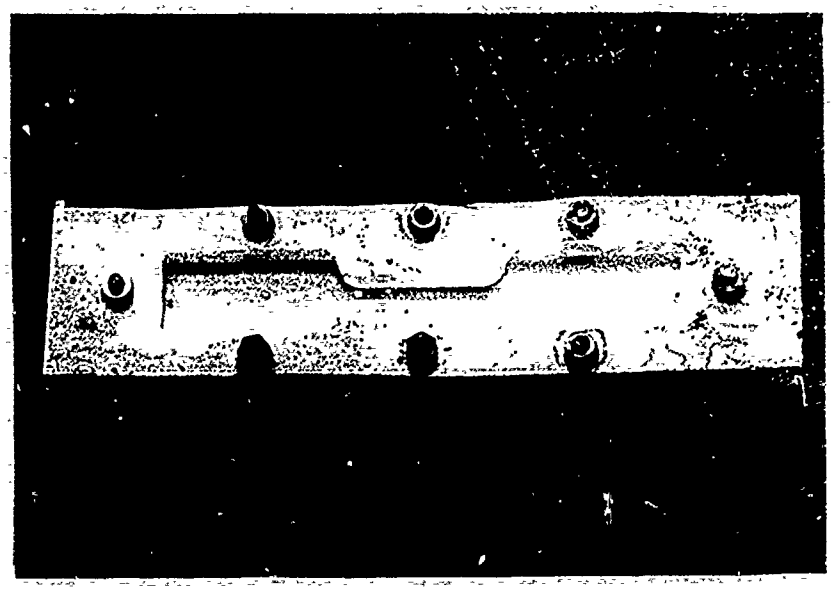

Figure 2.3 A " dog-bone " shaped PTFE mould.

a

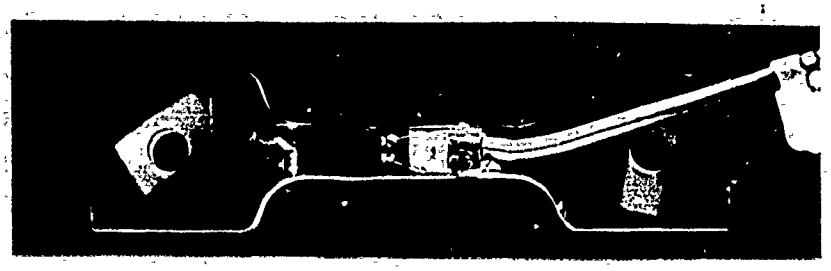

b

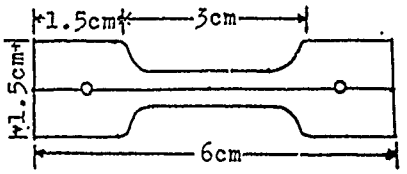

Figure 2.4 (a) Single fibre composite specimen.
The fibre is located at the centre of the specimen and a resistive strain gauge is attached to the outer surface.
(b) Sketch of specimen.

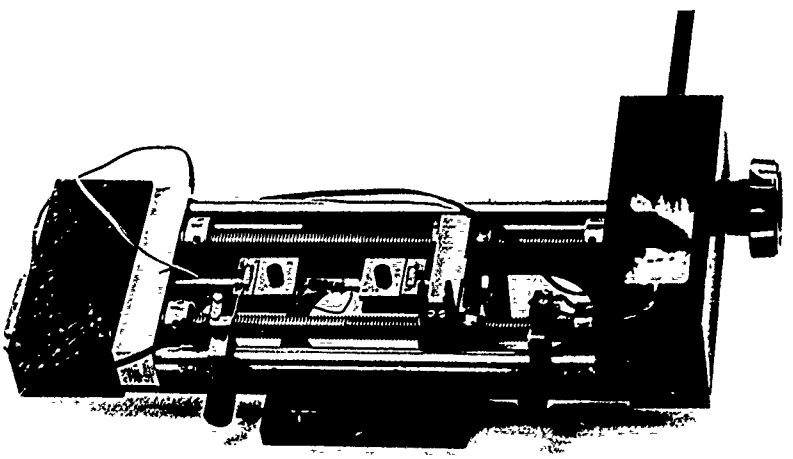

Figure 2.5 The Minimat with a tensile specimen in position.

2-4 Compression of composites

The composites used for the study of compression were the same as the ones used for the tensile test. They were obtained by cutting the two ends of the " dog-bone " shaped composites leaving a small rectangular block with a gauge length of about 1.2cm as shown in Figure 2.6. It was accomodated in a compression cage (Figure 2.7) where it was compressed. Grease was applied at both ends of the composite to lubricate the surfaces and hold it in place in the compression cage. Increments of compressive strain of about 0.03% was applied to the composite by the " Minimat " miniature materials tester through the cage up to a compressive strain of about 1%. A picture of the compression cage is shown in Figure 2.8.

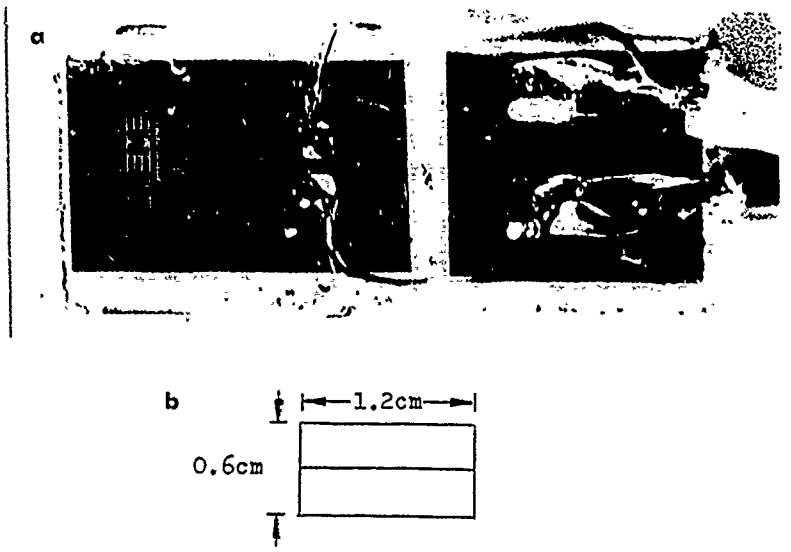

Figure 2.6 (a) Rectangular block single fibre composite with resistance strain gauge attached.
(b) Sketch of specimen.

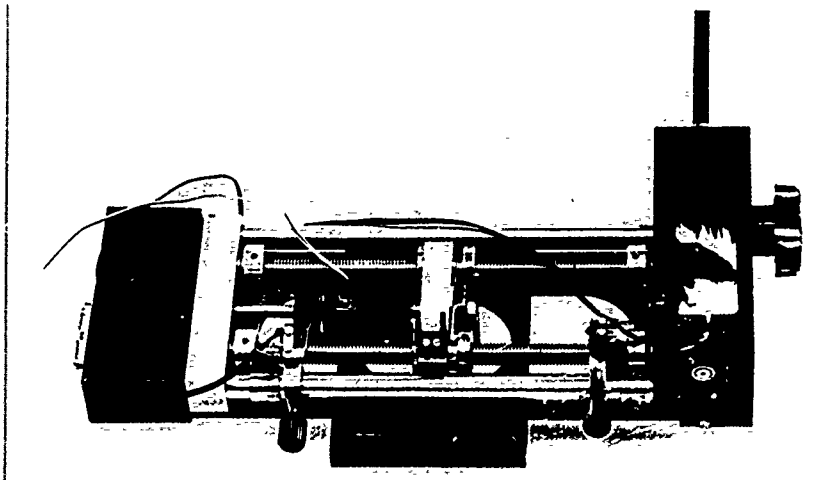

Figure 2.7 Minimat compression cage with the compression sample mounted.

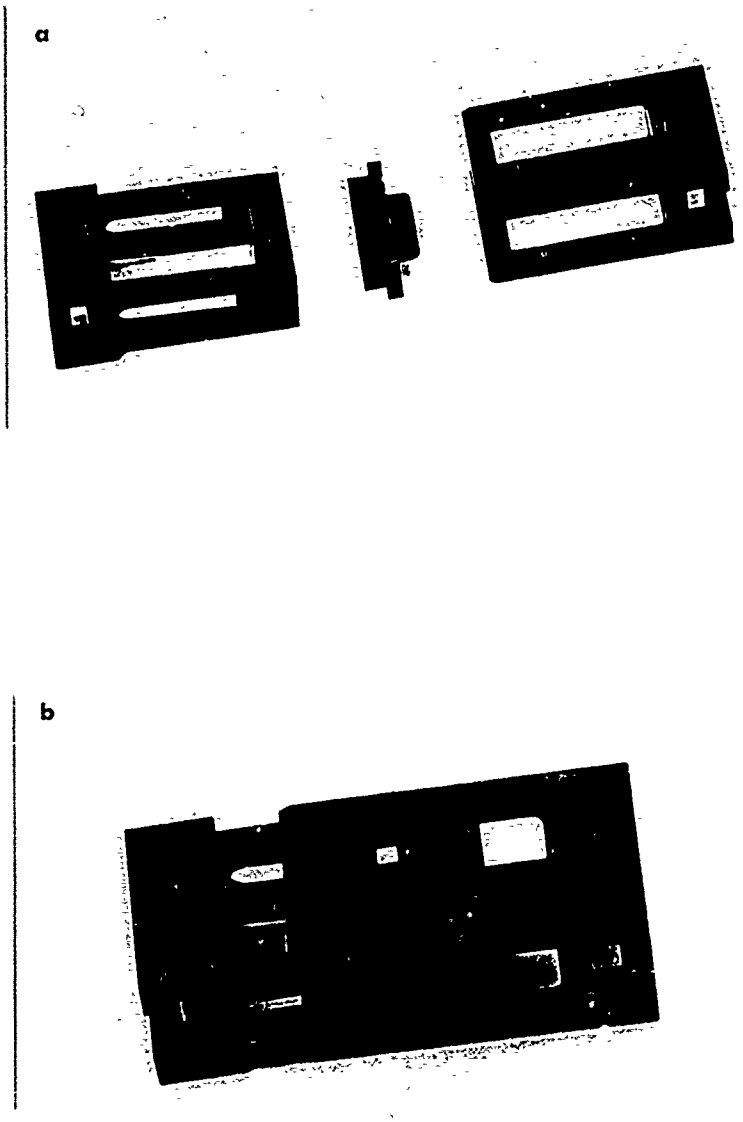

Figure 2.8 Compression cage.

(a) Dismantled; (b) assembled

2-5 Optical microscopy

An Olympus Manager optical microscope system was used to measure the diameter of the fibres for the calculation of stresses. Measurements were made at three different positions on the fibre using a x40 objective lens and the mean value of the diameter of each individual fibre was used for the calculation. A Olympus Vanox-T optical transmission microscope was used to view the kinkbands with a x20 objective lens and the polymer Laboratories " Minimat " was used to compress the sample. At each level of compressive strain an optical micrograph was taken. The film was developed later and the number of kinkbands at each level of strain was counted from a photographic print at a magnification of x400. The matrix strain was measured using resistance strain gauges. The optical micrographs of the as-received fibres and the fibres deformed by bending were also taken using an Olympus Vanox-T optical transmission microscope with a x40 objective lens.

3 RESULTS AND DISCUSSION

3-1 Characterisation of materials

3-1-1 Optical microscopy and scanning electron microscopy of as-received fibres

PBT fibres

Figures 3.1(a) and (b) show the optical micrographs of as-received AS and HT PBT fibres in air at the magnification of x400. It can be observed that kinkbands are already present and are perpendicular to the fibre direction although HT PBT fibres are more opaque compared to the as-spun fibres that make the appearance of the kinkbands less obvious. It was found that there are more kinkbands present in AS PBT fibres compared to the rest of the fibres studied. They may have been formed during processing or handling.

Figures 3.2(a) and (b) show the scanning electron micrographs of the surfaces of as-received AS and HT PBT fibres respectively. The surface of AS PBT fibres were found to be relatively smooth, defect-free and of uniform appearance whereas the surfaces of HT PBT fibres have a granular appearance. The granular appearance may be due to the high temperature treatment of PBT fibres (i.e 550 °C) giving rise to degradation. PBT fibres were found to have an approximately circular cross-section and to be relatively uniform in diameter along the fibre. The diameters of AS and HT PBT fibres obtained by Image Manager microscope are shown in Table 3.1. Measurements were made at three different points along each individual fibre for mechanical testing but a mean value from about 80 fibres is presented in Table

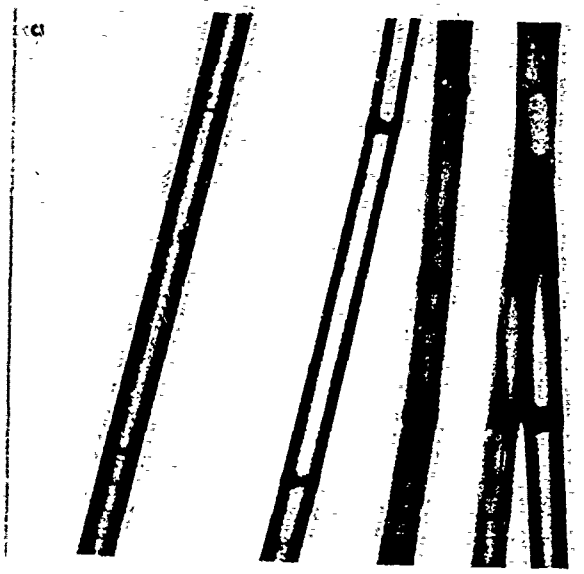

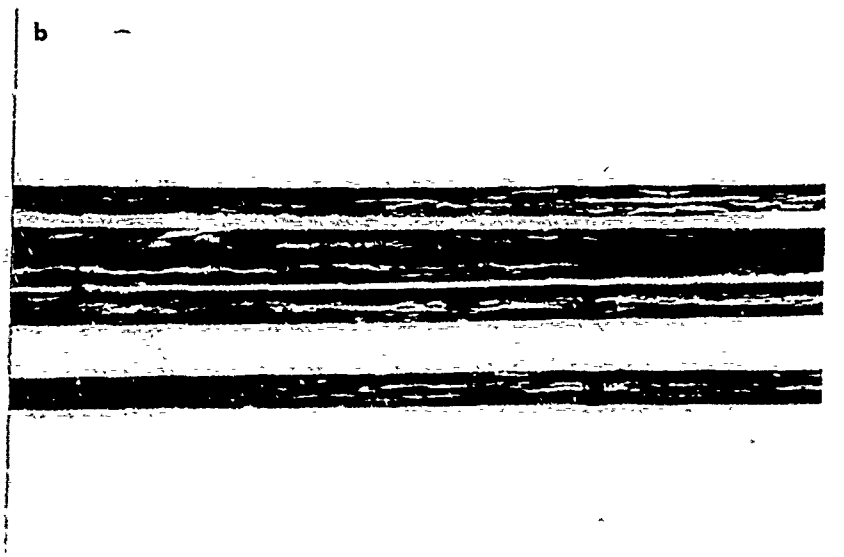

Figure 3.1 Optical micrographs of as-received PBT fibres in air. (a) As-spun; (b) heat treated

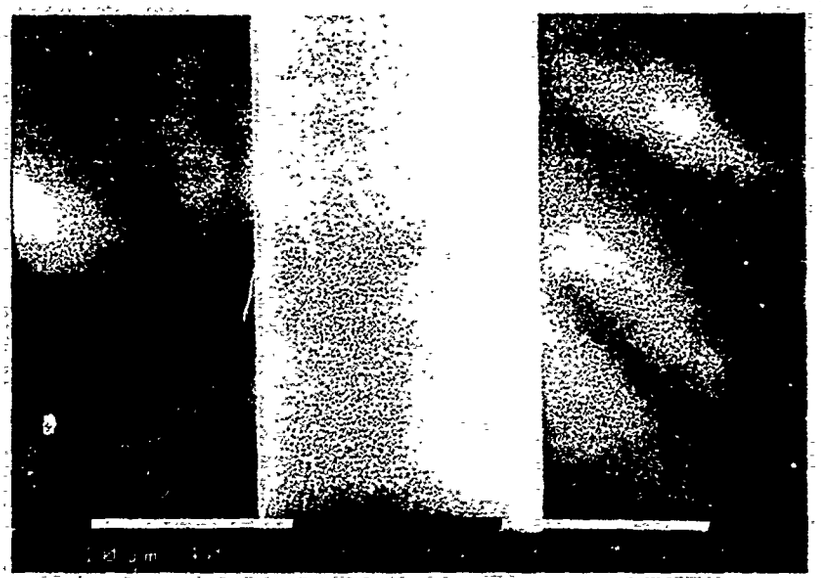

Figure 3.2 Scanning electron micrographs of as-received PBT fibres. (a) As-spun; (b) heat-treated

Materials	Diameter(um)
AS PBT	13.78 ± 0.18
HT PBT	13.97 ± 0.23
AS PBO	21.37 ± 2.03
HT PBO	16.43 ± 1.79
AS ABPBO	16.32 ± 1.16
HT ABPBO	15.96 ± 1.16

Table 3.1 Mean diameters of 80 measurements with standard deviations of AS and HT PBT, PBO and ABPBO fibres.

3.1. It can be seen that PBT fibres have a smaller diameter than PBO and ABPBO fibres. PBT fibres show no sign of kinkbands in the scanning electron micrographs.

PBO fibres

Figures 3.3(a) and (b) show the optical micrgraphs of as-received AS and HT PBO fibres in air at the magnification of x400. It can be observed that kinkbands are already present in both AS and HT PBO fibres. The kinkbands in AS PBO fibres are perpendicular to the fibre direction (similar to PBT fibres) while are at an angle in HT PBO fibres although HT PBO fibres are more opaque than the equivalent as-spun fibres which makes the appearance of the kinkbands less obvious.

Figures 3.4(a) and (b) show the scanning electron micrographs of the surfaces of as-received AS and HT PBO fibres respectively. The surfaces of AS PBO fibres are relatively smooth (but not as smooth as AS PBT fibres) compared to the HT PBO fibres. The granular appearance of HT PBO fibres (similar to HT PBT fibres) may be due to the high temperature treatment (i.e 600°C) giving rise to degradation. PBO fibres were found to have an approximately circular cross-section and some of them have a " figure-of-eight " cross-section. The diameters of AS and HT PBO fibres are shown in Table 3.1. It can be seen that PBO fibres have a larger diameter than the PBT and ABPBO fibres. The PBO fibres show no sign of kinkbands in the scanning electron micrographs.

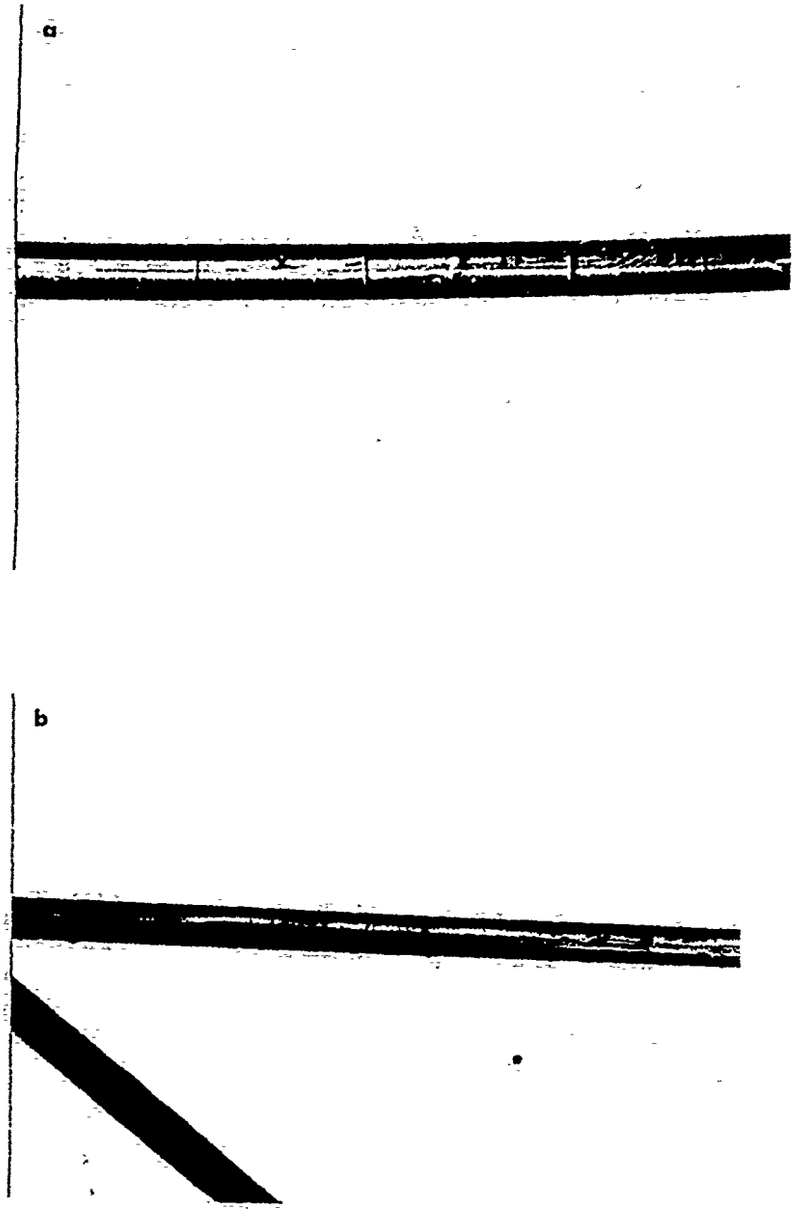

Figure 3.3 Optical micrographs of as-received PBO fibres in air. (a) As-spun; (b) heat treated

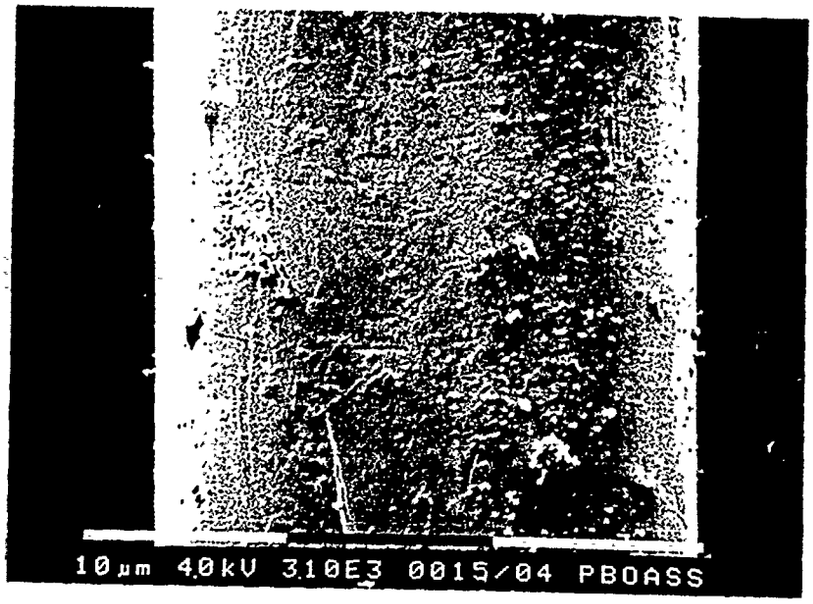

Figure 3.4 Scanning electron micrographs of as-received PBO fibres. (a) As-spun; (b) heat treated

ABPBO fibres

Figures 3.5(a) and (b) show the optical micrographs of as-received AS and HT ABPBO fibres in air at a magnification of x400. As can be seen, kinkbands are already present in both AS and HT ABPBO fibres. The kinkbands in AS ABPBO fibres are at an angle to the fibre direction (similar to HT PBO fibres) and for HT ABPBO fibres, a black V-shaped patterns of kinkbands can be seen along the fibre (quite different from the rest of the fibres).

Figures 3.6(a) and (b) show the scanning electron micrographs of the surfaces of as-received AS and HT ABPBO fibres respectively. The surfaces of both the AS and HT ABPBO fibres are relatively smooth (similar to AS PBO fibres) compared to the HT PBT and HT PBO fibres. ABPBO fibres were found to have approximately circular cross-section and some of them have a " figure-of-eight " cross-section. The diameters of AS and HT ABPBO fibres are shown in Table 3.1. ABPBO fibres show no sign of kinkbands in the scanning electron micrographs.

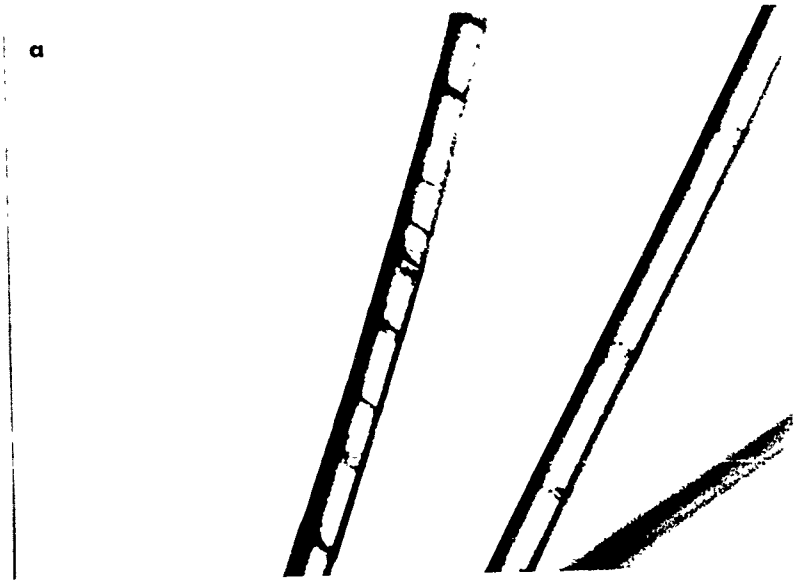

Figure 3.5 Optical micrographs of as-received ABPBO fibres in air. (a) As-spun; (b) heat treated

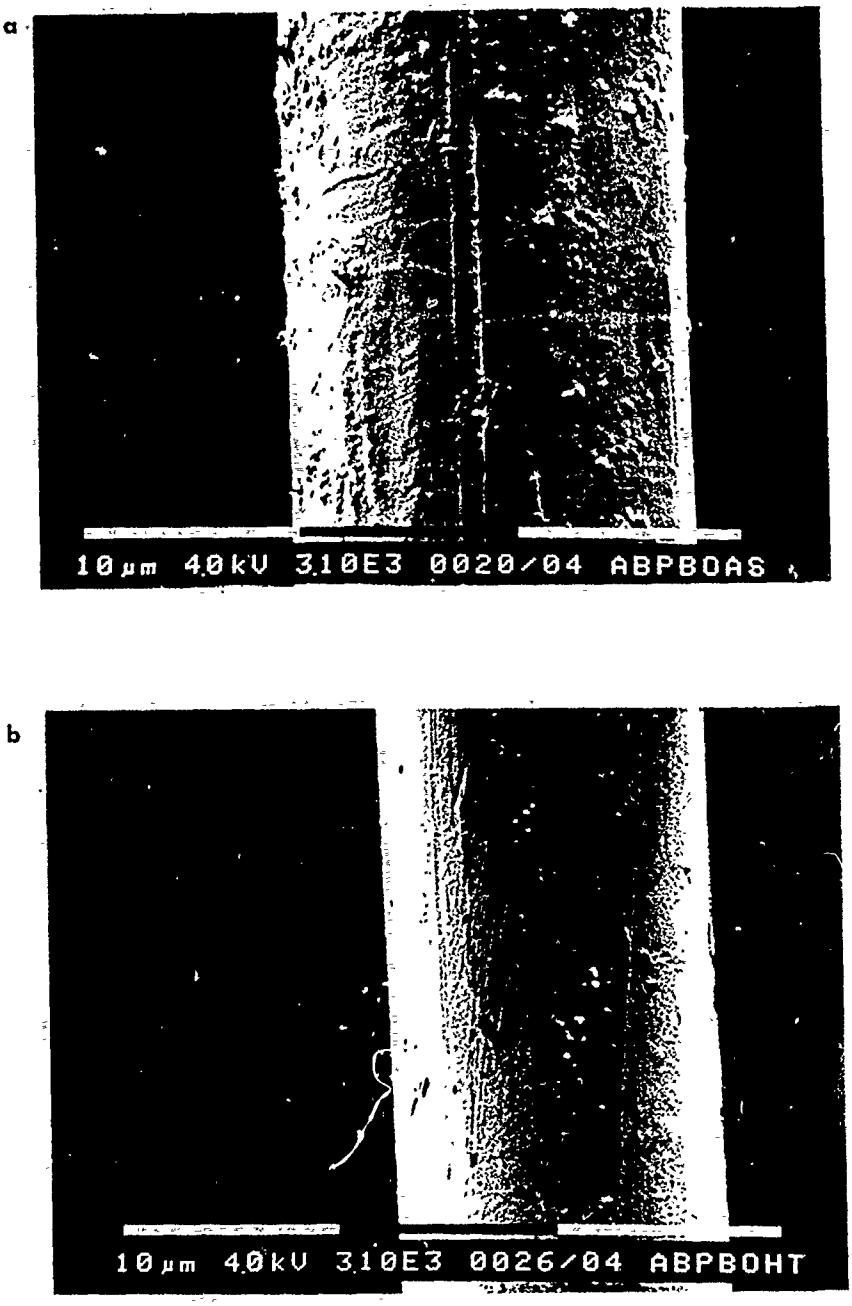

Figure 3.6 Scanning electron micrographs of as-received ABPBO fibres. (a) As-spun; (b) heat treated

3-1-2 X-ray diffraction

PBT fibres

The Wide-angle X-ray scattering (WAXS) patterns for the AS and HT fibres of PBT are shown in Figure 3.7. The as-spun fibers have a pattern consisting of diffuse equatorial peaks and weak layer lines (Figure 3.7(a)). The heat-treated fibres have sharper equatorial peaks and better defined layer lines (Figure 3.7(b)), indicating an improvement in structural order as reported previously(1). These WAXS patterns are also similar to those found by previous workers on PBT tapes(2,3). Odell et al(3) reported that the (00l) meridional reflections of PBT fibre were due to the periodicity of the repeat unit along the molecular axis (intramolecular interference). They also reported that only (hk0) equatorial reflections in selected area ·on diffraction (SAED) patterns were from crystalline material. T. ɔnce of (hkl) off-axis reflections as observed in Figure 3.7 indicates that the " crystallites " giving rise to the (hk0) reflections are not three-dimensionally (3D) ordered, but only 2D laterally ordered due to axial disorder of the molecules. It is thought that the heat treatment increases the conjugation length in the polymer by improving the planarity of the molecule. This leads to the colour change in the materials following heat treatment resulting in a better-defined molecular structure and improved orientation.

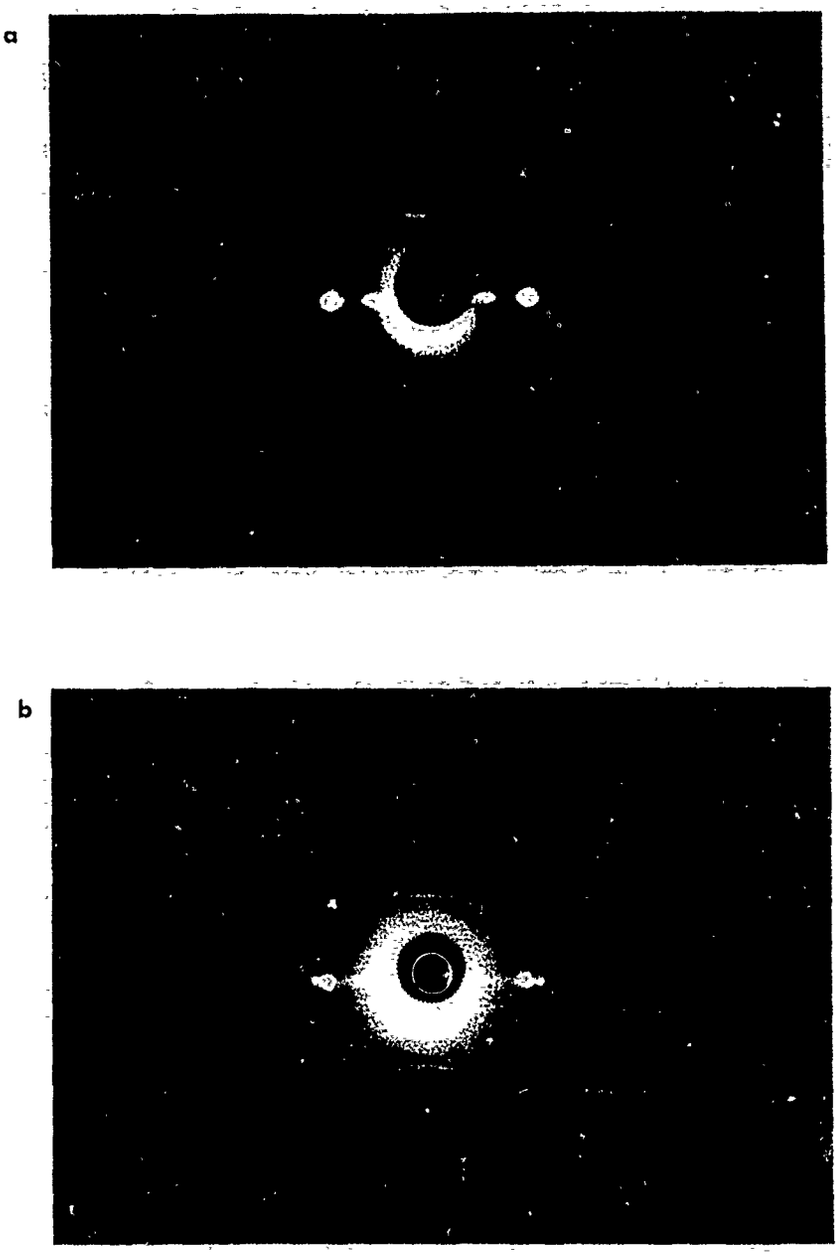

Figure 3.7 Wide-angle X-ray scattering patterns for bundles of PBT fibres. (a) As-spun; (b) heat treated

PBO fibres

WAXS patterns for the AS and HT PBO fibres are shown in Figure 3.8. The pattern for the as-spun fibres can be seen to consist of diffuse equatorial peaks which become sharper following heat treatment at 600°C, indicating an improvement in structural order. The patterns also show a limited number of weak, off-axis, first order (hkl) reflections, indicative of 3D crystallinity in the fibres in both the as-spun and the heat-treated conditions. Significant sharpening of the off-axis (hkl) reflections in the heat-treated fibres indicate that there is an increase in 3D order and/or crystallite size upon heat treatment as reported previously(4). The 3D crystallinity in PBO contrasts with the axial disorder in PBT where no off-axis (hkl) reflections are observed. It may be that, compared with non-planar PBT molecules, the planar molecules of PBO have improved chain axis registry, thus promoting 3D crystallinity in both the as-spun and heat-treated fibres. However, only first order (hkl) reflections are present in PBO, whereas many higher order (hkl) reflections are observed in aramids such as poly(p-phenylene terephthalamide)(PPTA), indicating that the PBO crystalline structure is not as well ordered as PPTA.

a

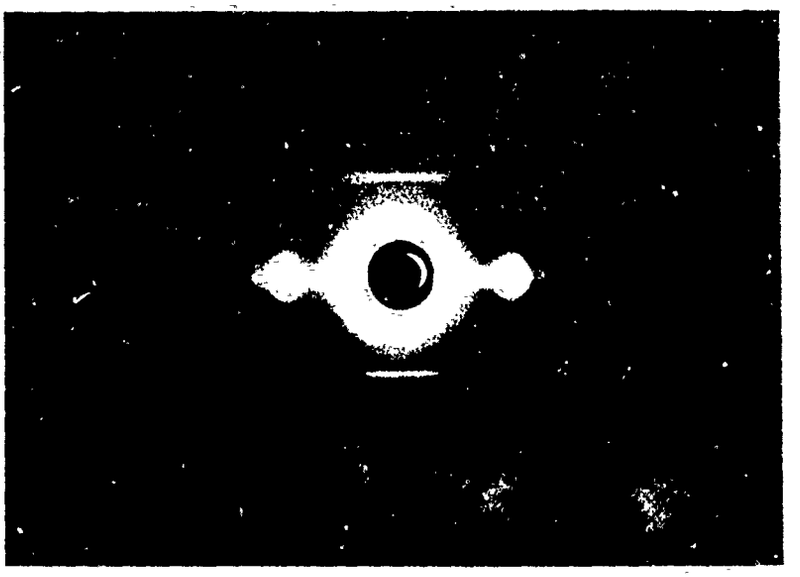

b

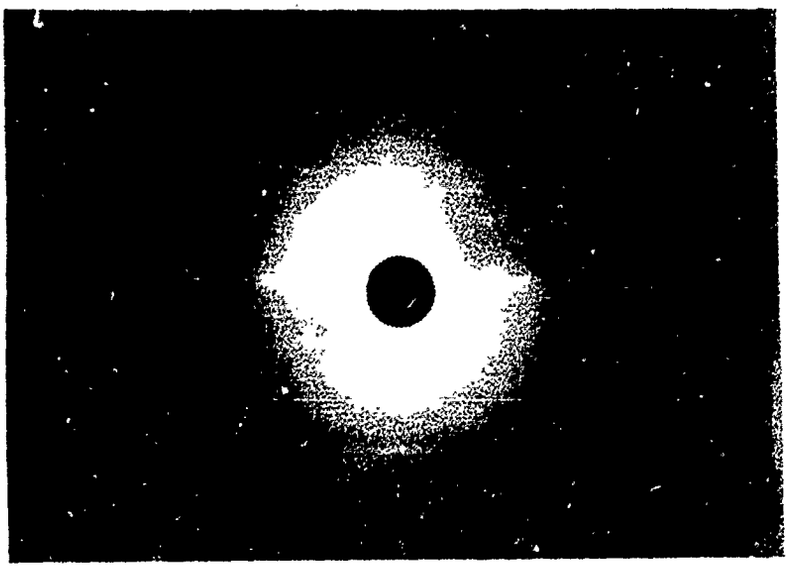

Figure 3.8 Wide-angle X-ray scattering patterns for bundles of PBO fibres. (a) As-spun; (b) heat treated

ABPBO fibres

WAXS patterns for the AS and HT ABPBO fibres are shown in Figure 3.9. The pattern for the as-spun fibres can be seen to consist of diffuse equatorial peaks which become sharper following heat treatment as reported previously(4) and observed in as-spun and heat-treated PBT and PBO fibres. It should be noted that very well-defined off-axis first order (hkl) reflections develop following the heat treatment, indicative of 3D crystallinity for ABPBO fibres in heat-treated condition. It has been reported(4) that the WAXS pattern for as-spun ABPBO shows a limited number of well defined, off-axis, first order(hkl) reflections but this is not apparent in Figure 3.9(a).

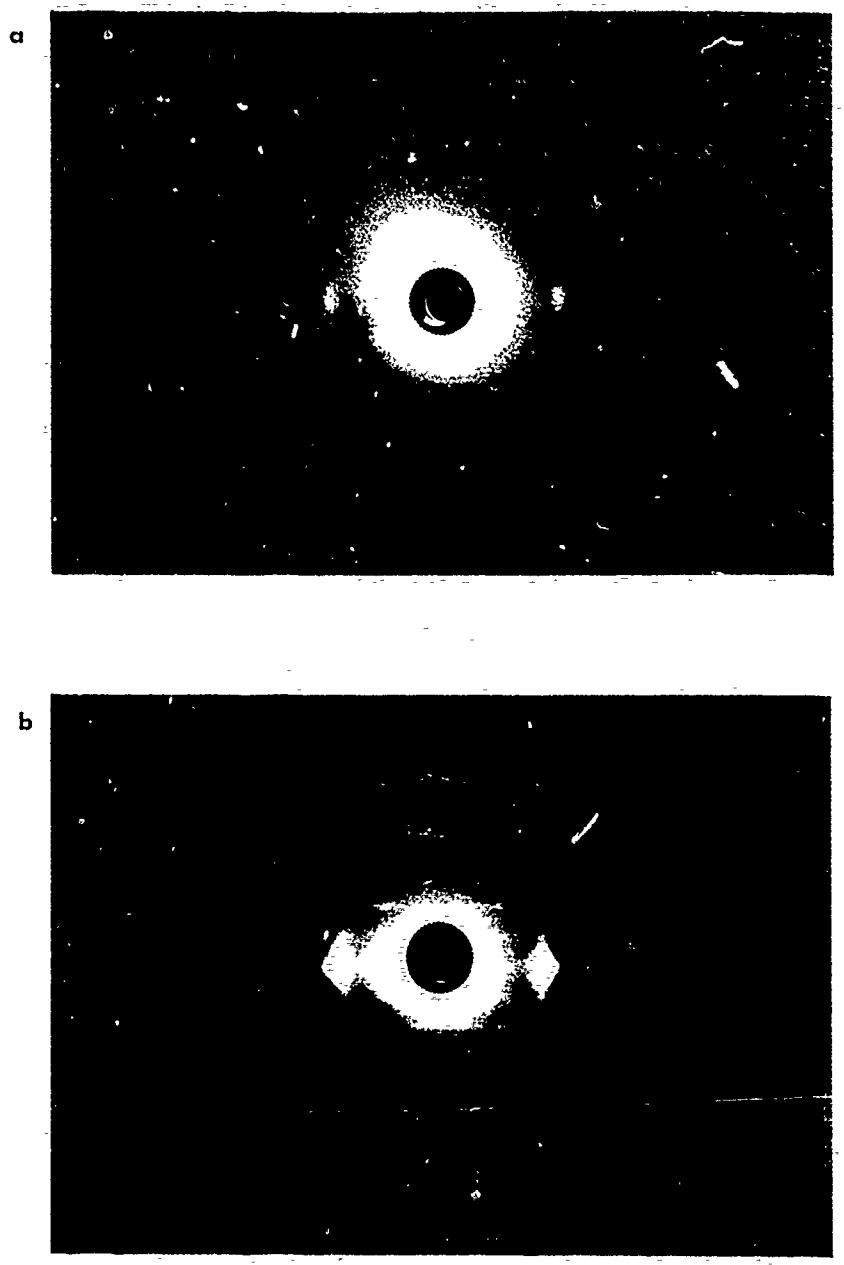

Figure 3.9 Wide-angle X-ray scattering patterns for bundles of ABPBO fibres. (a) As-spun; (b) heat treated

3-1-3 Mechanical testing

Stress-strain curves

Four sets of specimens with various gauge lengths namely; 50, 84, 110, 130 mm for AS and HT PBT , PBO and ABPBO fibres were tested. Typical stress-strain curves for individual AS and HT PBT, PBO and ABPBO fibres at 50mm gauge length are shown in Figures 3.10, 3.11 and 3.12 respectively. The curves for AS PBT, PBO and ABPBO fibres show pronounced deviations from linearity at strains of about 0.8%, 0.8% and 1.3% respectively. In contrast the curves for the HT PBT, PBO and ABPBO fibres are approximately linear up to fracture with no indication of yield. Similar behaviour has been found by other workers for PBT fibres(1,5). However, the behaviour is quite different from that of a different batch of AS PBO fibres reported previously(6) where the stress-strain curves were found to be approximately linear with no yield or inelastic behaviour. This may be due to batch-to-batch variation of fibre properties.

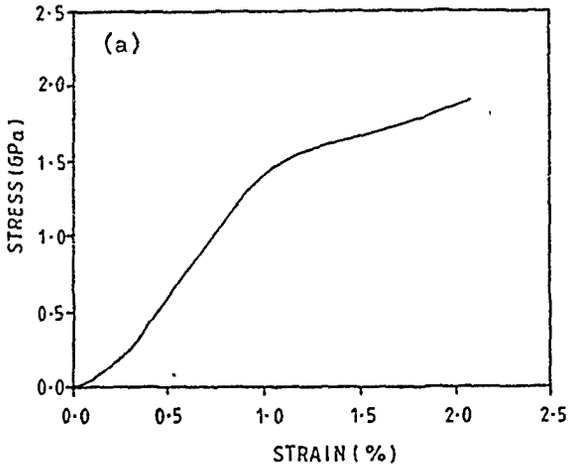

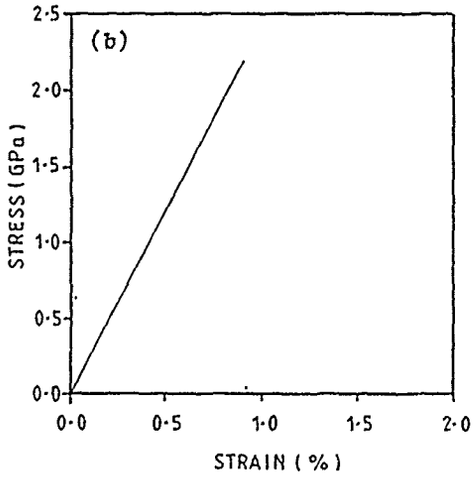

Figure 3.10 Stress-strain curves for individual PBT fibres.
(a) As-spun; (b) heat treated

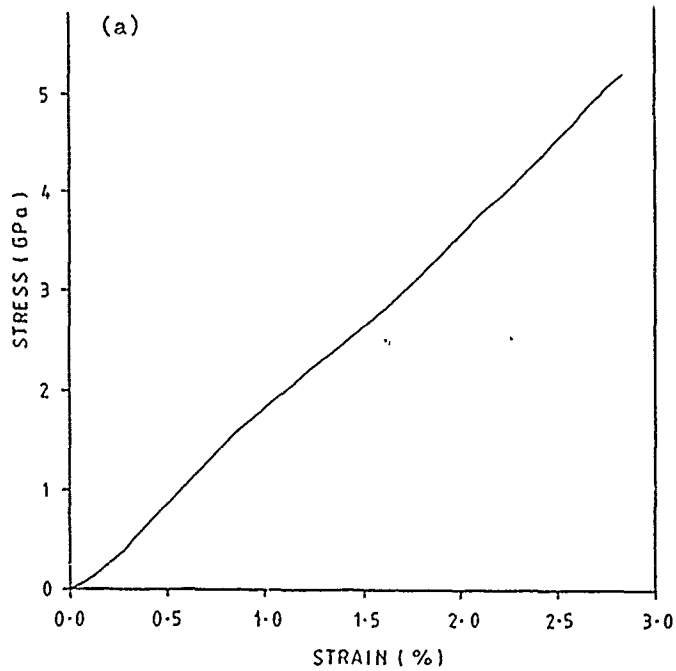

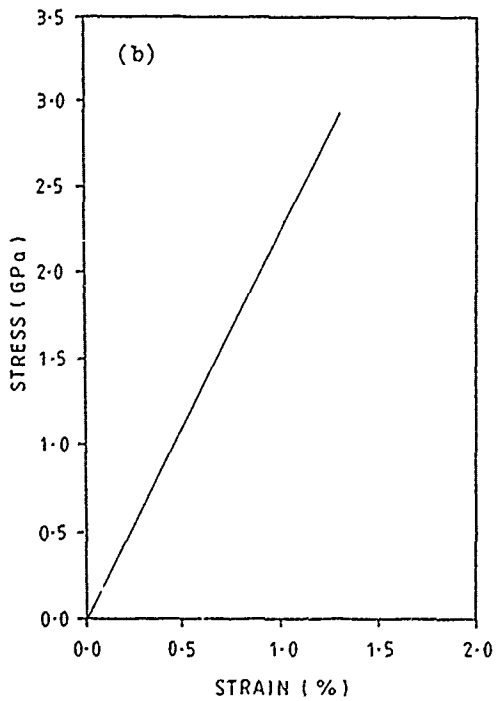

Figure 3.11 Stress-strain curves for individual PBO fibres.
(a) As-spun; (b) heat treated

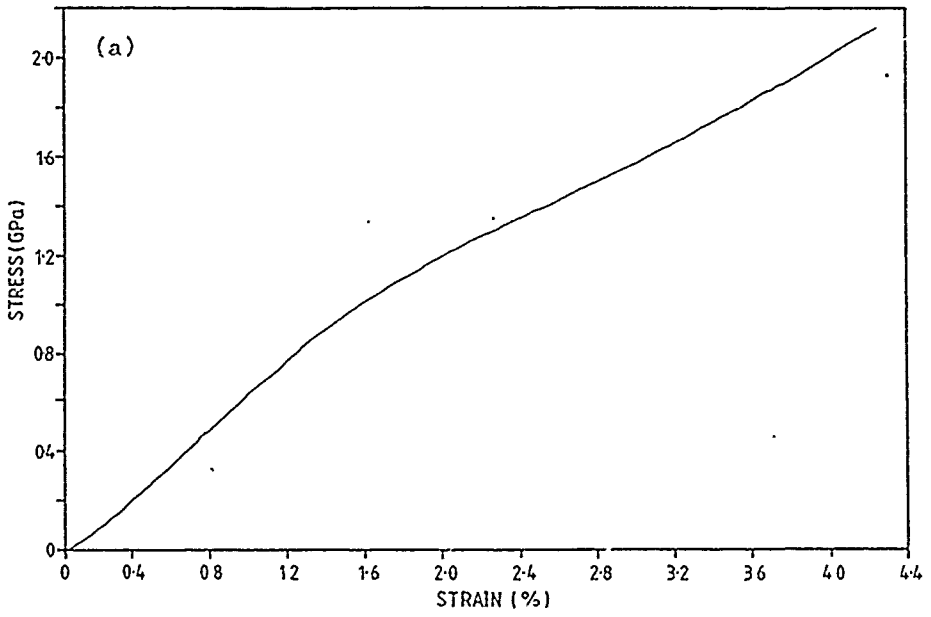

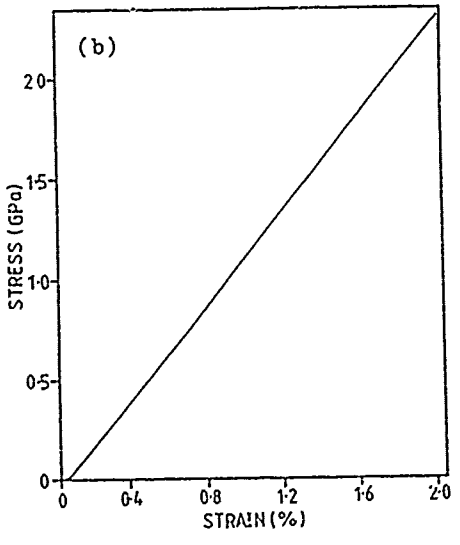

Figure 3.12 Stress-strain curves for individual ABPBO fibres.
(a) As-spun; (b) heat treated

Scanning electron micrographs of fractured fibres from mechanical testing

SEM images of fracture surfaces of AS and HT PBT, PBO and ABPBO fibre are shown in Figures 3.13, 3.14 and 3.15 respectively. All fibres show limited ductility and spliting of the fibre along the fibre direction at the point of fracture. Some fibrillation of the fibres also occured in all types of fibre.

The response of the fibres to mechanical deformation varies somewhat. Away from the fracture surface, some fibrillation on the sides of the fibres was observed in the AS PBT fibres (Figure 3.16(a)) and AS ABPBO fibres (Figure 3.18(a)) while a skin-core structure was observed in AS PBO fibres (Figure 3.17(a)). Cracking along the fibre direction can be seen in the HT PBT (Figure 3.16(b)), HT PBO (Figure 3.17(b)), AS ABPBO (Figure 3.18(a)) and HT ABPBO fibres (Figure 3.18(b)) while HT ABPBO fibres show fewer instances of cracking along the fibre direction. Figures 3.18(a) and (b) show the presence of voids in AS and HT ABPBO fibres respectively although there is some contamination on HT ABPBO fibres. Further away from the fracture region, kinkbands caused by the recoil forces acting on the broken ends of a fibre after tensile failure can be seen in all types of fibre (Figures 3.19, 3.20 and 3.21). This damage is the result of compressive stresses developed during snap-back, or recoil, the magnitude of which exceeds the compressive strength of the fibre(7). The recoil damage is most severe in AS PBO fibres (Figure 3.20(a)) while is less apparant in HT ABPBO fibres (Figure 3.21(b)). The production of these kinkbands has been used by Allen (7) to investigate the compressive properties of these types of fibres.

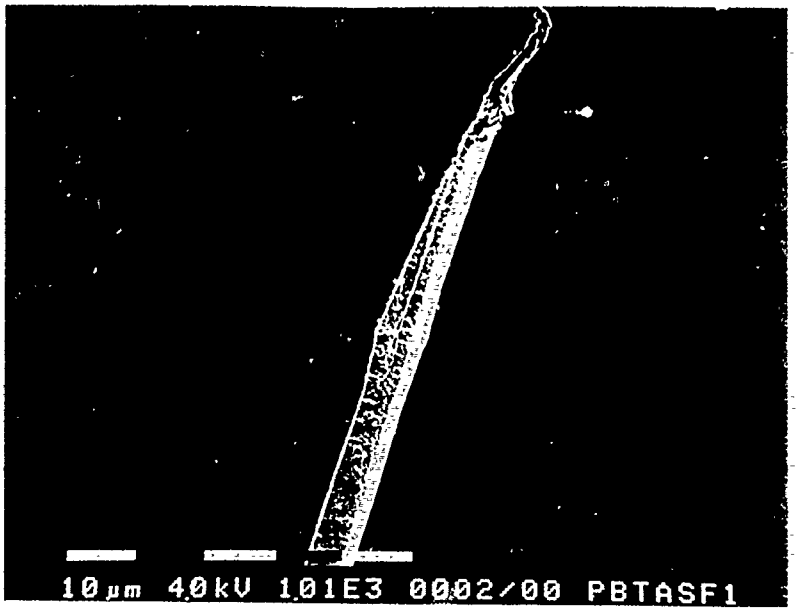

Figure 3.13(a) SEM of AS PBT fibre fracture surfaces.

Figure 3.13(b) SEM of HT PBT fibre fracture surfaces.

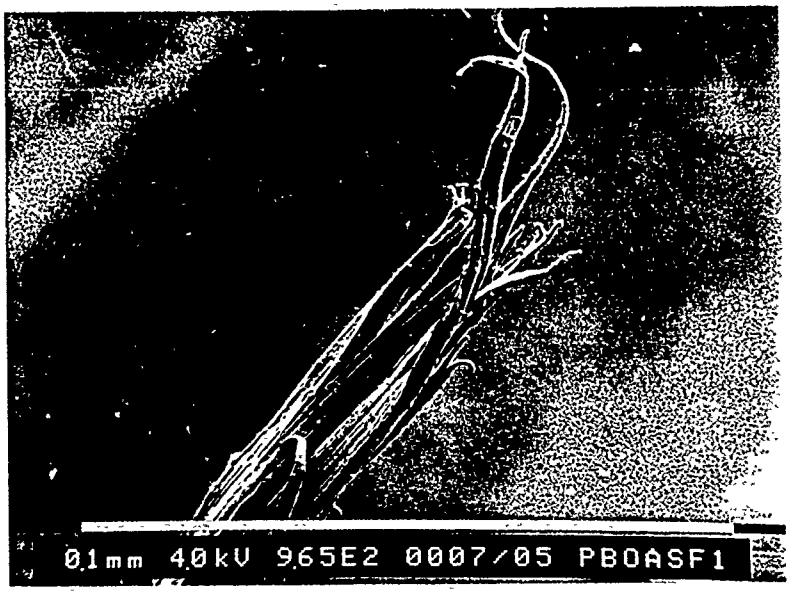

Figure 3.14(a) SEM of AS PBO fibre fracture surfaces.

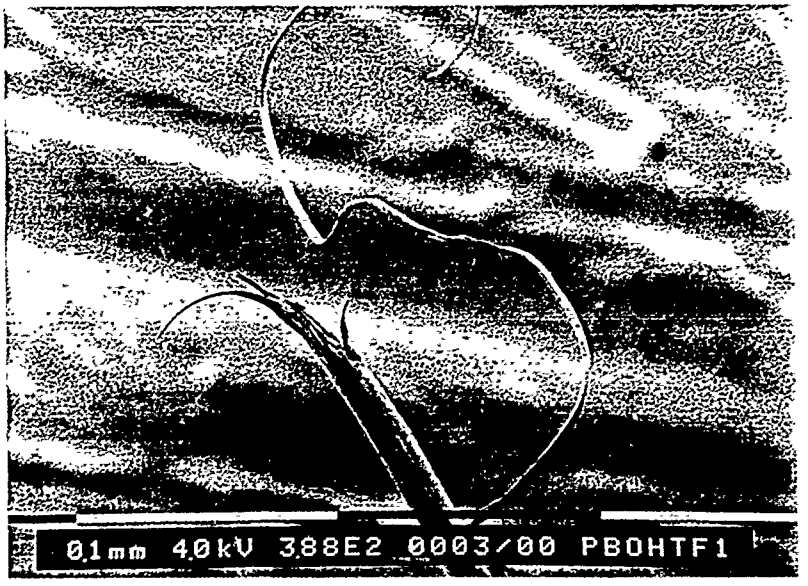

Figure 3.14(b) SEM of HT PBO fibre fracture surfaces.

Figure 3.15(a) SEM of AS ABPBO fibre fracture surfaces.

Figure 3.15(b) SEM of HT ABPBO fibre fracture surfaces.

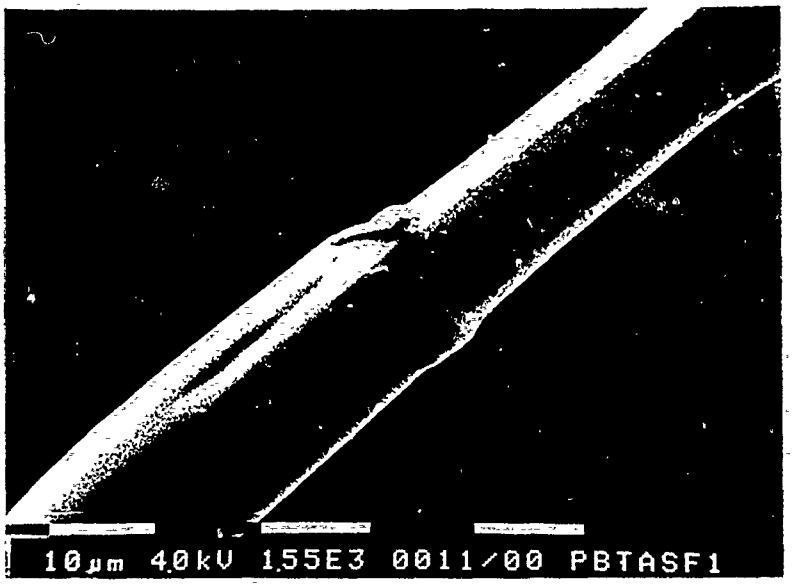

Figure 3.16(a) Fibrillation on the side of AS PBT fibre.

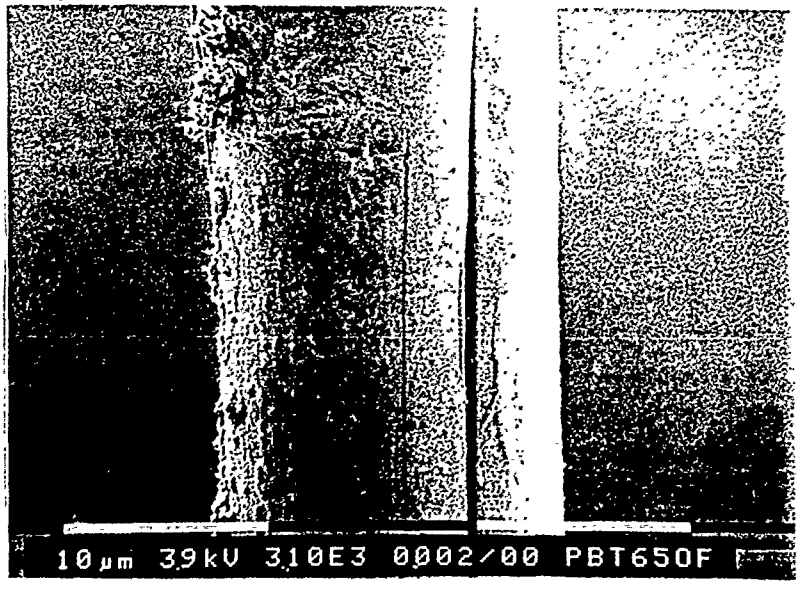

Figure 3.16(b) Cracking along fibre direction in HT PBT fibre.

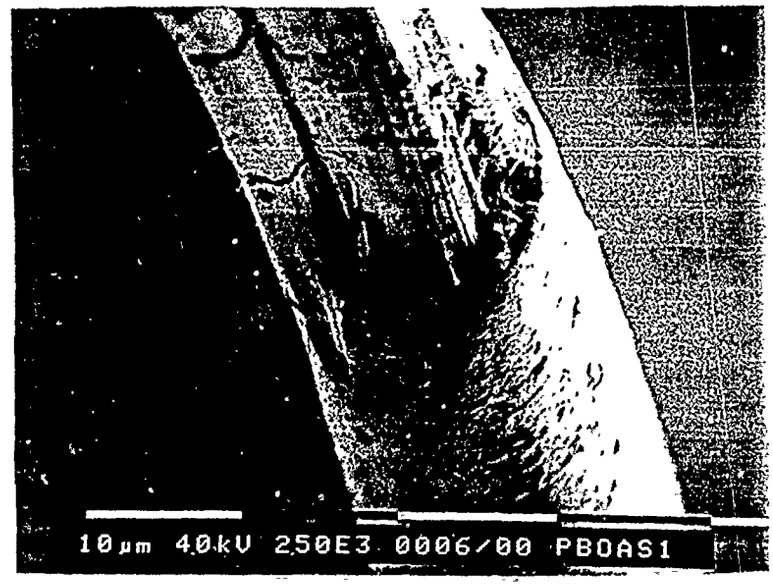

Figure 3.17(a) Skin core structure of AS PBO fibre.

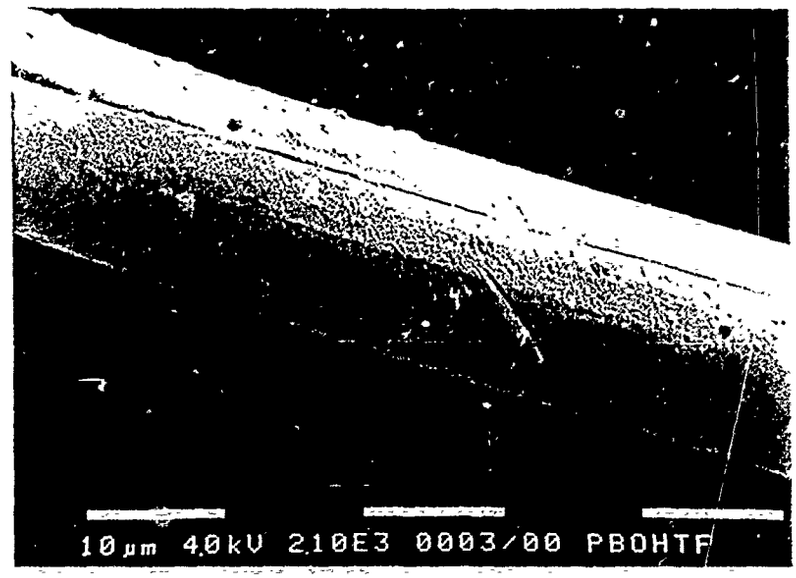

Figure 3.17(b) Cracking along fibre direction in HT PBO fibre.

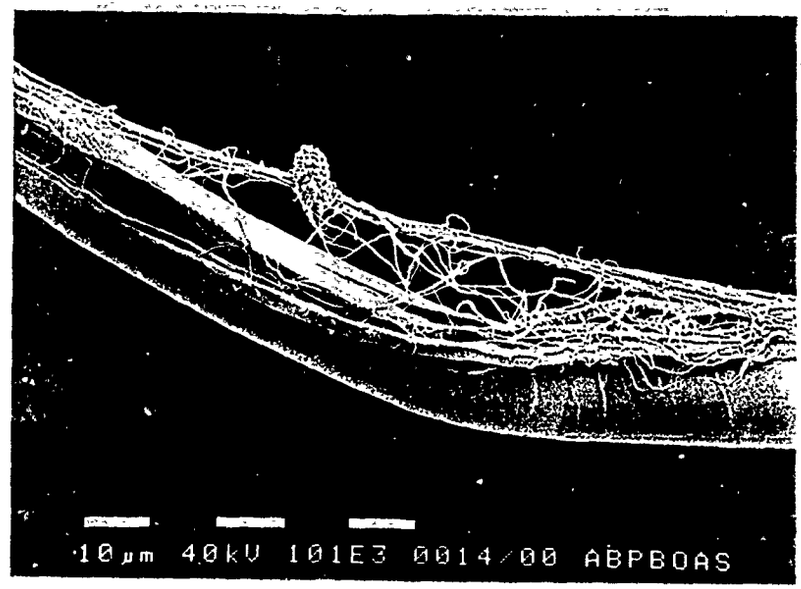

Figure 3.18(a) SEM of AS ABPBO fibre revealing the presence of a void.

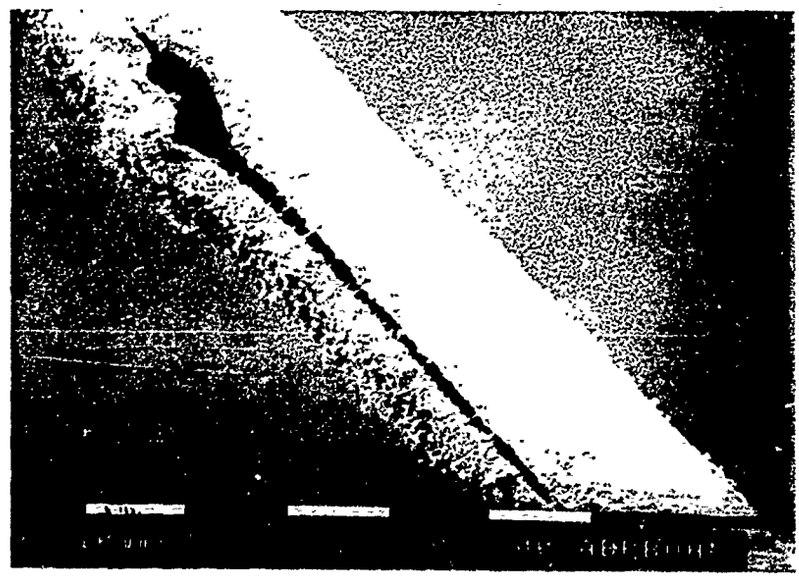

Figure 3.18(b) SEM of HT ABPBO fibre revealing the presence of a void.

Figure 3.19(a) Tensile recoil damage observed in AS PBT fibre.

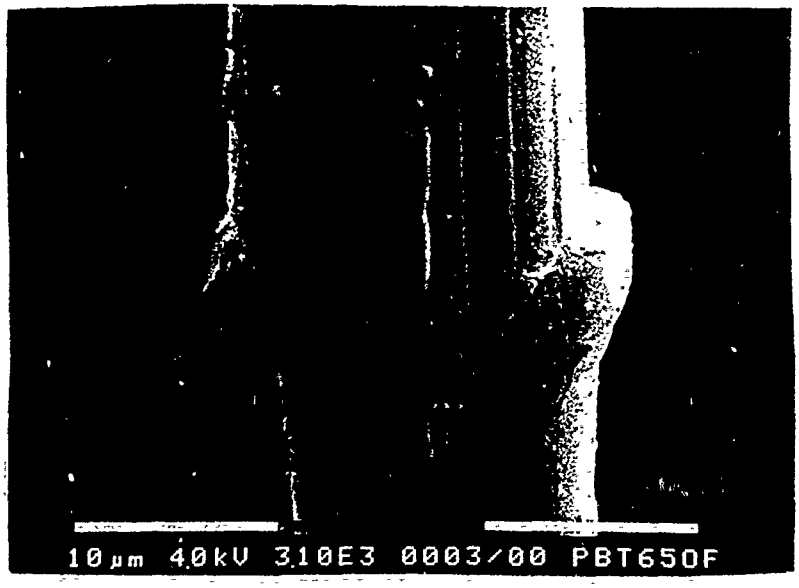

Figure 3.19(b) Tensile recoil damage observed in HT PBT fibre.

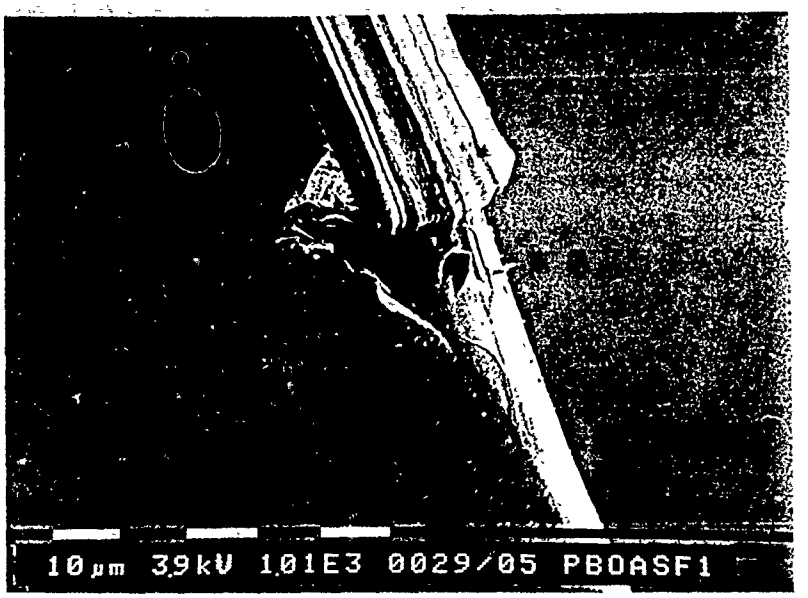

Figure 3.20(a) Tensile recoil damage observed in AS PBO fibre.

Figure 3.20(b) Tensile recoil damage observed in HT PBO fibre.

Figure 3.21(a) Tensile recoil damage observed in AS ABPBO fibre.

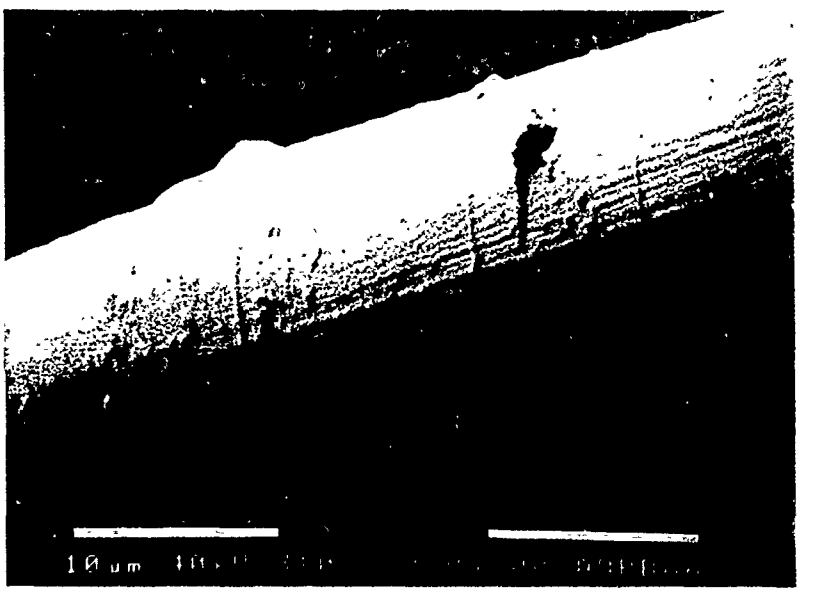

Figure 3.21(b) Tensile recoil damage observed in HT ABPBO fibre.

Effect of gauge length on mechanical properties

The diameter of the individual fibres was measured using the Image Manger microscope. Measurements were made at three different points along each individual fibre and a mean value of the three was obtained and used for the calculation of stresses. The mechanical properties of AS and HT PBT, PBO and ABPBO fibres for four sets of different gauge lengths are shown in Table 3.2 and each set represents the average of at least 10 specimens. The Young 's modulus vs 1/length curves for AS and HT PBT, PBO and ABPBO fibres are shown in Figures 3.22, 3.23 and 3.24 respectively. The corrected Young's modulus are obtained by extrapolating the straight line to infinite gauge length i.e 1/length=0. It was found that the corrected Young's modulus was higher than the practical Young's modulus. This is due to the fact that the end effects are eliminated at infinite gauge length. The factors that give rise to the end effects are discussed below:

(1) Effective gauge length: The stress in the fibres will not disappear at the edge of the clamp but will fall to zero at some point within it. The gauge length of the fibres as measured will thus be less than the true (or effective) gauge length which is undergoing the test. This means that the measured stress-strain curve will not be the true stress-strain curve. The strain will tend to be overestimated giving a lower value of modulus. This effect is assumed to be constant for the different gauge length, hence the reduction in modulus due to this effect is greater for shorter gauge length fibres and can be removed by extrapolating to infinite gauge length.

(2) Slippage: Another problem encountered in the tensile test is that of clamping. Slippage may or may not occur depending on the amount of adhesive used and how well it is adhers to the fibres on the paper cards. This is more likely to occur at low, rather than high rates of extension. However, slippage can be recognised from the

Materials	Gauge Length (mm)	Modulus (GPa)	Tensile Strength (GPa)	Elongation to break (%)
AS PBT	50	183.3 ± 12.8	1.99 ± .18	1.88 ± .26
	84	186.1 ± 14.5	1.95 ± .15	1.73 ± .21
	110	189.2 ± 11.5	1.84 ± .17	1.72 ± .31
	130	191.3 ± 7.1	1.79 ± .18	1.66 ± .31
HT PBT	50	233.8 ± 13.5	2.42 ± .35	1.10 ± .16
	84	248.8 ± 9.5	2.50 ± .40	1.06 ± .17
	110	251.6 ± 8.2	2.41 ± .47	1.00 ± .18
	130	253.6 ± 7.0	2.44 ± .49	1.02 ± .19
AS PBO	50	124.3 ± 9.8	3.03 ± .47	2.72 ± .27
	84	127.8 ± 10.1	2.73 ± .55	2.28 ± .31
	110	132.0 ± 10.37	2.69 ± .34	2.29 ± .19
	130	139.2 ± 12.61	2.81 ± .42	2.27 ± .22
HT PBO	50	210.2 ± 19.2	2.73 ± .46	1.33 ± .21
	84	235.9 ± 20.3	2.88 ± .36	1.27 ± .19
	110	229.0 ± 17.5	2.67 ± .58	1.18 ± .24
	130	248.2 ± 26.2	2.68 ± .76	1.08 ± .24

Table 3.2(a) Mechanical properties of AS and HT PBT and PBO fibres for four sets of different gauge length with standard deviation.

Materials	Gauge Length (mm)	Modulus (GPa)	Tensile Strength (GPa)	Elongation to break (%)
AS ABPBO	50	70.3 ± 5.2	1.99 ± .25	3.82 ± .40
	84	80.2 ± 6.1	1.98 ± .34	3.38 ± .56
	110	79.1 ± 7.6	1.90 ± .35	3.08 ± .64
	130	84.0 ± 5.4	1.90 ± .26	2.96 ± .45
HT ABPBO	50	119.5 ± 9.0	2.00 ± .43	1.80 ± .28
	84	125.4 ± 9.7	1.87 ± .33	1.48 ± .25
	110	126.9 ± 14.8	1.87 ± .39	1.52 ± .21
	130	127.8 ± 13.3	1.65 ± .26	1.35 ± .21

Table 3.2(b) Mechanical properties of AS and HT ABPBO fibres for four sets of different gauge length with standard deviation.

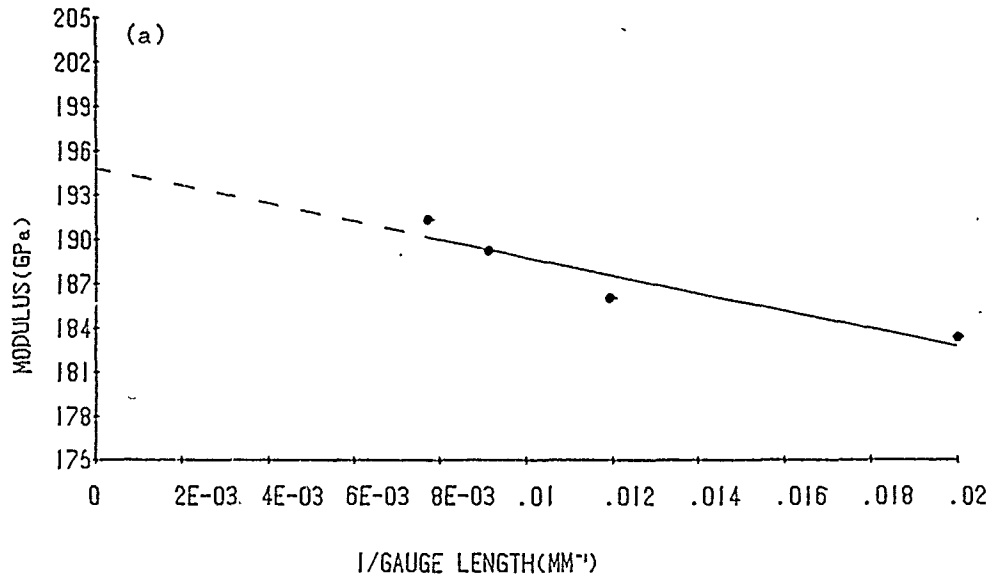

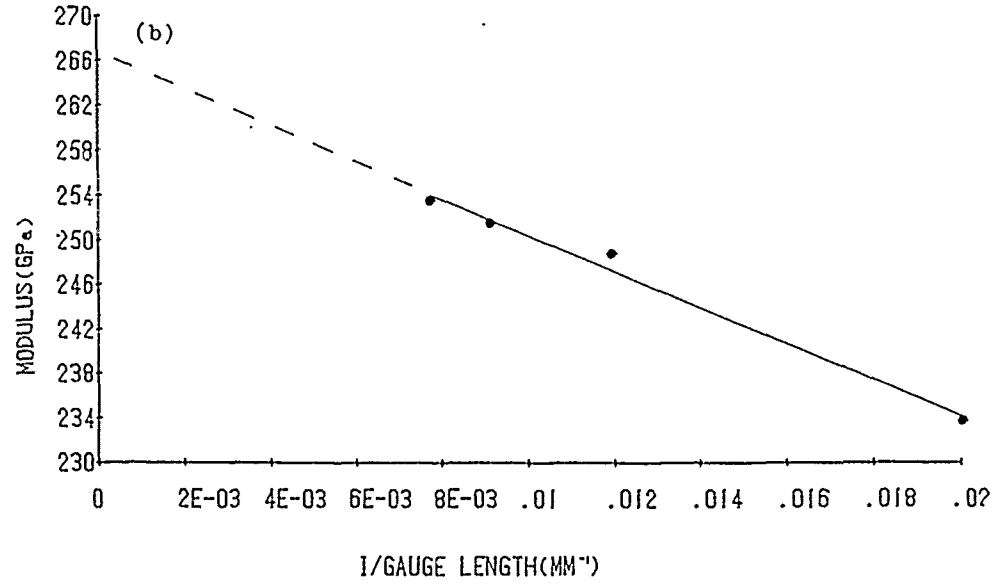

Figure 3.22 Young' modulus versus 1 /gauge length curves for PBT fibres. (a) As-spun; (b) heat treated

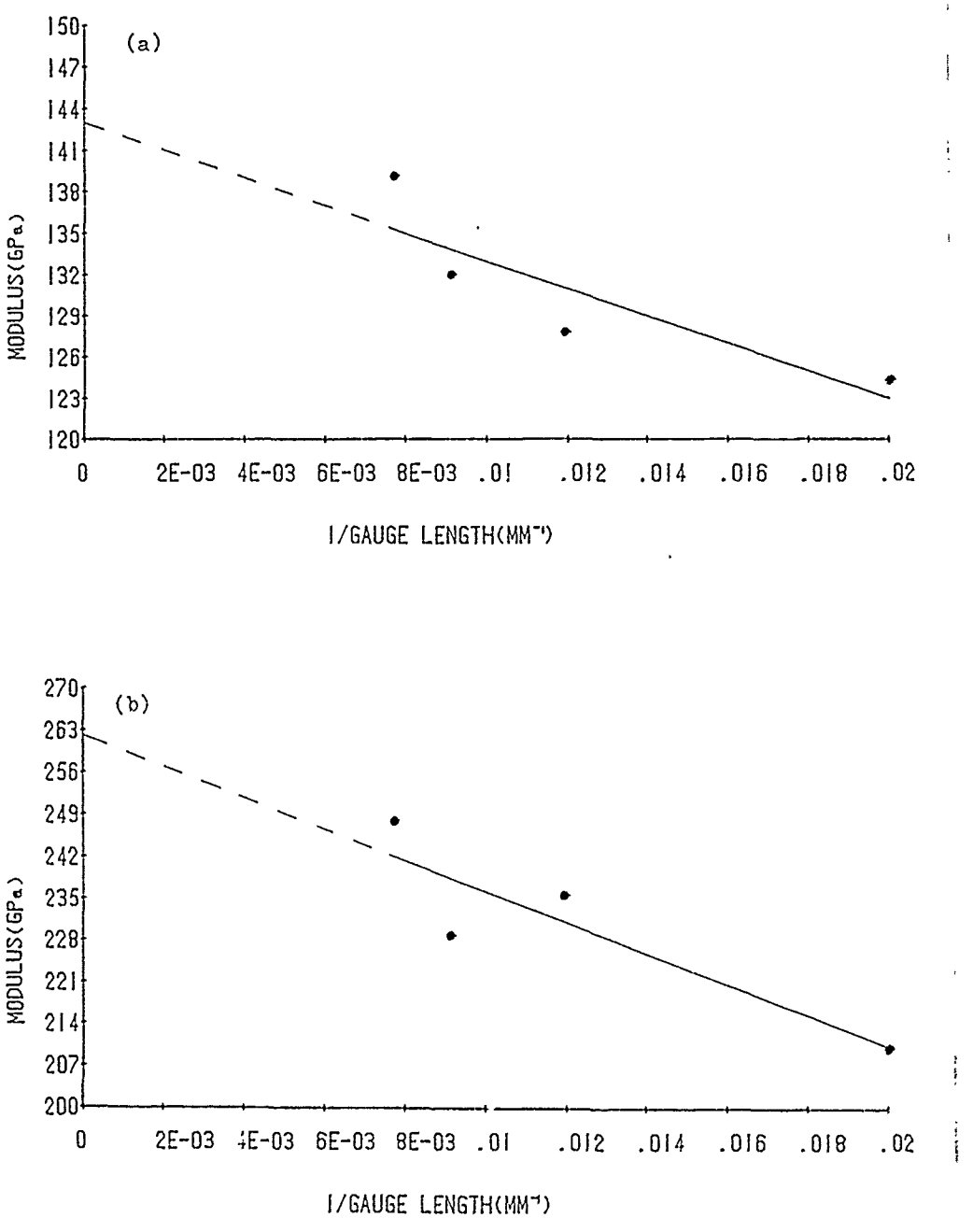

Figure 3.23 Young' modulus versus 1 /gauge length curves for PBO fibres. (a) As-spun; (b) heat treated

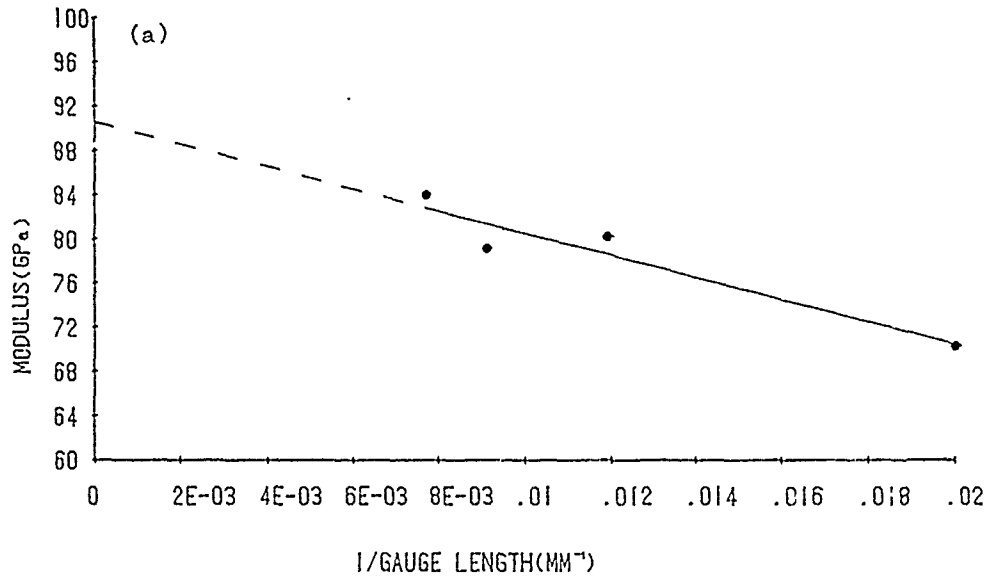

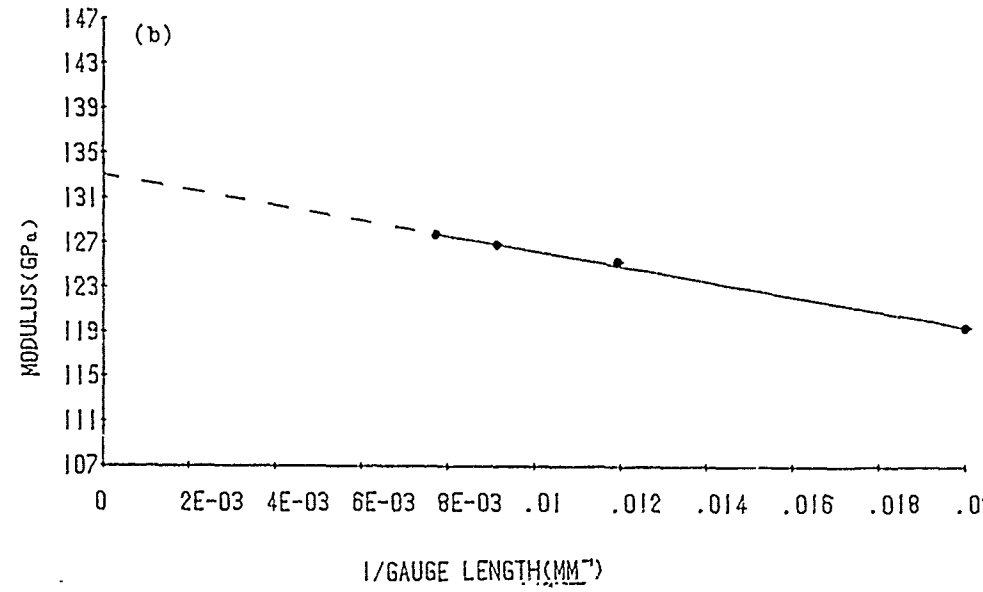

Figure 3.24 Young' modulus versus 1 /gauge length curves for ABPBO fibres. (a) As-spun; (b) heat treated

load/displacement curves which are disregarded when it takes place.

(3) Strain rate: The speed of extension used in this experiment is constant i.e 1mm/min for different gauge length. Hence it is expected that the strain-rate (which is defined as the extension rate divided by the gauge length) will be different for different gauge length. However, the difference in strain rate between gauge lengths of 50mm and 130mm is relatively small (i.e only a factor of 2.6). Hence the effect of strain rate on the stress-strain curve i.e the mechanical properties of these types of fibre (with high glass transition temperature and melting temperature) at room temperature can be neglected.

Figures 3.25, 3.26 and 3.27 show the variation of tensile strength with gauge length and Figures 3.28, 3.29 and 3.30 show the % elongation to break with gauge length for AS and HT PBT, PBO and ABPBO fibres respectively. The corrected tensile strength and % elongation to break are obtained by extrapolating a straight line joining the data points to zero gauge length. It was found that the corrected tensile strength and % elongation are higher than the practical values for the AS and HT PBT, PBO and ABPBO fibres. This is because the shorter the gauge length, the fewer the number of defects in the fibres and hence the higher the tensile strength and % elongation to break. It is thought that the types of defects that may be present are kinkbands and flaws (Figures 3.1-3.6).

The slopes of Young's modulus vs 1/length and tensile strength and % elongation to break vs gauge length plots for AS and HT PBT, PBO and ABPBO fibres are shown in Table 3.3. It can be seen that the slope varies slightly from fibre to fibre. However they are of the same order

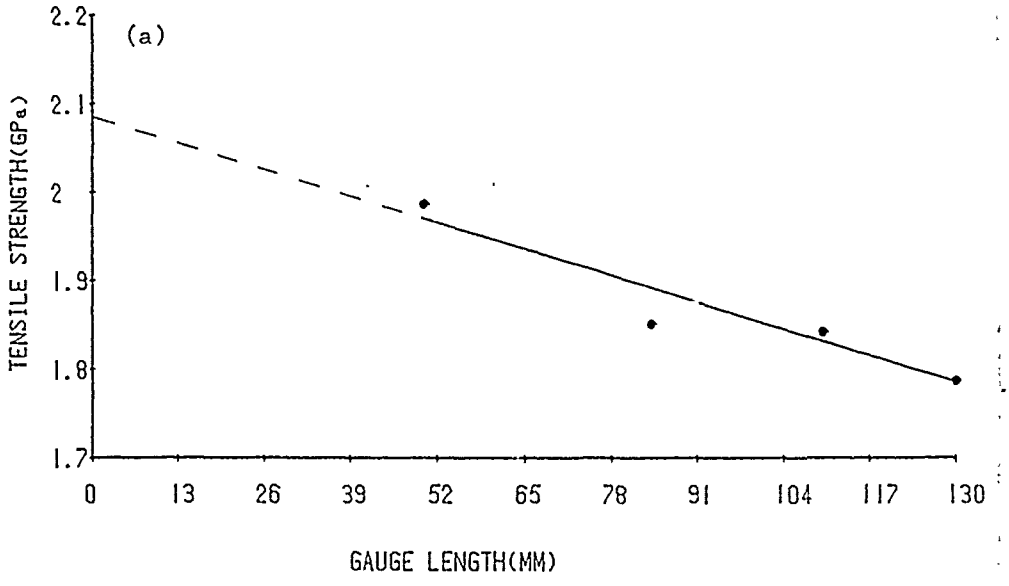

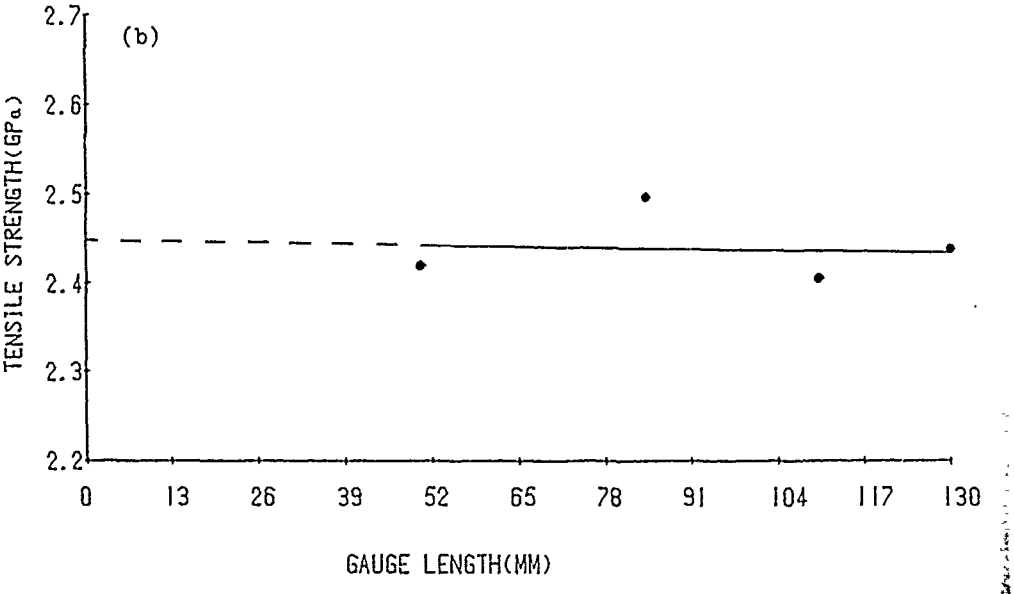

Figure 3.25 Tensile strength versus gauge length curves for PBT fibres, (a) As-spun: (b) heat treated

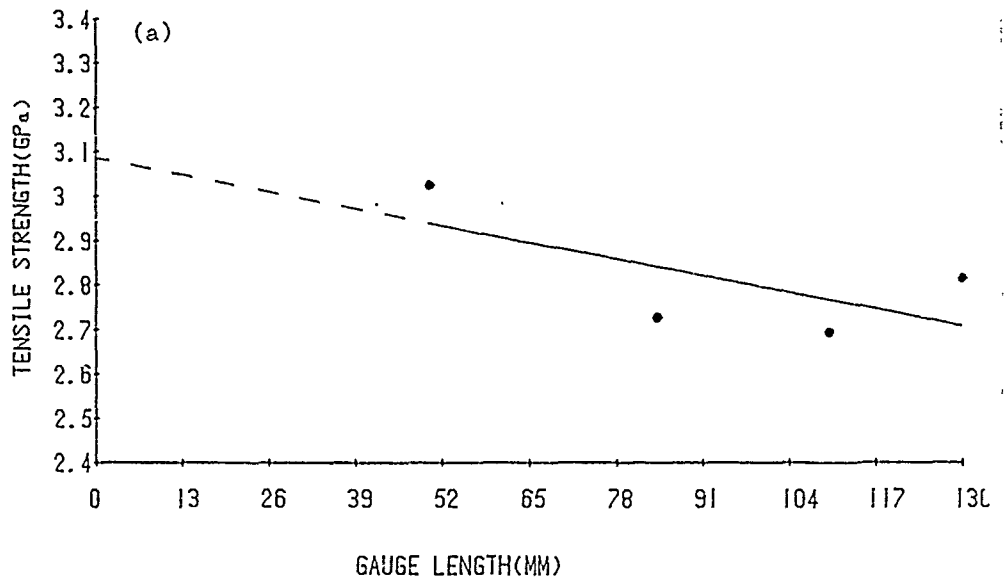

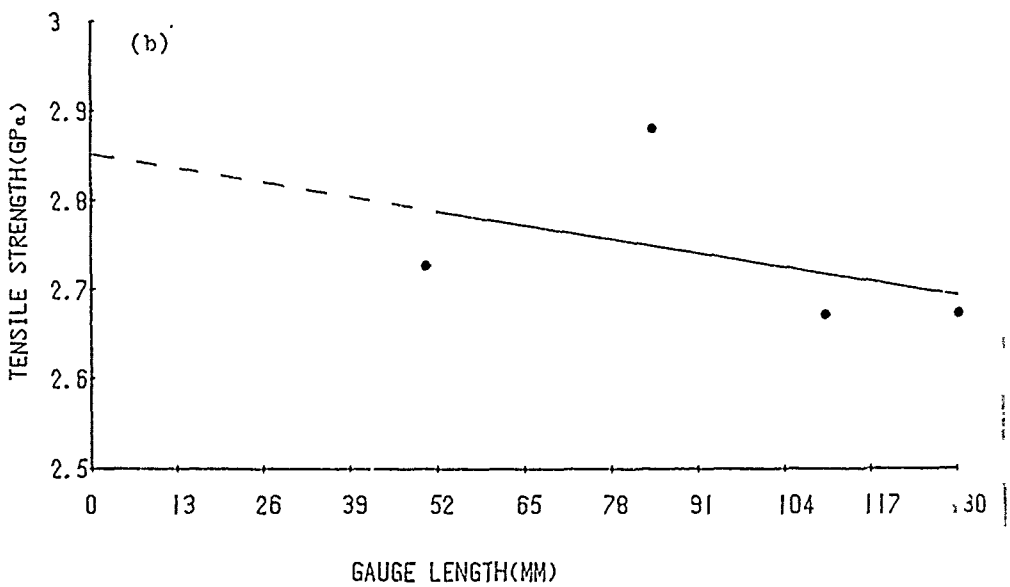

Figure 3.26 Tensile strength versus gauge length curves for PBO fibres. (a) As-spun; (b) heat treated

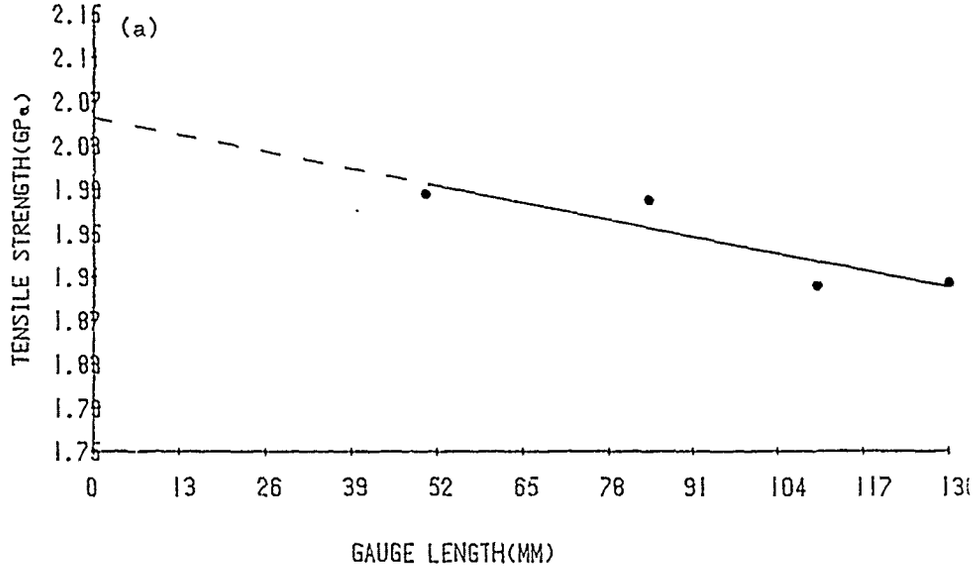

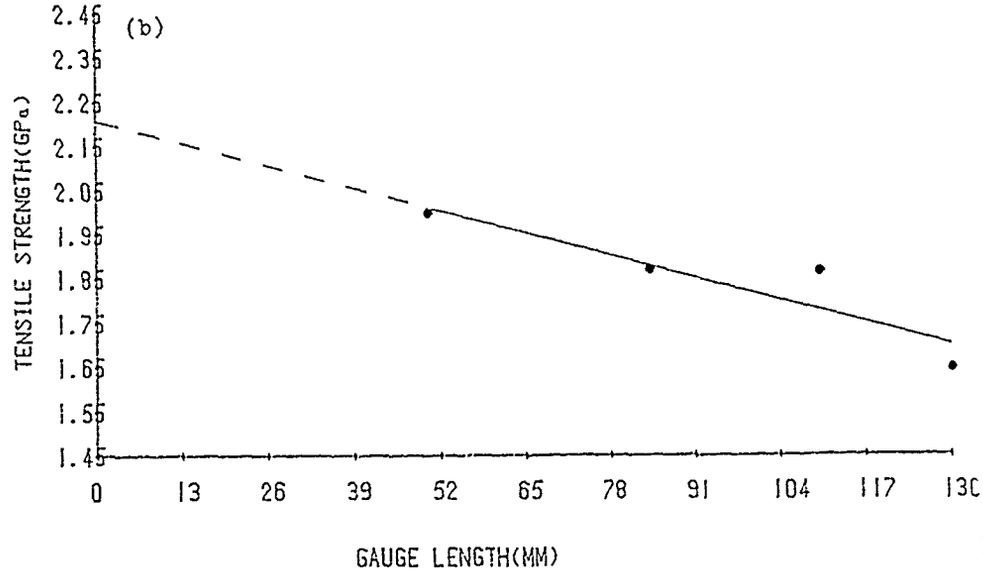

Figure 3.27 Tensile strength versus gauge length curves for ABPBO fibres. (a) As-spun; (b) heat treated

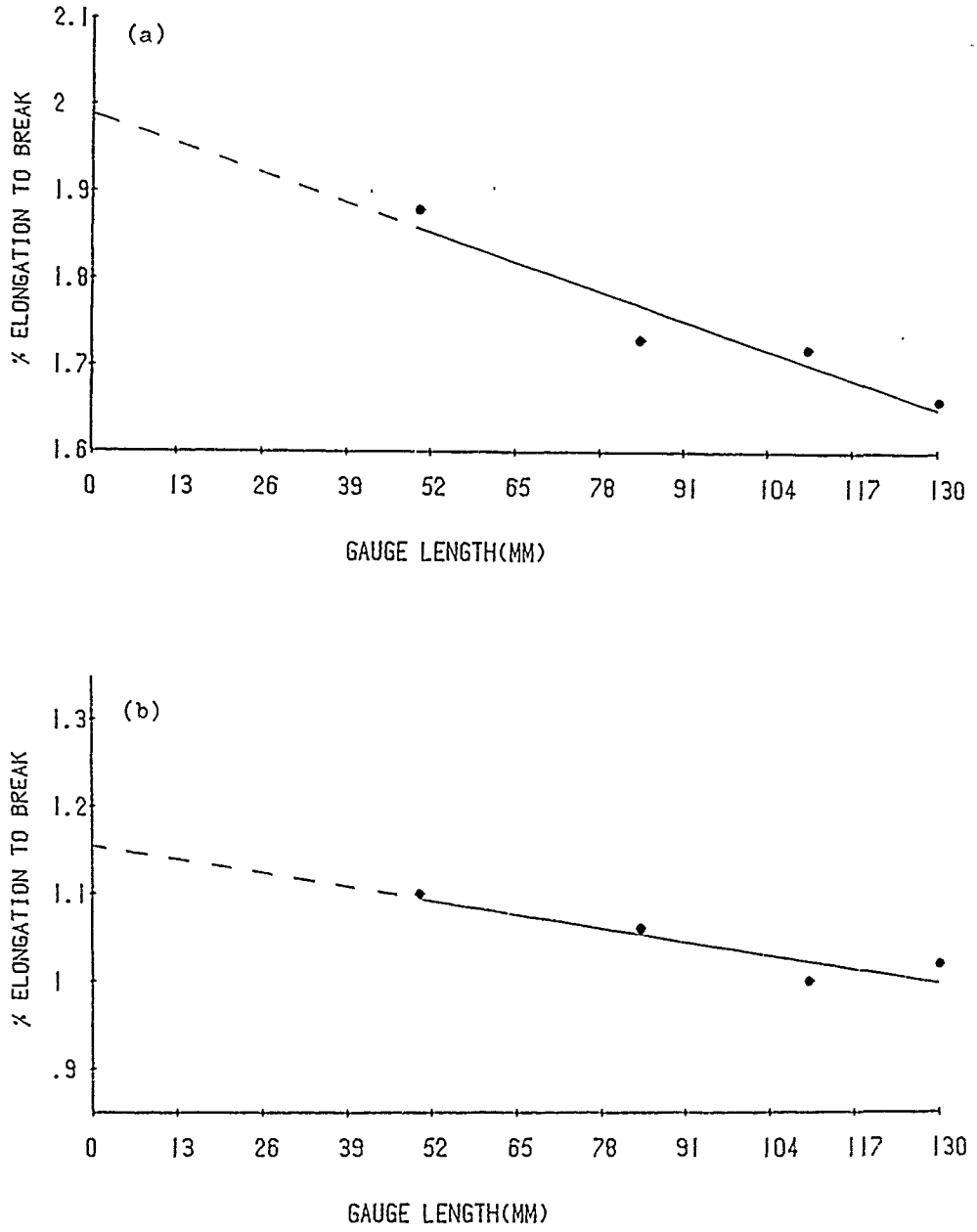

Figure 3.28 % elongation to break versus gauge length curves for PBT fibres. (a) As-spun; (b) heat treated

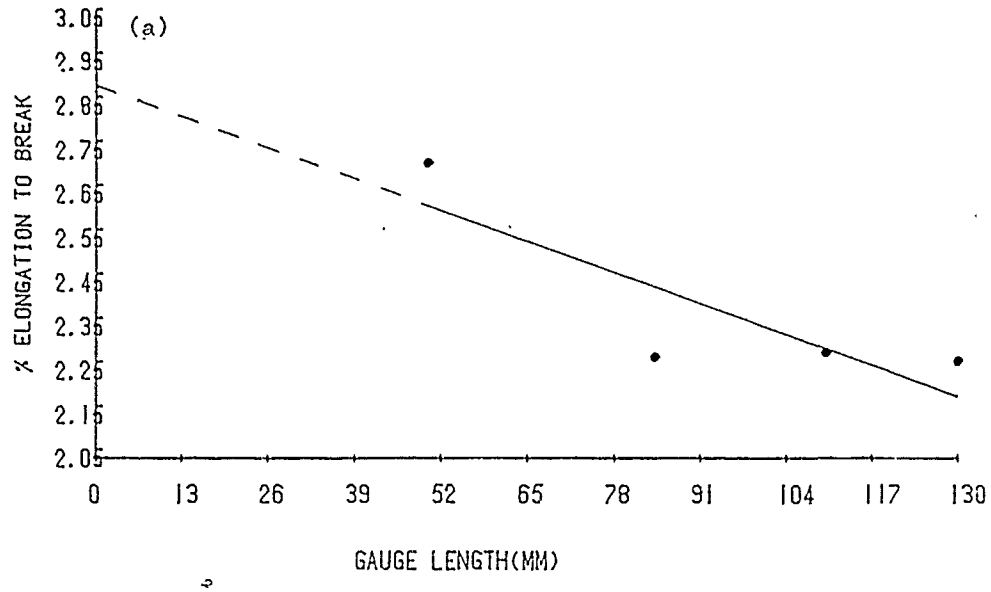

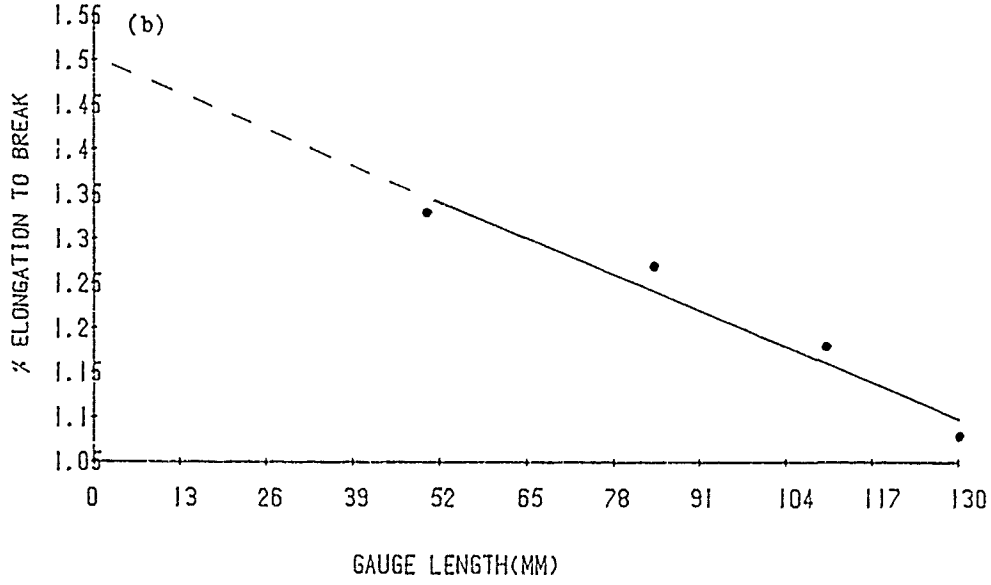

Figure 3.29 % elongation to break versus gauge length curves for PBO fibres. (a) As-spun; (b) heat treated

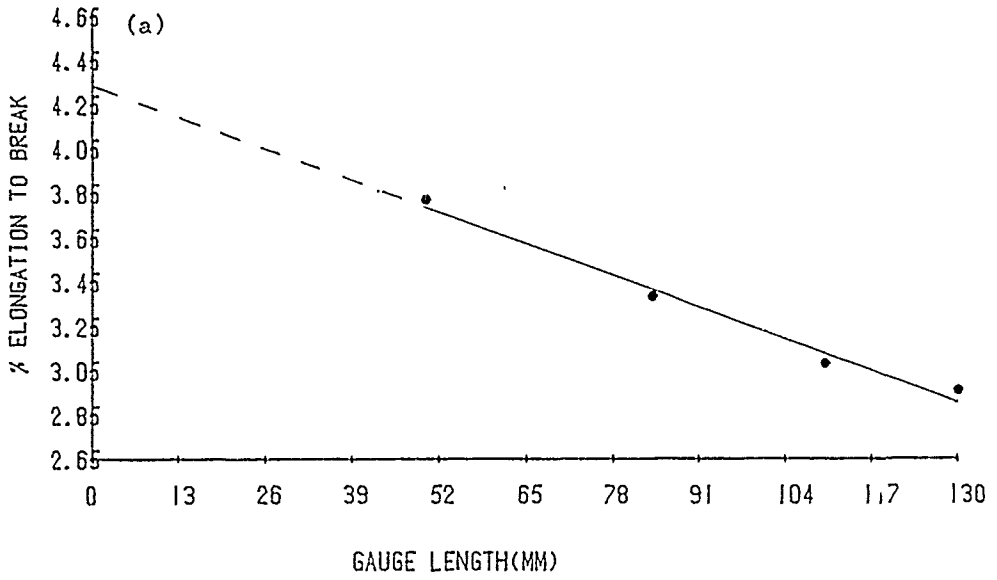

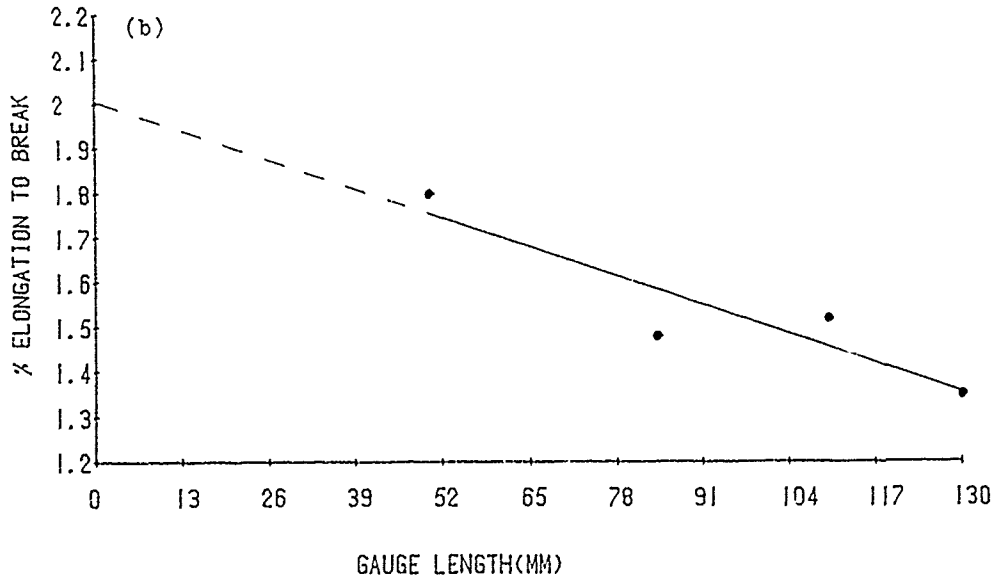

Figure 3.30 % elongation to break versus gauge length curves for ABPBO fibres. (a) As-spun; (b) heat treated

Materials	Slopes		
	Modulus vs (gauge length)$^{-1}$ (GPa mm)	Tensile strength vs gauge length (GPa/mm)	% elongation to break vs gauge length (%/mm)
AS PBT	-600.30	-2.3×10^{-3}	-2.6×10^{-3}
HT PBT	-1622.24	-0.1×10^{-3}	-1.2×10^{-3}
AS PBO	-1002.66	-2.9×10^{-3}	-5.4×10^{-3}
HT PBO	-2586.71	-1.2×10^{-3}	-3.1×10^{-3}
AS ABPBO	-1004.81	-1.2×10^{-3}	-10×10^{-3}
HT ABPBO	-677.74	-3.9×10^{-3}	-5×10^{-3}

Table 3.3 Slopes of Young 's modulus vs 1/length and tensile strength and % elongation to break vs gauge length for AS and HT PBT, PBO and ABPBO fibres.

and all have a negative slope. The significance of these variations is not clear, but it can be reasoned that the variation of tensile strength and % elongation with gauge length will depend on the number of defects in the particular fibre. On the other hand, the variation of modulus with gauge length is a geometrical factor which would be expected to be relatively constant for the different fibres.

Comparison of corrected mechanical properties between different fibres

The corrected Young's modulus, tensile strength and % elongation to break obtained from four sets of specimens with various gauge lengths and the approximate yield strains are given in Table 3.4. The yield strains were obtained from the average of 10 specimens at the gauge length of 50mm. It can be seen that the corrected Young's modulus values of the heat-treated fibres are considerably higher than the equivalent figures for the as-spun fibres. The corrected tensile strengths of the HT PBT and ABPBO fibres are higher than the equivalent as-spun fibres except for the HT PBO fibre. The corrected % elongation to break of the heat-treated fibres is lower than for the equivalent as-spun fibres. The increase of Young's modulus after heat-treatment is accompanied by an improvement in structural order as shown earlier in section 3-1-2. It seems that the improvement of the structural order due to heat-treatment also reduces the elongation to break.

It can also be seen that the corrected modulus of the PBT fibres is higher than that of the PBO fibres which is different as reported(4,8) previously. This may be due to the batch-to-batch variation. It was also observed that some of the PBO and ABPBO fibres have a " figure-of-eight " cross-section, whereas in the calculation of the stresses and modulus, the fibres were assumed to have circular cross-sections. It should be noted that the results of modulus and stress measurements depend strongly on the diameter used. If the

Materials	Corrected modulus (GPa)	Corrected tensile strength (GPa)	Corrected elongation to break (%)	Approximate yield strain (%)
AS PBT	194.8 ± 11.5	2.09 ± .17	1.99 ± .27	0.78 ± .04
HT PBT	266.8 ± 9.6	2.45 ± .43	1.15 ± .18	
AS PBO	143.0 ± 10.7	3.32 ± .45	2.89 ± .25	0.78 ± .09
HT PBO	262.3 ± 20.8	2.85 ± .54	1.50 ± .22	
AS ABPBO	90.7 ± 5.3	2.06 ± .30	4.34 ± .51	1.28 ± .14
HT ABPBO	133.2 ± 11.7	2.21 ± .35	2.01 ± .27	

Table 3.4 Corrected mechanical properties and approximate yield strain for AS and HT PBT, PBO and ABPBO fibres with standard deviation.

diameter of the fibres cannot be obtained accurately, then the results of modulus and stresses will not be very reliable.

3-2 Raman microscopy

3-2-1 Raman spectra

PBT fibres

Raman spectra could be obtained from any position on the AS and HT PBT fibres using relatively low powers of laser radiation 488.0nm line of an laser 5mW Ar/Ion. Typical spectra from undeformed AS and HT PBT fibres are shown in Figures 3.31(a) and (b) respectively. The spectra consist of a few well-defined intense peaks on a strong fluorescent background. The level of the fluorescence increases with heat-treatment due probably to some degradation of the fibres.

It can be seen from Figures 3.31(a) and (b) that three principal bands are found in the Raman spectra of AS and HT PBT fibres between 1100 and 1700 cm^{-1}. These are located at approximately 1175, 1475 and 1600 cm^{-1} with the 1475 cm^{-1} band being the most intense for an excitation wavelength of 488.0nm. It also has the highest strain sensitivity (i.e highest Raman shift per % strain) and a better-defined peak(1) than the others. Hence it was chosen for further study. Detailed changes in the spectra during deformation are described in the next section. The 1475 cm^{-1} band was tentatively assigned to a stretching mode of the heterocyclic rings and the 1600 cm^{-1} band was thought to be due to stretching of the phenyl rings but may also contain contributions from other vibrations(9). The 1175 cm^{-1} band, which has not been reported in PBT solutions or solid PBT pellets(10), may be due to stretching of the C-C link between the aromatic rings, or possibly residual acid(11).

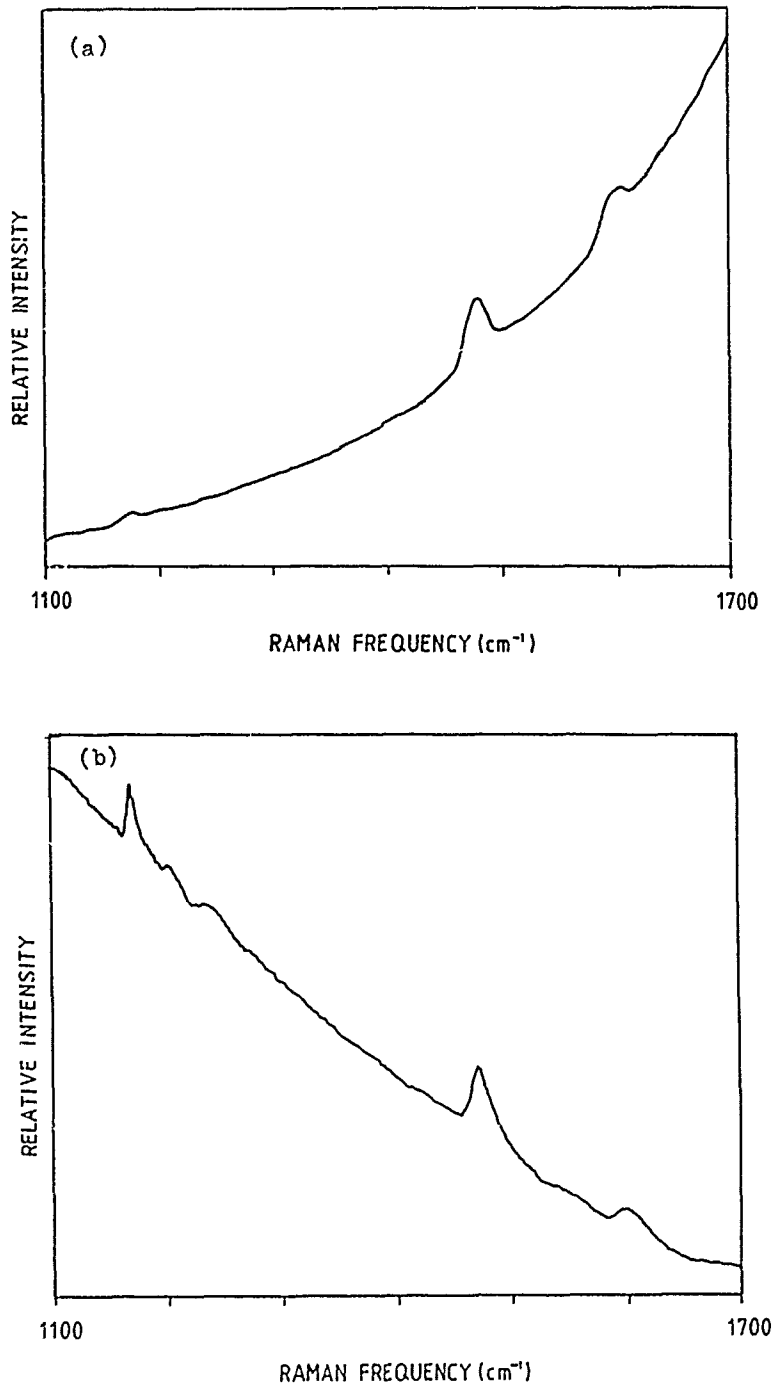

Figure 3.31 Raman spectra in the range of 1100-1700 cm^{-1} for individual PBT fibres obtained at 0% fibre strain. (a) As-spun; (b) heat treated

PBO fibres

Typical spectra from undeformed AS and HT PBO fibres obtained using He/Ne laser (for AS PBO) and Ar/Ion laser (for HT PBO) are shown in Figures 3.32(a) and (b) respectively. It can be seen that there are five principal bands between 1100-1700 cm^{-1} region in AS PBO fibres. These are located approximately 1170 cm^{-1}, 1275 cm^{-1}, 1305 cm^{-1}, 1540 cm^{-1} and 1617 cm^{-1} with 1617 cm^{-1} band being the most intense. The 1275 cm^{-1} band has been used for further study because it has the highest strain sensitivity and a better defined peak(6) than the others. Detailed changes in the spectra during deformation are described in the next section. It can also be observed that the level of the fluorescence increases with heat-treatment due probably to some degradation of the fibres (similar to HT PBT fibres). In fact there is so much fluorescence for HT PBO fibres that it is difficult to see the bands in Figure 3.32(b). It has not been possible to assign them all to molecular vibrations for PBO fibres due to the lack of Raman studies upon model materials and of theoretical analyses.

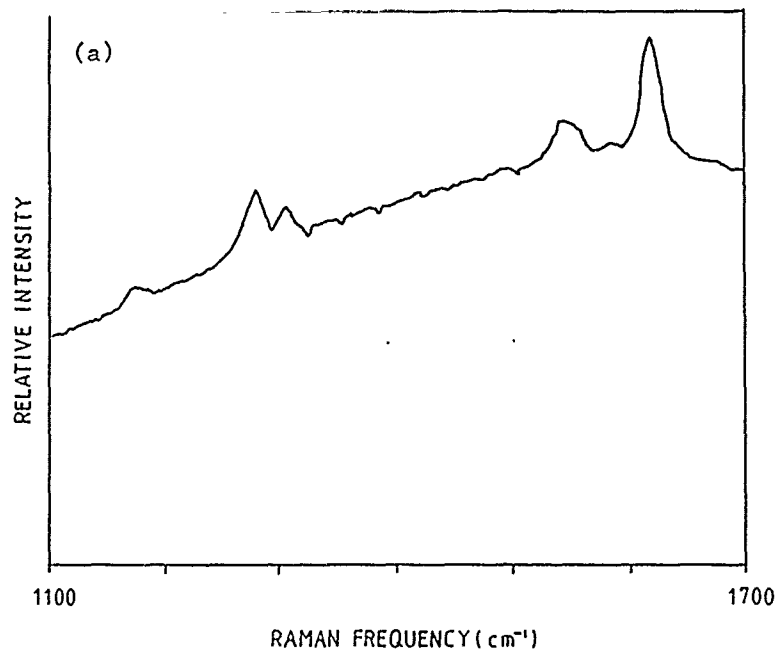

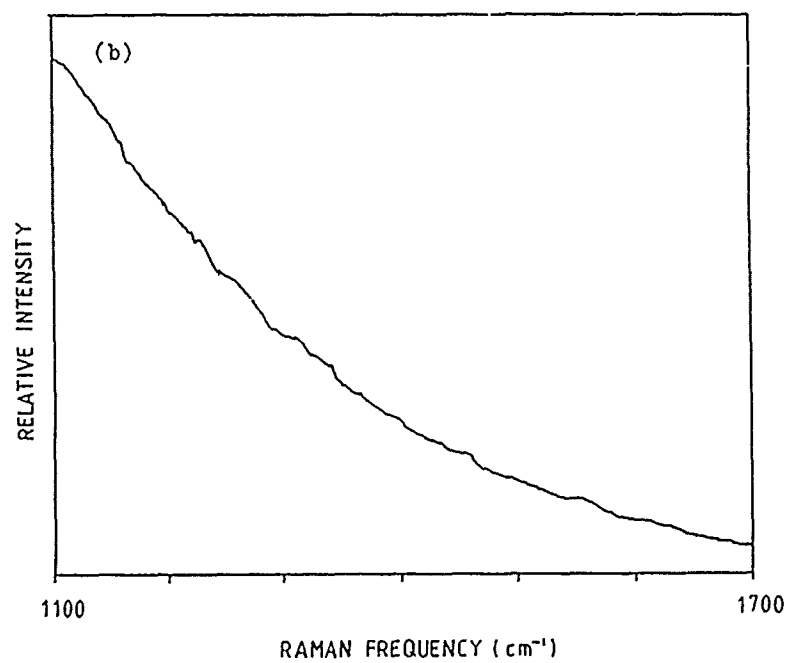

Figure 3.32 Raman spectra in the range of 1100-1700 cm^{-1} for individual PBO fibres obtained at 0% fibre strain. (a) As-spun; (b) heat treated

ABPBO fibres

Typical spectra from undeformed AS and HT ABPBO fibres obtained using He/Ne laser (for AS ABPBO) and Ar/Ion laser (for HT ABPBO) are shown in Figure 3.33(a) and (b) respectively. It can be seen that there are nine principal bands between 1100 and 1700 cm^{-1} in AS ABPBO fibres. They are located approximately 1231 cm^{-1}, 1261 cm^{-1}, 1311 cm^{-1}, 1339 cm^{-1}, 1430 cm^{-1}, 1457 cm^{-1}, 1552 cm^{-1}, 1611 cm^{-1} and 1629 cm^{-1} with the 1552 cm^{-1} band being the most intense. It also has the highest strain sensitivity and a better defined peak than the others. Hence it was chosen for further study. Detailed changes in the spectra during deformation are described in the next section. It can also be observed that the level of the fluorescence increases with heat-treatment due probably to some degradation of the fibres (similar to HT PBT and HT PBO fibres). Again the fluorescence is so strong for the HT ABPBO fibre that it is difficult to see the peaks in the spectrum. It has not been possible to assign the bands to molecular vibrations for ABPBO fibres due to the lack of Raman studies upon model materials and of theoretical analyses.

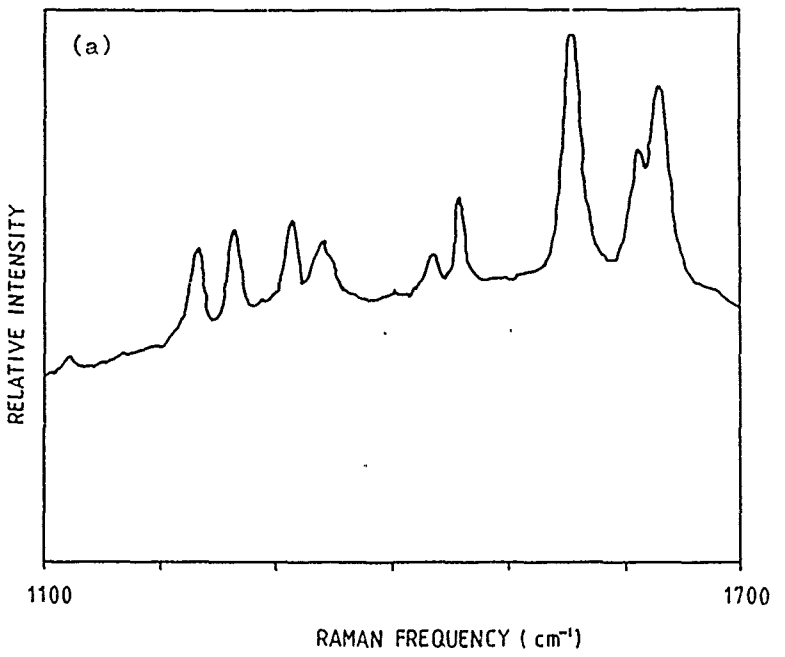

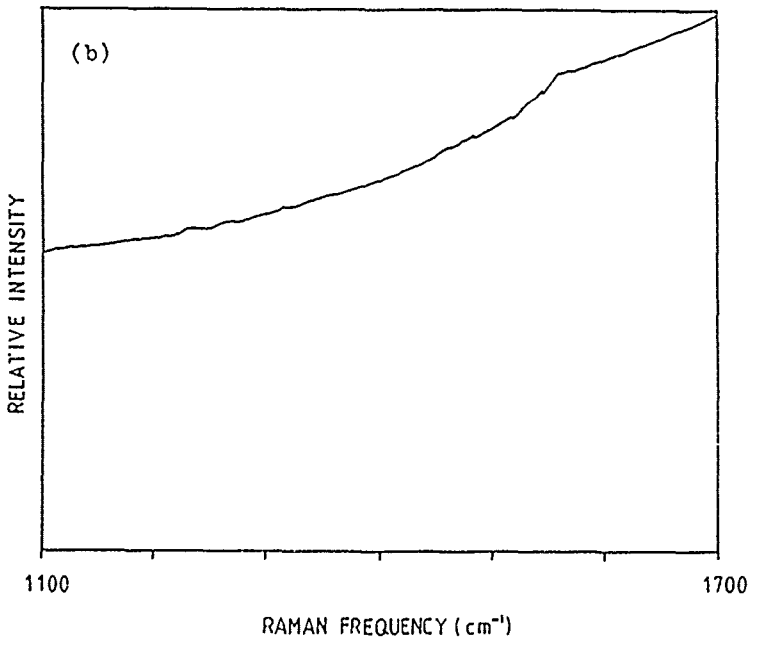

Figure 3.33 Raman spectra in the range of 1100-1700 cm^{-1} for individual ABPBO fibres obtained at 0% fibre strain. (a) As-spun; (b) heat treated

3-2-2 Effect of deformation on the Raman spectra

PBT fibres

Spectra of AS and HT PBT fibres (Figures 3.34(a) and (b) respectively) were obtained using Ar/Ion laser because the spectrum was not as good using He/Ne laser. It has been reported that very well defined spectra can be obtained when using a He/Ne laser for AS and HT PBT fibres(1) with a photomultiplier detector, this may be again due to batch-to-batch variation between fibres and the characteristics of the CCD camera. Figures 3.34(a) and (b) show the spectra for AS and HT PBT fibres of undeformed and deformed to 2% strain in the 1435-1515 cm^{-1} region and it can be seen that there is a significant change in the position of the 1475 cm^{-1} band during deformation. It can also be seen that there is some broadening of the peak during deformation. The shift shows that within the individual fibres the molecules are experiencing different levels of stress. The broadening shows that there is an average level of stress but some molecules appear to be overstressed and others understressed. Similar behaviour has been reported by Wool and coworkers(12-14) from their infra-red studies on polypropylene fibres, although they bear little structural similarity to PBT fibres.

The effect of deformation upon the 1475 cm^{-1} peak for AS and HT PBT fibres can be seen in more detail in Figures 3.35(a) and (b) respectively where peak position is plotted as a function of strain. A few AS PBT fibres were taken out from the bundles at random for testing and found to have a slight different slopes in a Raman frequency against fibre strain plot as shown in Figure 3.35(a). This shows that there appears to be a variation between individual fibres. It can also be seen in Figure 3.35(a) that there is a linear shift in Raman

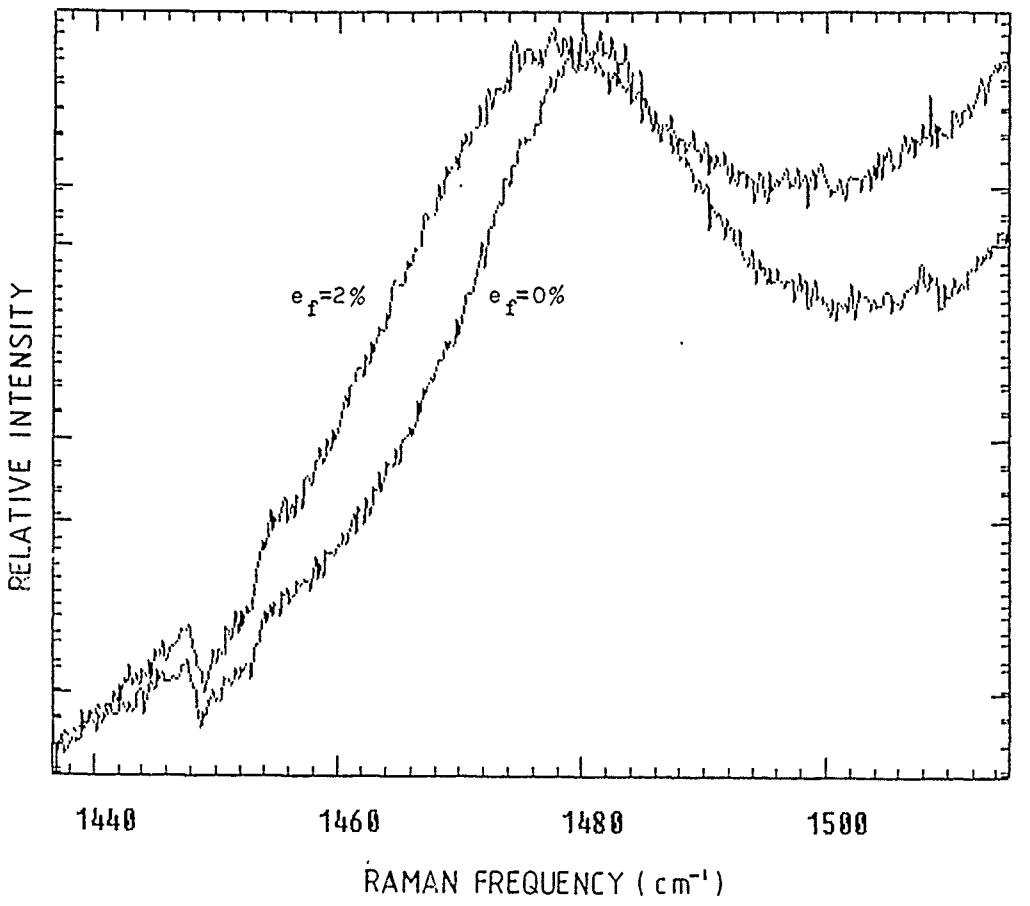

Figure 3.34(a) Raman spectra in the region of the 1475 cm^{-1} band for an AS PBT fibre obtained at fibre strain (e_f) of 0% and 2% showing the peak shift using Ar/Ion laser.

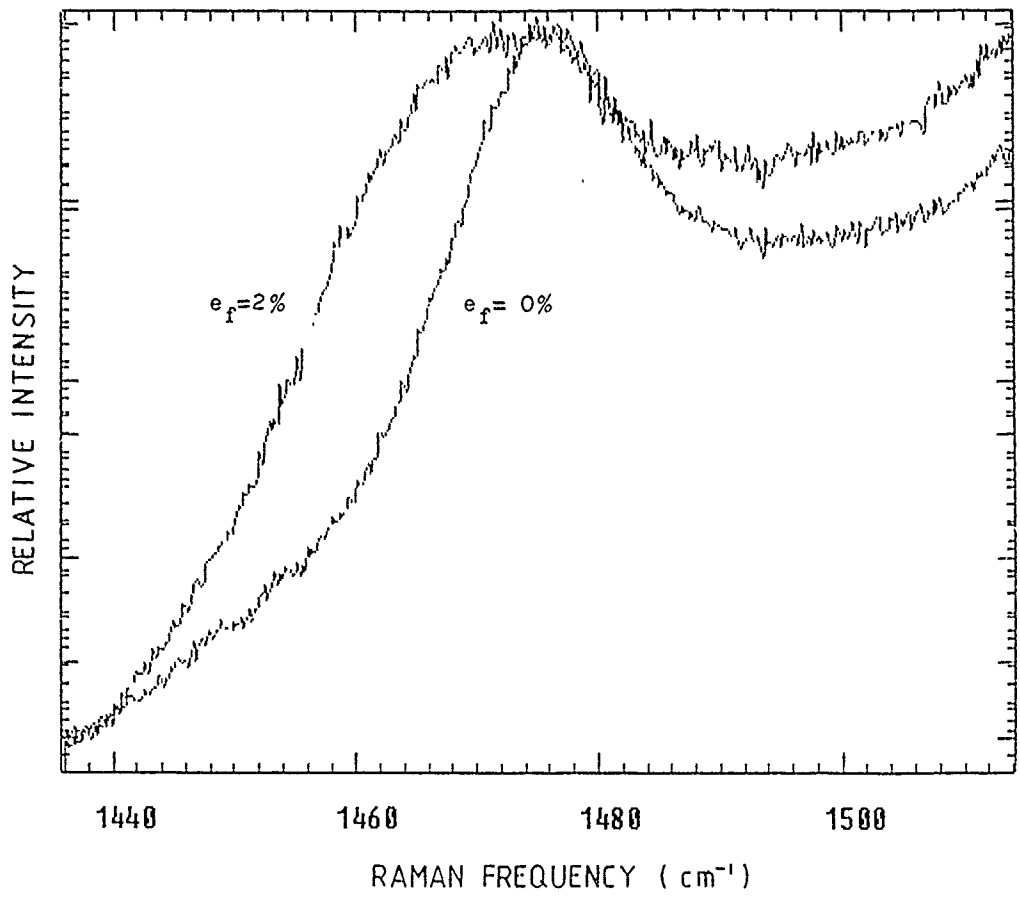

Figure 3.34(b) Raman spectra in the region of the 1475 cm^{-1} band for a HT PBT fibre obtained at fibre strain (e_f) of 0% and 2% showing the peak shift using Ar/Ion laser.

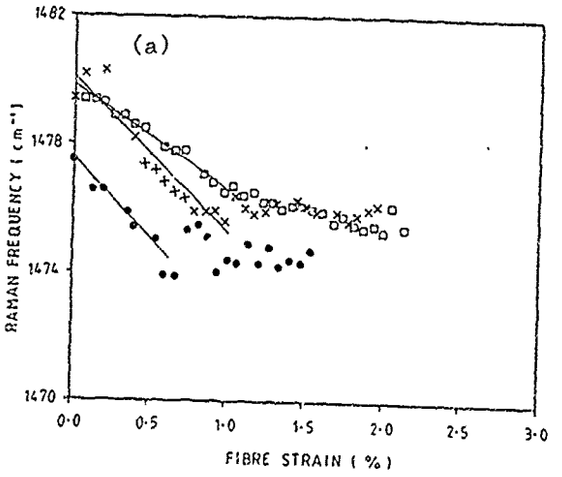

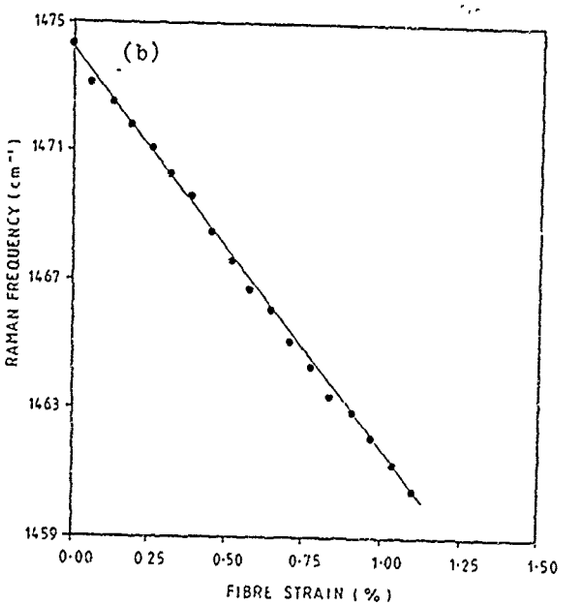

Figure 3.35 Variation of the position of the 1475 cm^{-1} peak with fibre strain for PBT fibres. (a) As-spun; (b) heat treated

frequency up to a strain of an average of about 0.9% and then there is no further shift. It is highly likely that the discontinuity is due to yielding in the AS PBT fibres since the stress and strain curves of the fibres show an yield point of about 0.8% (Table 3.4), although differet strain rates were used for the two types of test. It was shown in the mechanical testing that the deformation of the heat-treated higher modulus PBT fibres is more elastic than the as-spun ones since they do not undergo yield. This is confirmed in Figure 3.35(b) where there is a linear decrease in frequency of the peak with increasing fibre strain up to fracture. The unstrained peak position, Raman shift factor (i.e slope) and the intercept for the plot of Raman frequency against fibre strain is shown in Table 3.5. An average Raman shift factor of -4.51 cm^{-1}/% strain for AS PBT fibres and 12.50 cm^{-1}/% strain for HT PBT fibres can be seen in Table 3.5. This is much lower for AS PBT fibres compared to previous report(1) (i.e-8.3 cm^{-1}/% strain) but is about the same for HT PBT fibres. The difference between the AS PBT fibres could be due to the variation in the method of manufacture. The yield strain and strain to failure is shown in Table 3.6 and compare well with the values obtained during mechanical testing.

Figure 3.36 shows the plot of Raman shift factor (i.e slope of the plots in Figures 3.35) against tensile modulus for PBT fibres. It can be seen that the rate of Raman shift is higher for the heat-treated fibres than the as-spun ones which has also been reported(1) previously. The different values of modulus due to a variety of heat-treatments reflect different degrees of molecular alignment in such fibres. The HT PBT fibres with better aligned molecules (shown in the X-ray diffraction pattern in section 3-1-2) have the highest levels of modulus because more stress is being taken directly by the covalent

Materials	Peak position (cm^{-1})	$\bar{\nu}$ (cm^{-1}/%)	Average $\bar{\nu}$ (cm^{-1}/%)	Intercept (cm^{-1})	Average intercept (cm^{-1})
AS PBT	1475	-3.23	-4.51±.91	1479.8	1479.1±1.2
		-4.99		1480.1	
		-5.31		1477.5	
HT PBT		-12.50	-12.50	1474.2	1474.2
AS PBO	1275	-5.26	-5.08±.61	1278.6	1278.1±0.5
		-4.78		1277.4	
		-4.25		1277.8	
		-5.00		1278.6	
		-6.09		1278.2	
HT PBO		-8.75	-8.75	1276.1	1276.1
AS ABPBO	1552	-3.74	-3.92±.24	1554.1	1554.2±0.5
		-3.89		1555.0	
		-3.72		1554.2	
		-4.31		1553.6	
HT ABPBO		-5.92	-5.92	1557.8	1557.8

Table 3.5 Peak position, Raman shift factor (i.e slope, $\bar{\nu}$) and intercept for the plot of Raman frequency against fibre strain of AS and HT PBT, PBO and ABPBO fibres with standard deviations.

Materials	Yield strain (%)	Average yield strain (%)	Strain to failure (%)	Average strain to failure (%)
AS PBT	0.97	0.86 ± .18	2.13	1.90 ± .26
	1.00		2.04	
	0.60		1.54	
HT PBT			1.36	1.36
AS PBO	1.07	0.81 ± .22	4.00	3.41 ± .47
	1.08		2.80	
	0.72		3.14	
	0.66		3.91	
	0.53		3.20	
HT PBO			1.22	1.22
AS ABPBO	1.34	1.14 ± .19	3.66	3.98 ± .43
	1.32		4.61	
	0.94		4.40	
	0.97		3.64	
HT ABPBO			1.74	1.74

Table 3.6 Yield strain and strain to failure with standard deviation of AS and HT PBT, PBO and ABPBO fibres.

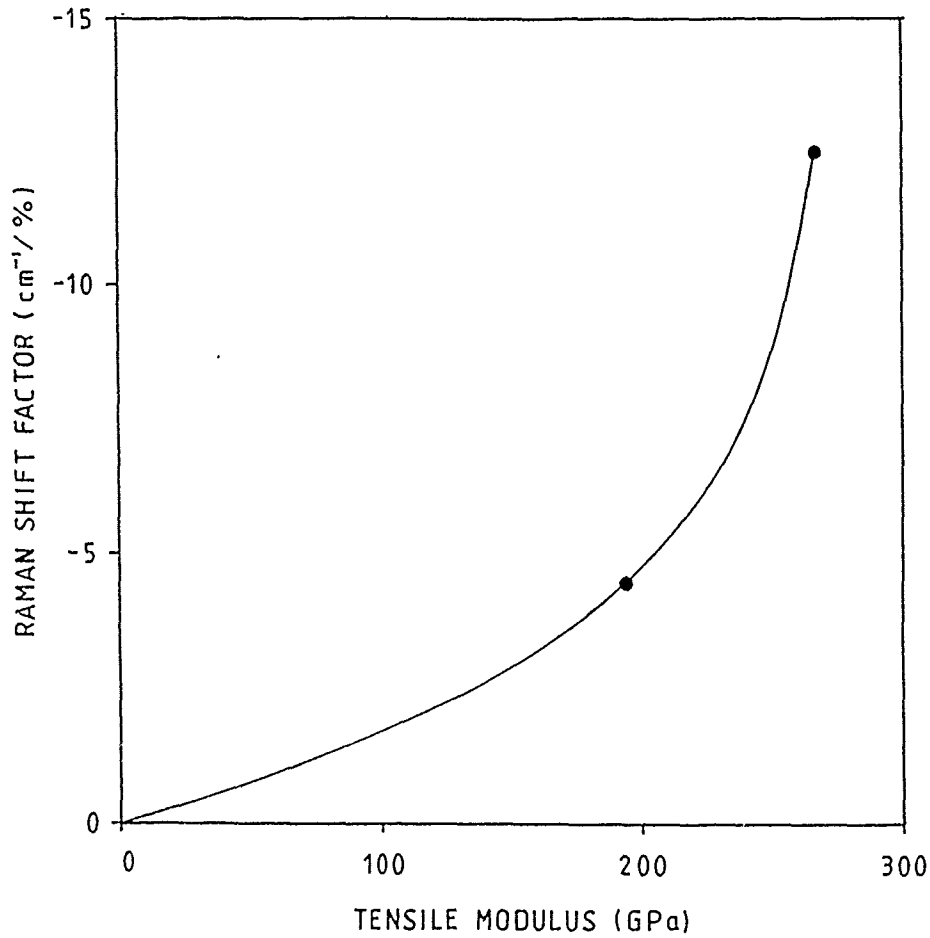

Figure 3.36 Raman shift factor as a function of the tensile modulus for PBT fibres.

bonds in the molecular backbone. This is then reflected in the magnitude of the strain induced frequency shifts that would be expected. Hence, when the technique is being used to study the deformation of individual fibres or their behaviour in composites, it will be more sensitive and accurate for the higher modulus fibres.

PBO fibres

Figures 3.37(a) and (b) show the spectra for AS and HT PBO fibres, undeformed and deformed state of 2% strain in the 1255-1295 cm^{-1} and 1240-1320 cm^{-1} regions respectively. It can be seen that there is a significant change in the 1275 cm^{-1} band. Spectra of HT PBO fibres were obtained using an Ar/Ion laser because no good spectra could be obtained using He/Ne laser. It can also be seen that there is some broadening of the peak during deformation (similar to PBT fibres).

The effect of deformation upon the 1275 cm^{-1} peak for AS and HT PBO fibres can be seen in more detail in Figures 3.38(a) and (b) respectively. It was found that there is a slight different slopes in the plots of Raman peak frequency against fibre strain for a few fibres tested at random and this shows that there is a variation between each individual fibre (similar to AS PBT fibres). It can also be seen in Figure 3.38(a) that there is a linear shift in frequency up to a strain of an average of about 0.8% and then there is a change in slope. Again it is highly likely that the discontinuity is due to yielding in the AS PBO fibres since the stress and strain curves of the fibre also show a yield point of about 0.8% (Table 3.4). It was shown in the mechanical test that the deformation of heat-treated higher modulus fibres are more elastic than the as-spun ones since they do not undergo yield. This is confirmed in Figure 3.38(b) where it can be seen that there is

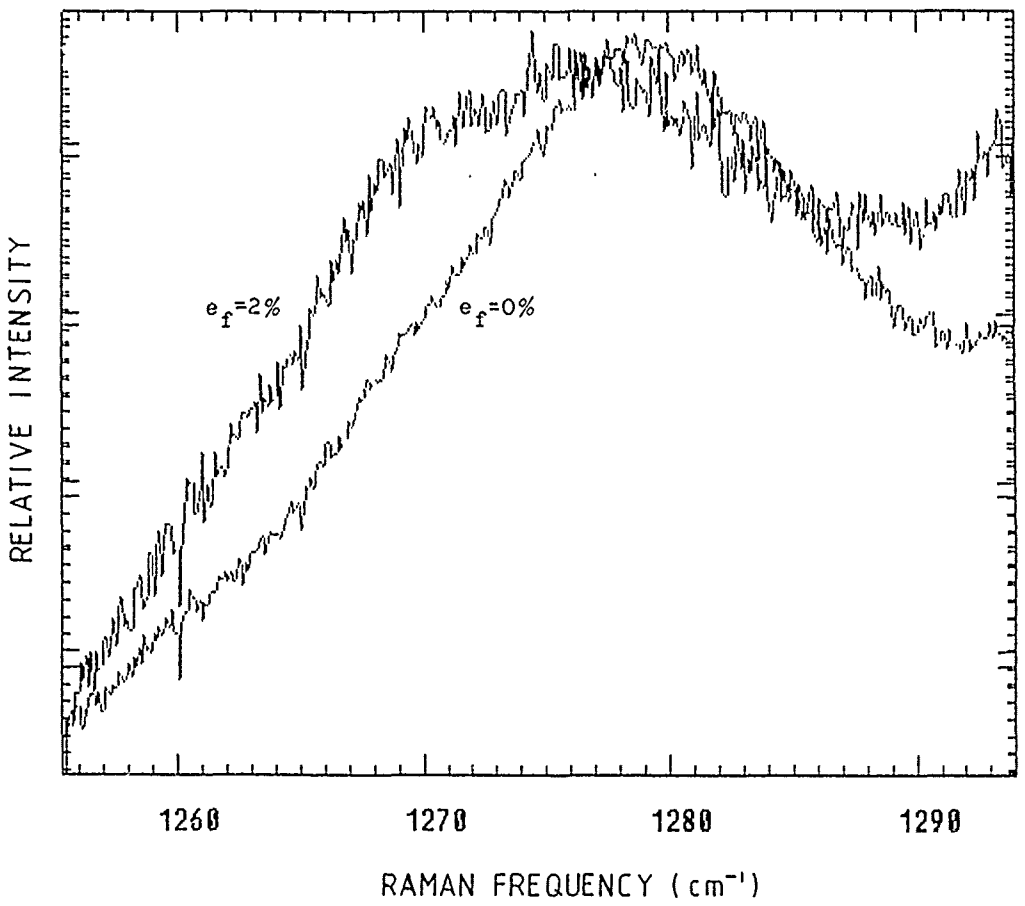

Figure 3.37(a) Raman spectra in the region of the 1275 cm^{-1} band for an AS PBO fibre obtained at fibre strain (e_f) of 0% and 2% showing the peak shift using He/Ne laser.

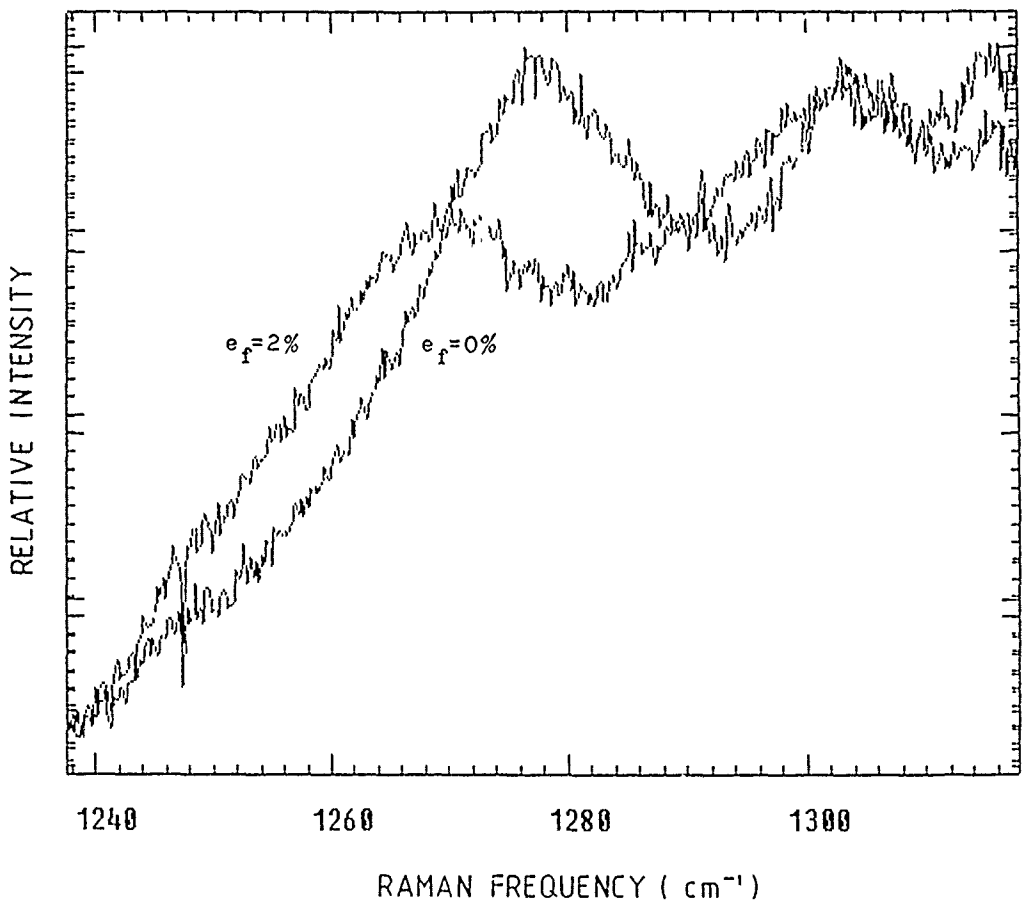

Figure 3.37(b) Raman spectra in the region of the 1275 cm^{-1} band for a HT PBO fibre obtained at fibre strain (ε_f) of 0% and 2% showing the peak shift using Ar/Ion laser.

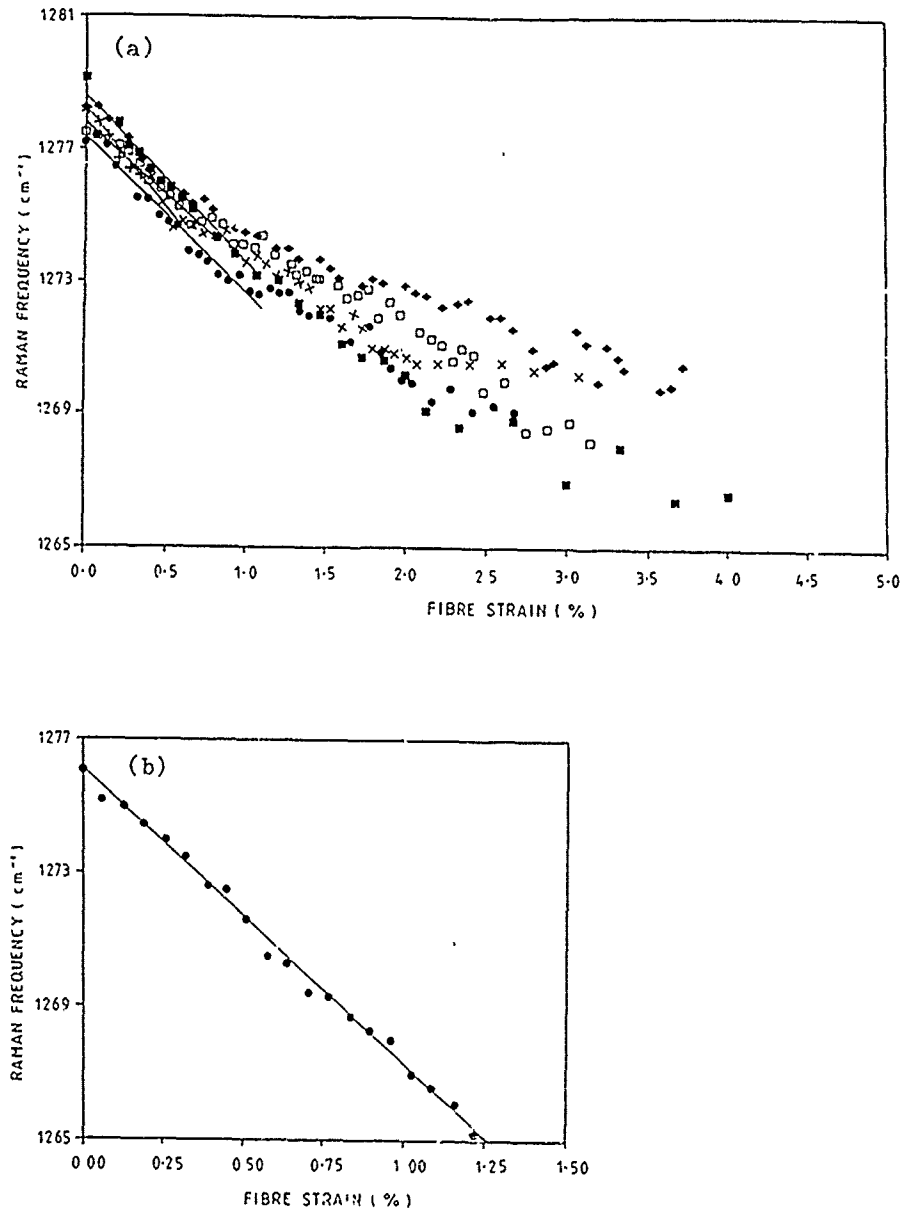

Figure 3.38 Variation of the position of the 1275 cm^{-1} peak with fibre strain for PBO fibres. (a) As-spur; (b) heat treated

a linear decrease in frequency of the peak with increasing fibre strain up to fracture. The peak position, Raman shift factor (i.e slope) and the intercept for the plot of Raman frequency against fibre strain is shown in Table 3.5. The yield strain and strain to failure is shown in Table 3.6.

Figure 3.39 show the plot of Raman shift factor against modulus for PBO fibres. It can be seen that the rate of shift is higher for HT PBO fibres than AS PBO fibres which has also been reported(6) previously (again similar to PBT fibres.

ABPBO fibres

Figures 3.40(a) and (b) show the spectra in the region of 1535-1570 cm^{-1} and 1515-1590 cm^{-1} for AS and HT ABPBO in the undeformed and deformed state and it can be seen that there is a significant change in the position of the 1552 cm^{-1} band with deformation. Spectra of HT ABPBO fibres were obtained using Ar/Ion because the spectrum obtained by He/Ne laser is not as well defined as spectra obtained by Ar/Ion laser. It can also be seen that there is some broadening of the peak during deformation (similar to PBT and PBO fibres).

The effect of deformation upon the 1552 cm^{-1} peak for AS and HT ABPBO fibres can be seen in more detail in Figures 3.41(a) and (b, respectively. A few AS ABPBO fibres were taken out from the bundles at random for testing and found to have a slight different slopes in frequency against fibre strain plot as shown in Figure 3.41(a) (similar to AS PBT and AS PBO fibres). This shows that there is a slight variation between individual fibres. It can also be seen in Figure 3.41(a) that there is a linear shift in frequency up to a strain of an average of about 1.1% and then there is no further shift. It is highly

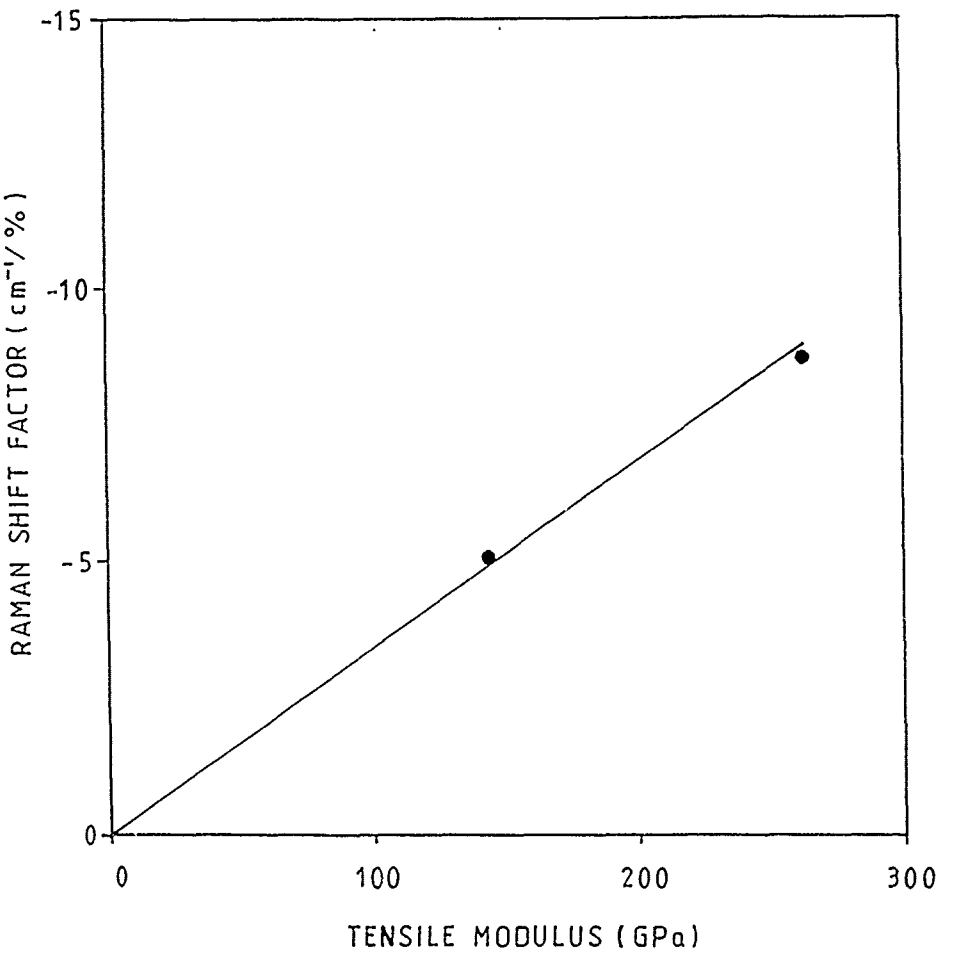

Figure 3.39 Raman shift factor as a function of the tensile modulus for PBO fibres.

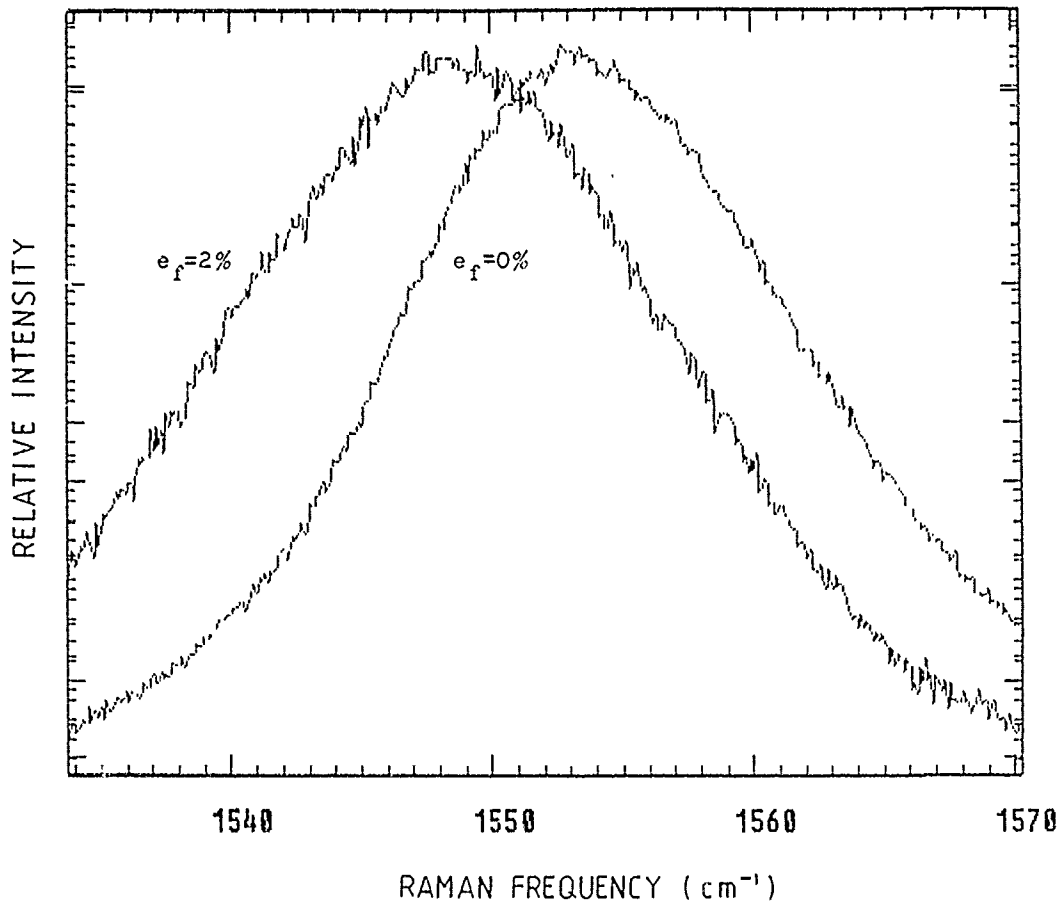

Figure 3.40(a) Raman spectra in the region of the 1552 cm^{-1} band for an AS ABPBO fibre obtained at fibre strain (e_f) of 0% and 2% showing the peak shift using He/Ne laser.

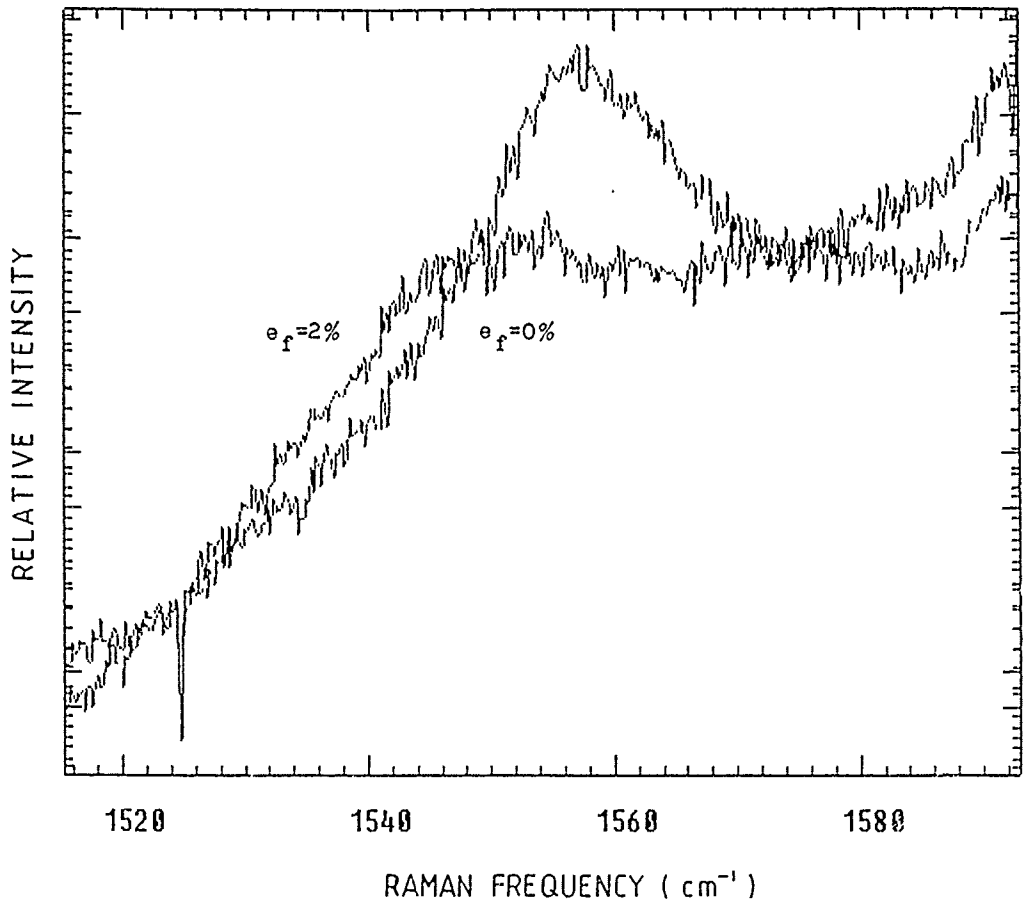

Figure 3.40(b) Raman spectra in the region of the 1552 cm^{-1} band for a HT ABPBO fibre obtained at fibre strain (e_f) of 0% and 2% showing the peak shift using Ar/Ion laser.

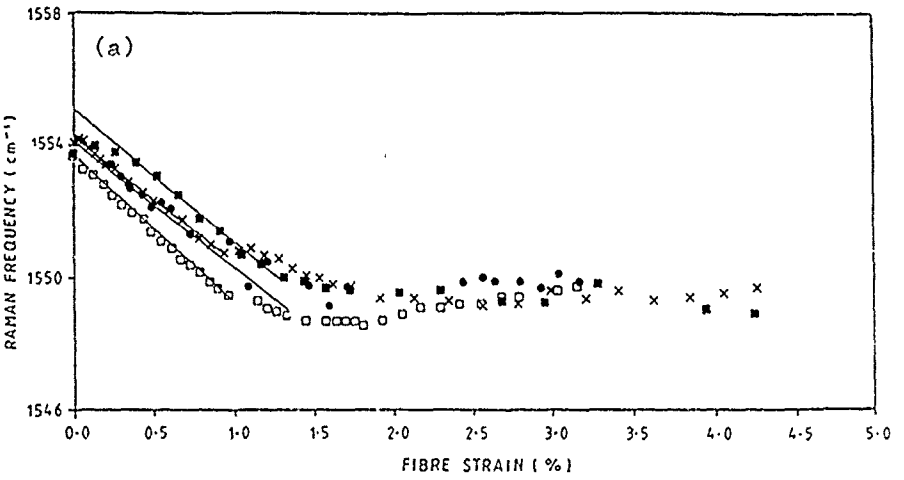

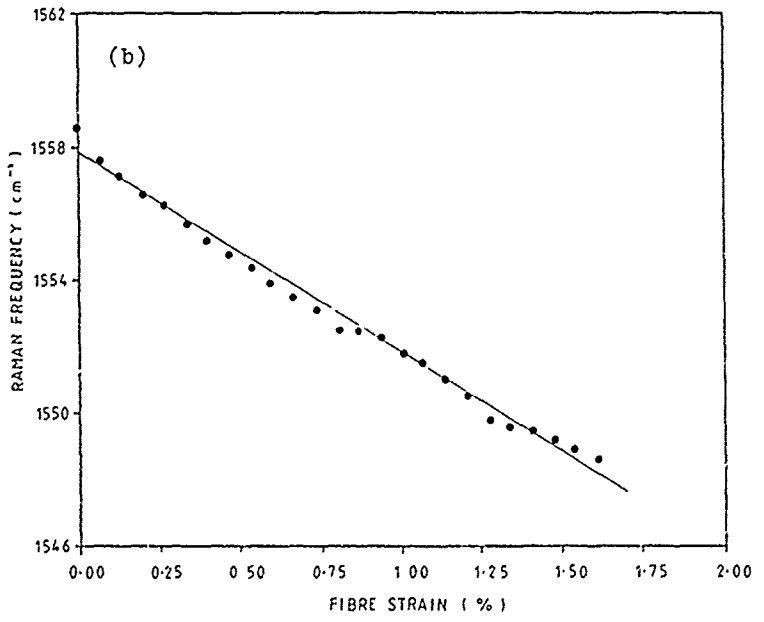

Figure 3.41 Variation of the position of the 1552 cm^{-1} peak with fibre strain for ABPBO fibres. (a) As-spun (b) heat treated

likely that the discontinuity is due to yielding in the AS ABPBO fibre since the stress and strain curves of the fibre show an yield point of about 1.3% (Table 3.4). It was shown in the mechanical testing that the deformation of the heat-treated higher modulus ABPBO fibres is more elastic than the AS ABPBO fibres since they do not undergo yield. This is confirmed in Figure 3.41(b) where it can be seen that there is a linear decrease in frequency of the peak with increasing fibre strain up to fracture. The peak position, Raman shift factor (i.e slope) and the intercept for the plot of Raman frequency against fibre strain is shown in Table 3.5. The yield strain and strain to failure of AS and HT ABPBO fibres is shown in Table 3.6.

Figure 3.42 shows the plot of Raman shift factor against modulus for ABPBO fibres. It can be seen that the rate of shift is higher for HT ABPBO fibres than AS ABPBO fibres (similar to PBT and PBO fibres) and consistent with heat treatment improving orientation and structural order.

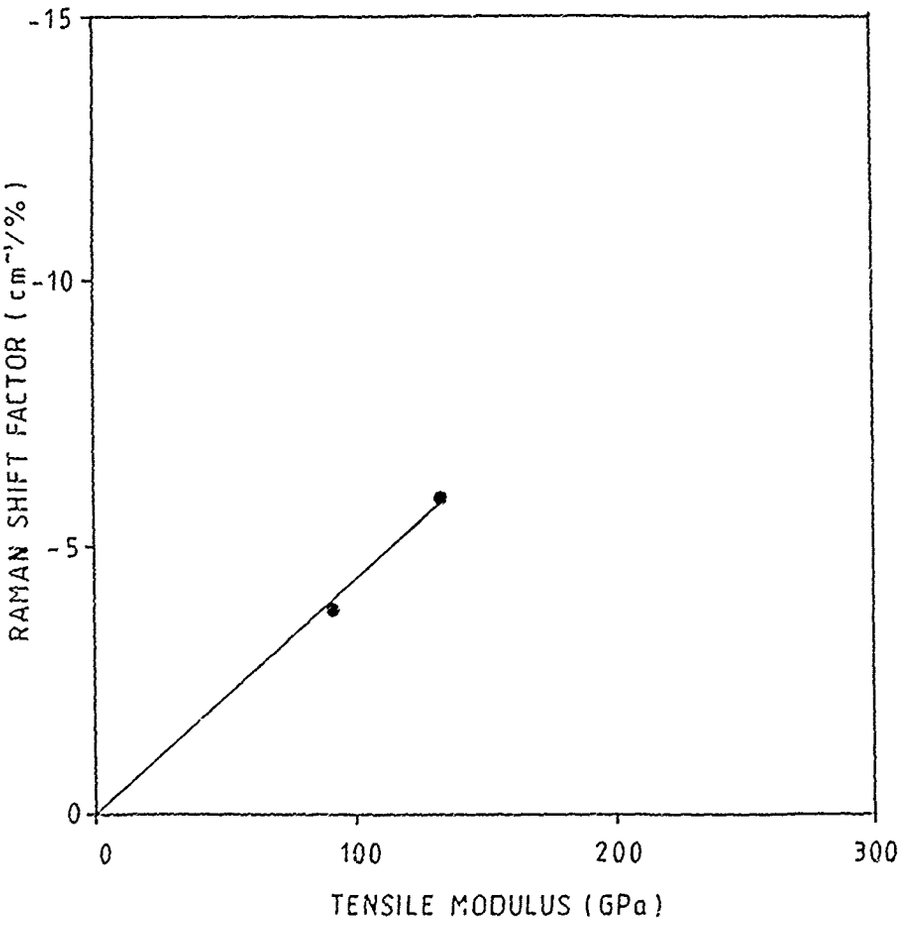

Figure 3.42 Raman shift factor as a function of the tensile modulus for ABPBO fibres.

3-2-3 Extension of the composites

Figures 3.43, 3.44 and 3.45 show the plots of the Raman frequency at the mid-point of the fibre against the composite tensile strain measured by the strain gauge for AS and HT PBT, PBO and ABPBO fibres respectively in the single continuous fibre composite samples. Table 3.7 shows the intercept and slope of Raman frequency against composite tensile strain and intercept and slope of fibre strain against composite tensile strain for that types of fibre. Figures 3.46, 3.47 and 3.48 show the plot of Raman shift factor against tensile modulus for PBT, PBO and ABPBO fibres respectively. As can be seen the slope of Raman frequency against composite tensile strain curves is higher for the heat-treated fibres than the as-spun fibres. It can also be observed that there is a slight different between the slope and intercept of the Raman frequency against composite tensile strain and the calibration curve for some of the fibres section. The slight difference in slope and intercept between them may be due to the better gripping of the fibres in the composite but also the higher noise and fluorescence cause by the epoxy resin. Hence it is suggested that in the future a spatial filter might be necessary to decrease the fluorescent or the camera gain should be reduced so as to increase the exposure time and hence reduce the noise. However, it can be seen that there is an approximately linear increase in the fibre strain calibrated using free-standing fibre data with composite tensile strain as would be expected from simple considerations of composite micromechanics (Figure 3.49). The Raman frequency may be converted into the fibre strain by the calibration curve which was obtained by using the same sample of the fibre as the composite i.e. half of the length of the fibre was used for the calibration test the slope and intercept of

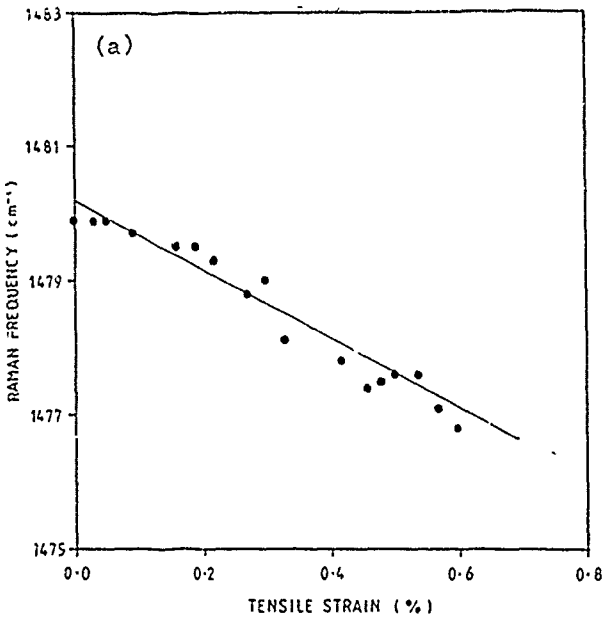

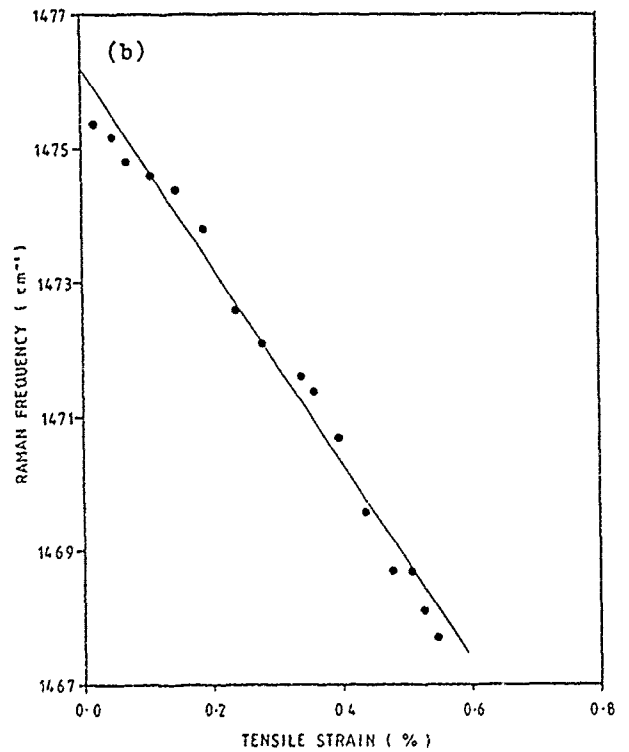

Figure 3.43 Variation of the position of the 1475 cm^{-1} peak with composite tensile strain for a single PBT fibre composite. (a) As-spun; (b) heat treated

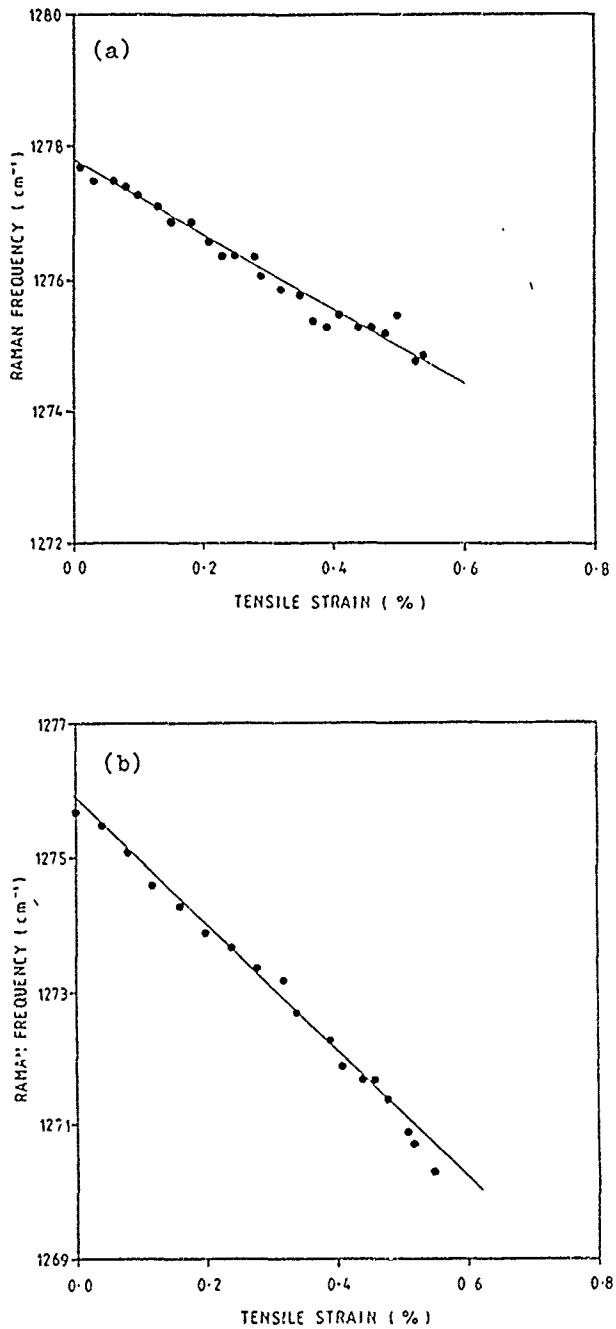

Figure 3.44 Variation of the position of the 1275 cm^{-1} peak with composite tensile strain for a single PBO fibre composite. (a) As-spun; (b) heat treated

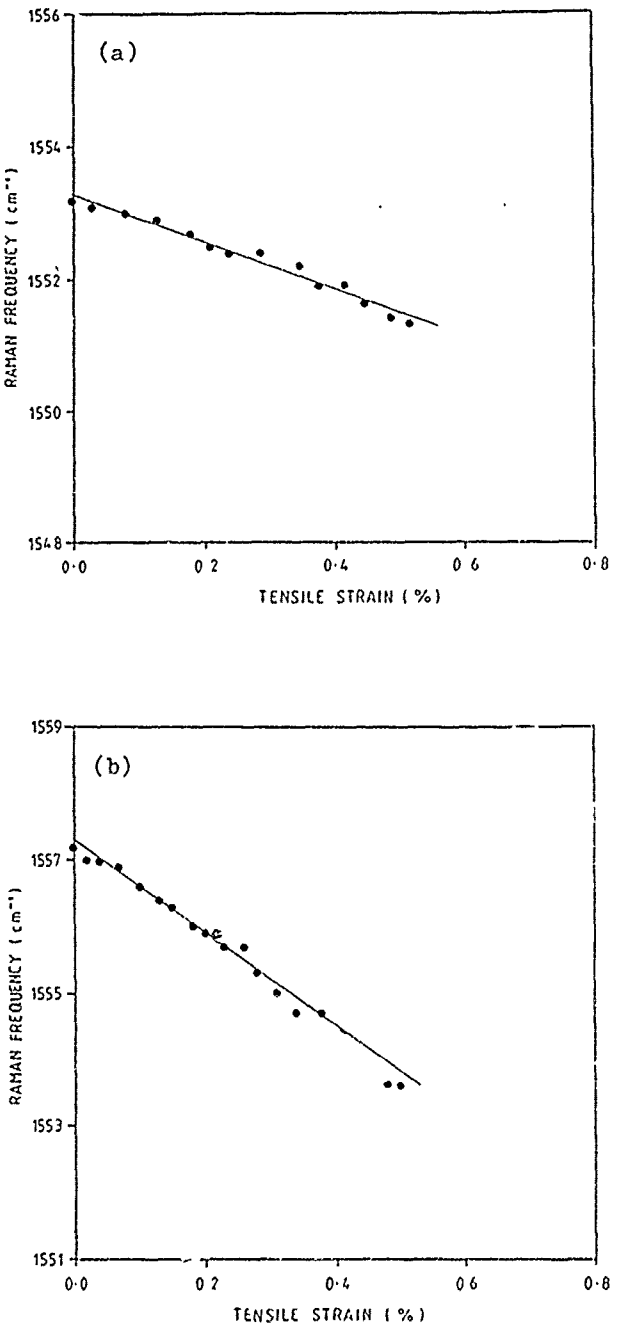

Figure 3.45 Variation of the position of the 1552 cm^{-1} peak with composite tensile strain for a single ARPBO fibre composite. (a) As-spun; (b) heat treated

Types of single fibre composite	Raman frequency vs composite strain		Fibre strain vs composite strain	
	Intercept	Slope	Intercept	Slope
AS PBT	1480.2 (1480.1)	-5.15 (-4.99)	-0.02	1.08
HT PBT	1476.2 (1474.2)	-14.70 (-12.50)	-0.22	1.32
AS PBO	1277.8 (1278.2)	-5.44 (-6.09)	0.07	0.90
HT PBO	1275.9 (1276.1)	-9.74 (-8.75)	0.02	1.08
AS ABPBO	1553.3 (1553.6)	-3.62 (-4.31)	0.07	0.84
HT ABPBO	1557.3 (1557.8)	-7.31 (-5.92)	0.21	0.84

Table 3.7 Intercept and slope of Raman frequency against composite tensile strain and fibre strain against composite tensile strain for AS and HT PBT, PBO and ABPBO fibres (The data in brackets are for free-standing fibres).

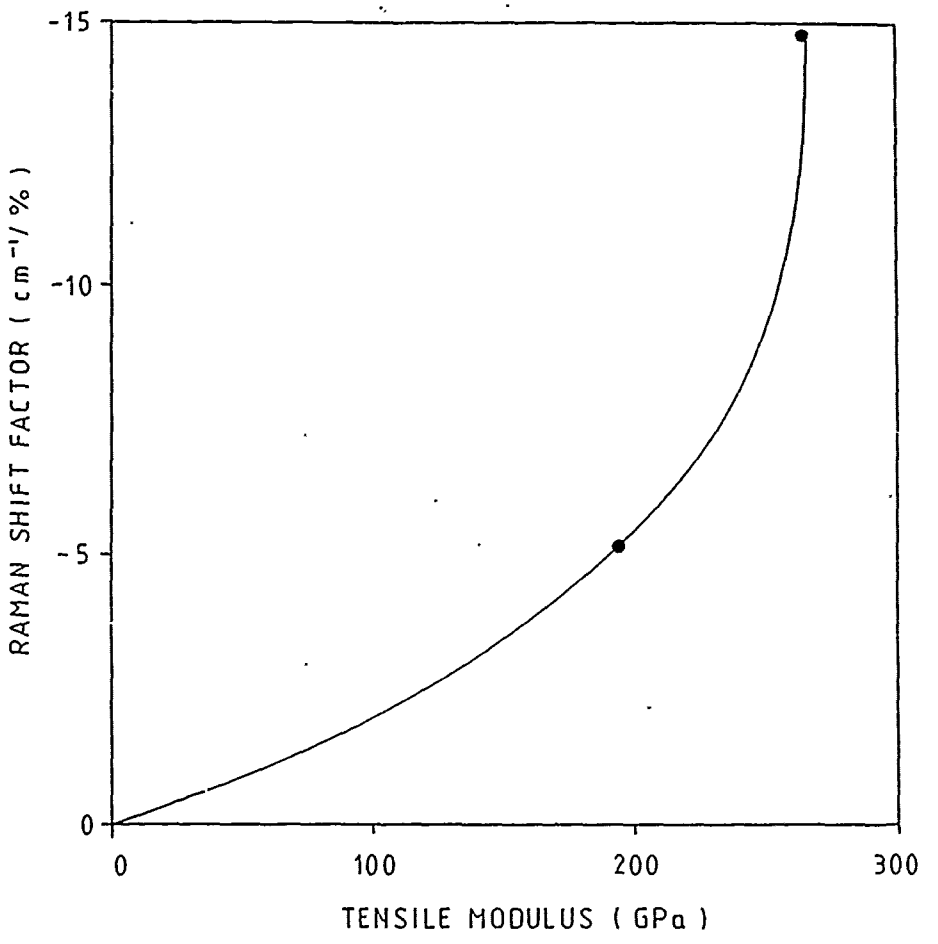

Figure 3.46 Raman shift factor as a function of the tensile modulus for PBT fibres.

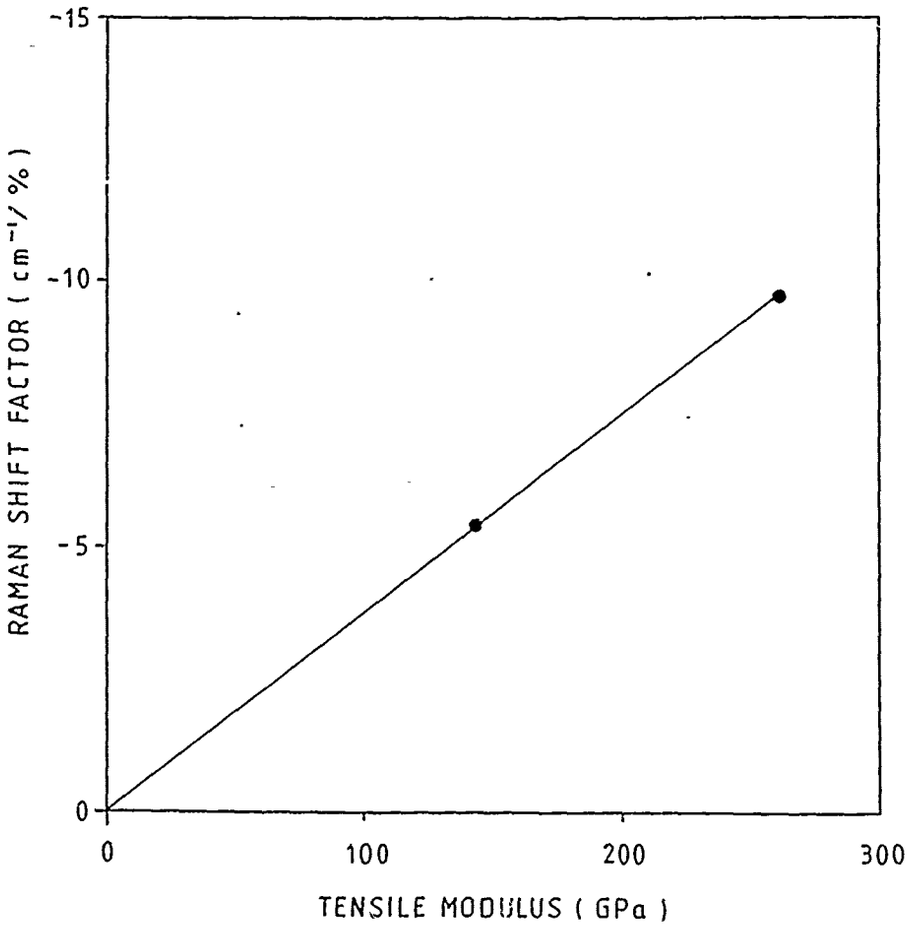

Figure 3.47 Raman shift factor as a function of the tensile modulus for PBO fibres.

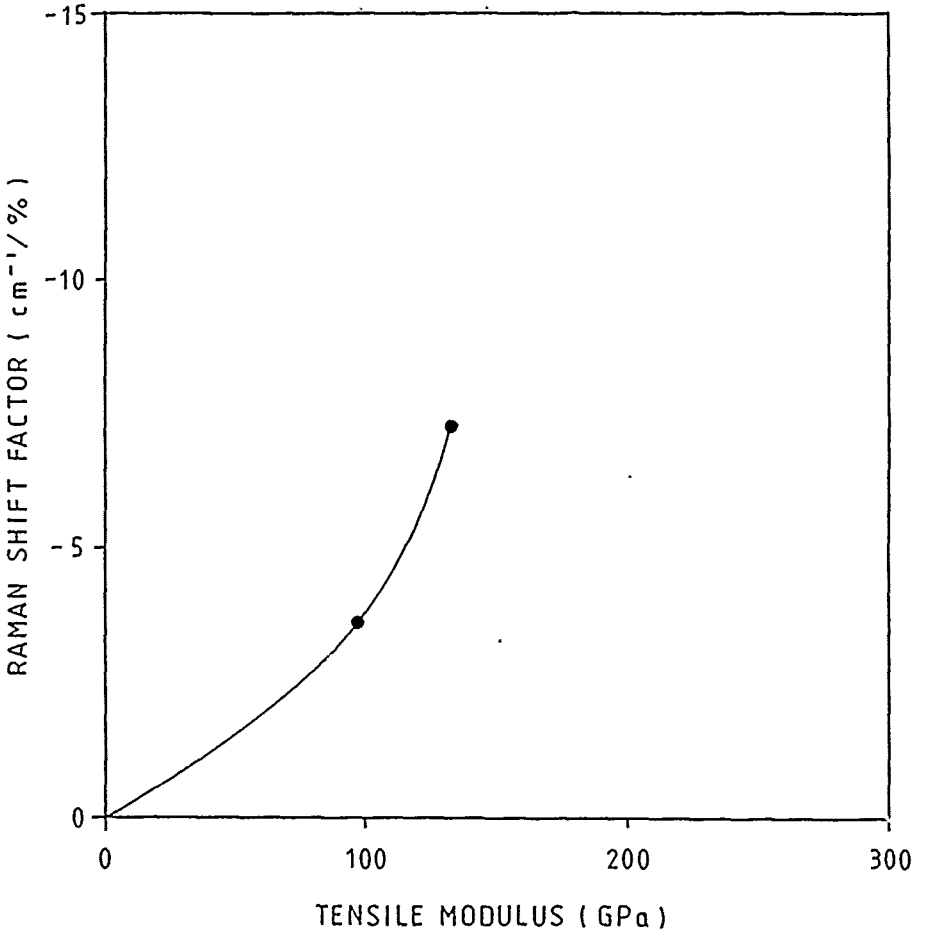

Figure 3.48 Raman shift factor as a function of the tensile modulus for ABPBO fibres.

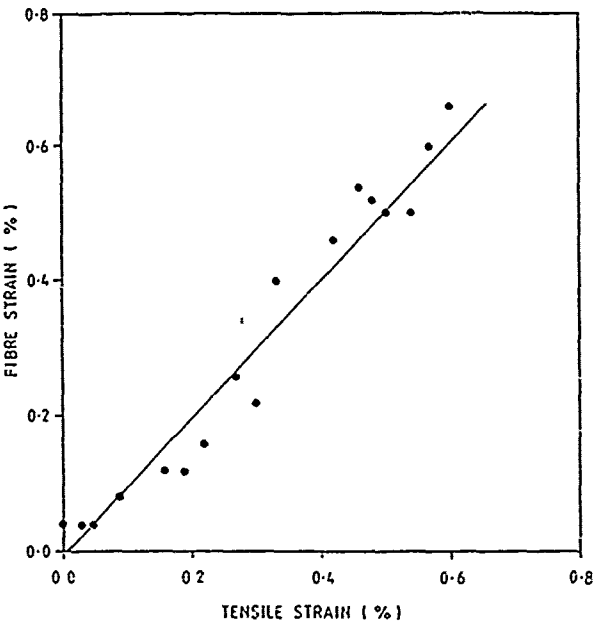

Figure 3.49 Variation of the fibre strain with applied composite tensile strain for a single AS PBT fibre composite.

the calibration curve for a free standing fibre is indicated in brackets in Table 3.7) and the other half was used to prepare the composite so as to minimize the effect due to variation between fibres. It is expected in this sample geometry that the fibre and matrix strain should be equal. This is similar to the behaviour found by Robinson et al(15) for a short polydiacetylene fibre and by Ang(8) for a long continuous HT PBT fibres.

3-2-4 Compression of the composites

PBT single fibre composites

Axial compression of highly-oriented high modulus polymeric fibres results in the formation of so-called kinkbands (17, 18, 19). Figures 3.50(a) and (b) show the plot of Raman frequency against compressive composite strain for AS and HT PBT fibres respectively. It must be noted that for the Raman microscopy technique the laser beam is focused at a small spot on the fibre, i.e it is a localised test method. It can be seen that the Raman frequency increases in the initial stages of compression until compressive failure of the fibre occurs. The frequency then remains approximately constant although there is scatter in the data. It will be shown later in section 3-3 that this region of constant frequency with increase compressive composite strain corresponds to the kinking of the fibre. As the fibres kink, the increase of compressive composite strain is not transferred directly to elastic deformation of the backbone of the molecule which has already been kinked but to the backbone of the molecule where kinkbands have not formed yet. Therefore there is an overall displacement of the composite but no further overall molecular straining and hence no increase in frequency is observed after the fibre has kinked at that particular point. It is therefore suggested that kinkbands are nucleated in a localised area at a certain critical fibre strain and then propagate at nearly constant overall compressive fibre strain. The intercept and initial slope of the plot in Figure 3.50, the ratio of the initial slope of the linear region of the compression curve to tensile curve (R) and the compressive composite

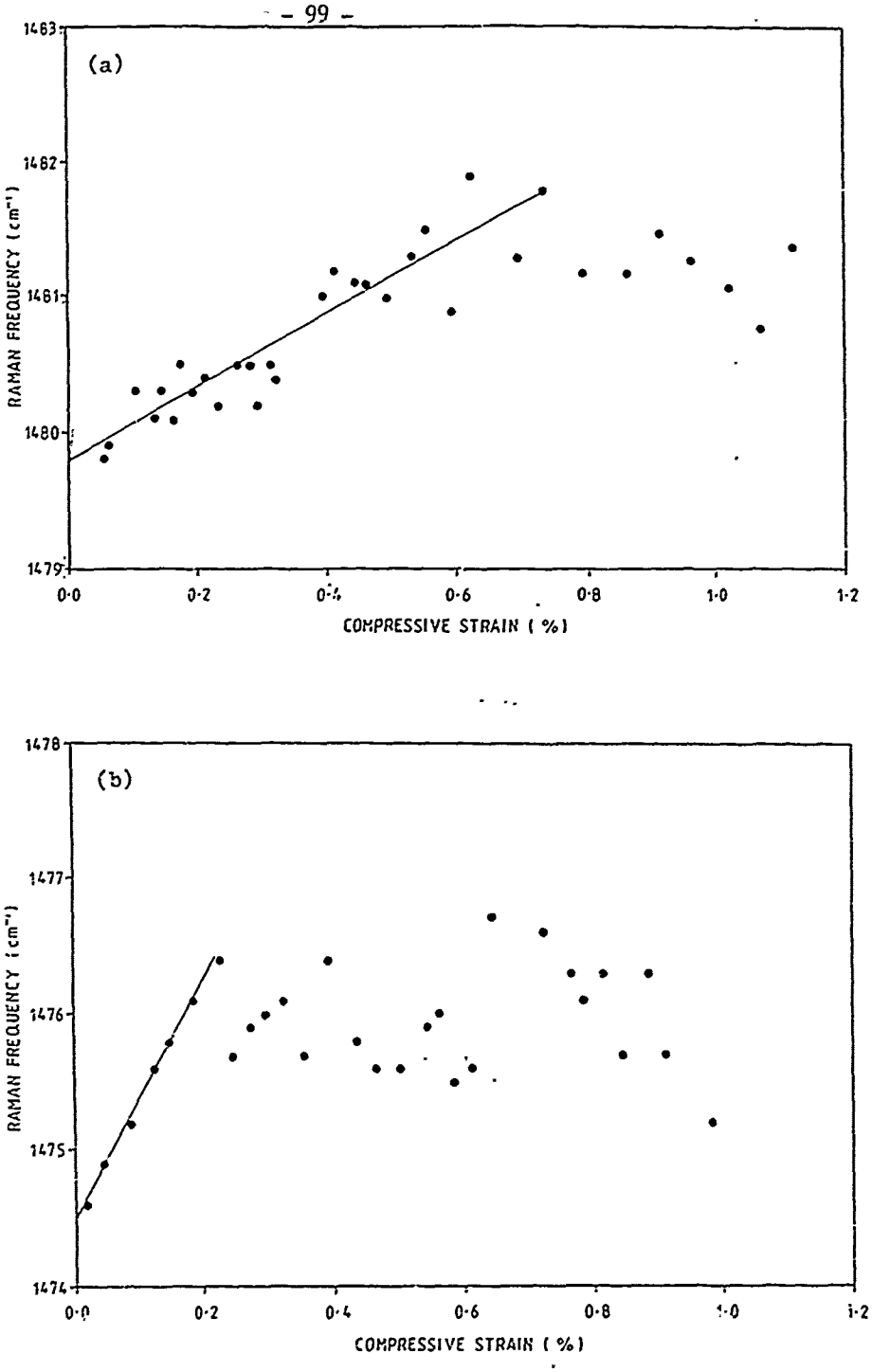

Figure 3.50 Variation of the position 1475 cm^{-1} peak with compressive composite strain for a single PBT fibre composite. (a) As-spun; (b) heat treated

strain at which compressive failure of the fibre occurs (e_{KR}) are all shown in Table 3.8. The slopes and intercepts in brackets are the data obtained from the extension of single fibre composite (see section 3-2-3). The two ends of the " dog bone " shaped composite (which was used in extension earlier) were cut off leaving a small rectangler block. The reason for using the same piece of sample for extension and compression is to minimize the effect due to variation between fibres and hence make comparison more reliable. The epoxy resin used for this study was cured at room temperature to avoid resin shrinkage and subsequent fibre compression. The value of e_{KR} is higher for AS PBT than for HT PBT fibres. It is noticeable that the deformation behaviour in the linear compressive region for the single fibre composites is not the same as that found in tensile tests. It can be seen that the slope of the linear region for the compression tests are lower than for the tensile tests. Reports for PBT fibres suggest a ratio of compressive to tensile modulus of 0.54-0.64 (18) and 0.7-1.0(19) which is in agreement with the results measured. The whole picture of the plot of Raman frequency shift against composite strain for extension and compression of AS and HT single PBT fibre composite can be seen in Figure 51(a) and (b) respectively.

Figure 3.52 shows the plot of Raman frequency against position along fibre scanned at the mid-point of the fibre with an interval of about 20 um at two different levels of applied compressive composite strain. It can be noted that the accuracy of measuring the peak is ± 0.05 cm^{-1}. It can be seen that there is considerable point-to-point variation due to kinkbands, the observed valleys of low strain correspond to the release of applied load through the formation of kinkbands in the fibre as has been found before in aramid/epoxy(20).

Types of single fibre composite	Raman frequency vs composite strain		e_{KR}	R
	Intercept	Slope		
AS PBT	1479.8 (1480.2)	2.70 (-5.15)	-0.73	0.52
HT PBT	1474.5 (1476.2)	8.64 (-14.70)	-0.23	0.59
AS PBO	1277.2 (1277.8)	4.70 (-5.44)	-0.61	0.86
HT PBO	1276.0 (1275.9)	7.46 (-9.74)	-0.17	0.77
AS ABPBO	1553.4 (1553.3)	3.85 (-3.62)	-0.60	1.06
HT ABPBO	1557.3 (1557.3)	6.07 (-7.31)	-0.27	0.83

Table 3.6 Intercept and slope of Raman frequency against compressive composite strain plot, compressive strain at which compressive failure of fibre occurs (e_{KR}) and the ratio of the slope of compression to tensile curve (R) for AS and HT PBT, PBO and ABPBO fibres (The data in brackets are for extension of composite).

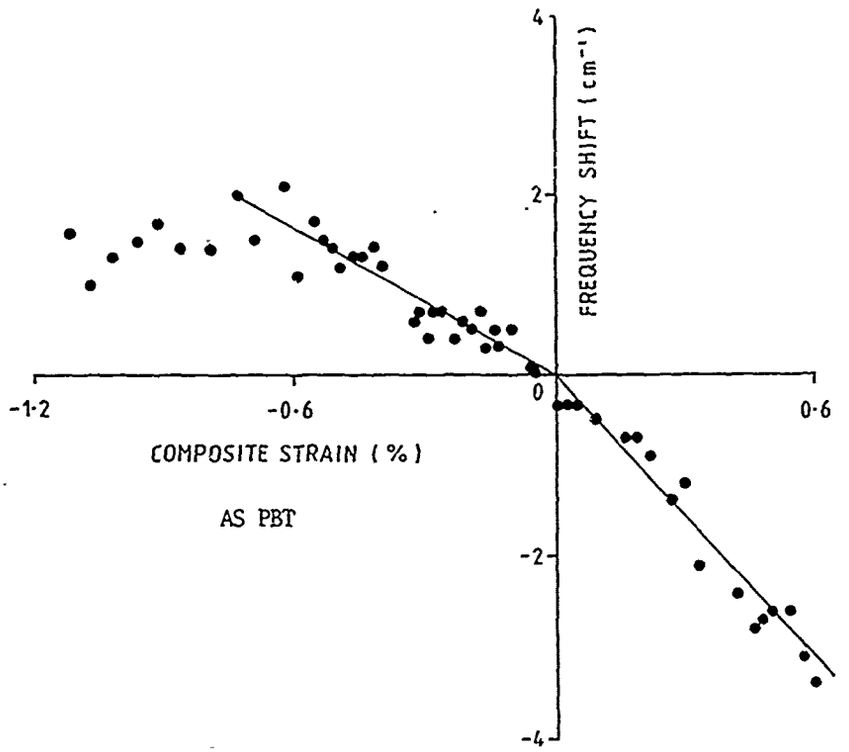

Figure 3.51(a) Raman frequency shift versus composite strain for extension and compression of single AS PBT fibre composite.

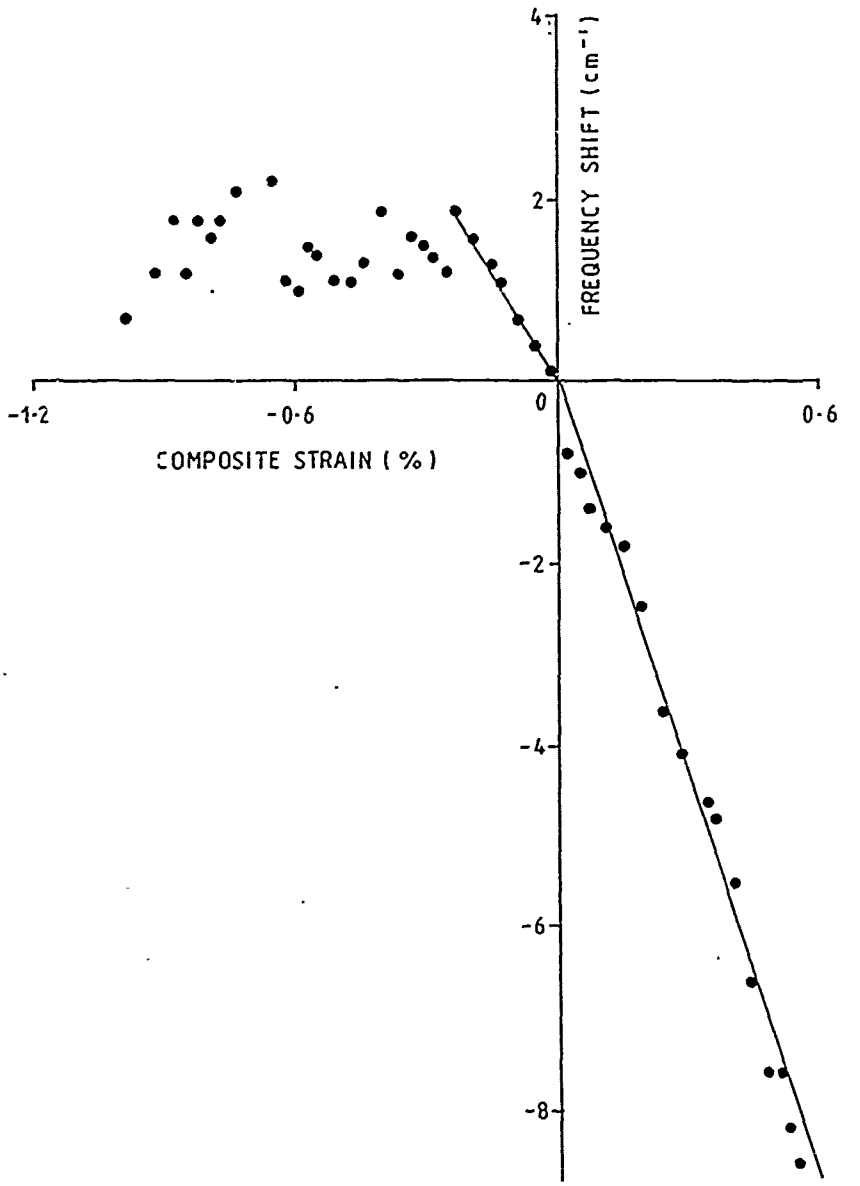

Figure 3.51(b) Raman frequency shift versus composite strain for extension and compression of single HT PBT fibre composite.

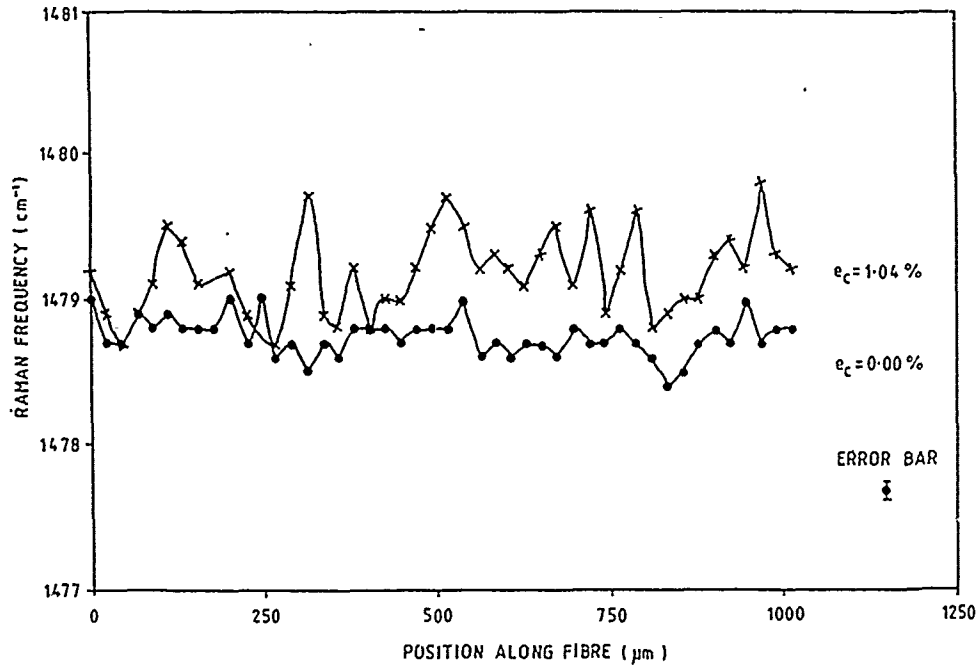

Figure 3.52 Variation of the position 1475 cm^{-1} peak with position along the AS PBT fibre for two different levels of applied compressive composite strain (e_c).

There is more point-to-point variation due to kinkbands at the higher level of compressive composite strain. The variation is less at 0% compressive composite strain and in this case the point-to-point variation may be due to the presence of kinkbands in the as-received fibre. (It was found from optical microscope in section 3-1-1 that there are more kinkbands present in the as-received AS PBT fibres compared to the others). It can be deduced that the uniformity of the strain along the fibre is less for higher compressive composite strains due to the presence of a large number of kinkbands. It should also be noted that the point-to-point variation for two different levels of compressive composite strain is very close due to the fact that the Raman frequency shift factor AS PBT fibres is relatively small. However it can be seen that for a higher level of compressive composite strain, the points are generally at a higher Raman frequency.

PBO single fibre composites

Figures 3.53(a) and (b) show the plot of Raman frequency against compressive composite strain for AS and HT PBO fibres respectively. It can be seen that the Raman frequency increases in the initial stages of compression until compressive failure of the fibre occurs. The frequency then remains approximately constant although there is scatter in the data (similar to PBT fibres). The intercept and initial slope of the above plot, the ratio of the initial slope of the linear region of the compression curve to tensile curve (R) and the compressive strain at which the compressive failure of the fibre occur (e_{kR}) are all shown in Table 3.8. Again the value of e_{kR} is higher for the AS PBO fibres compared to the HT PBO fibres (as for PBT fibres). It is also noticeable that the slope of the plots in the linear compressive region for the PBO single fibre composites is not the same as that found in tensile tests. However the ratio of these for PBO fibres is higher than for PBT fibres. The whole picture for the plot of Raman frequency shift against composite strain for both extension and compression of AS and HT PBO single fibre composites can be seen in Figure 3.54(a) and (b) respectively. The difference in slope for the compressive and tensile regions is apparant.

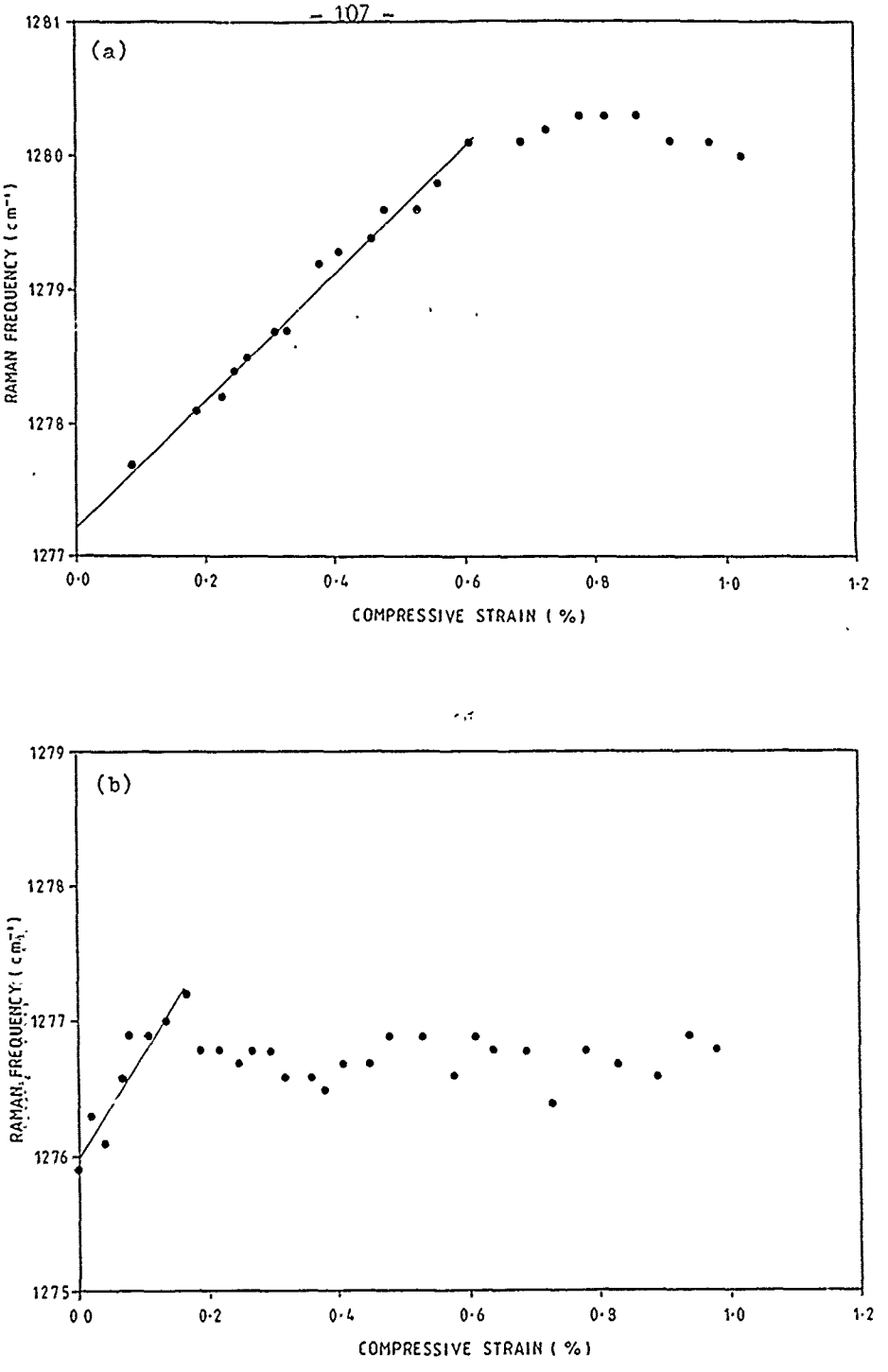

Figure 3.53 Variation of the position 1275 cm^{-1} peak with compressive composite strain for a single PBO fibre composite. (a) As-spun; (b) heat treated

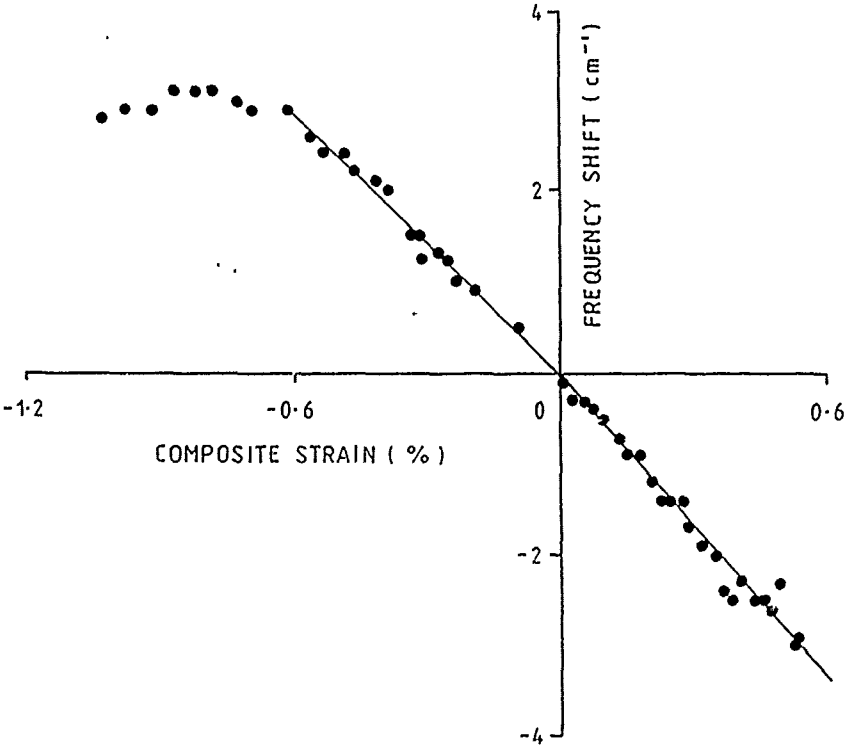

Figure 3.54(a) Raman frequency shift versus composite strain for extension and compression of single AS PBO fibre composite.

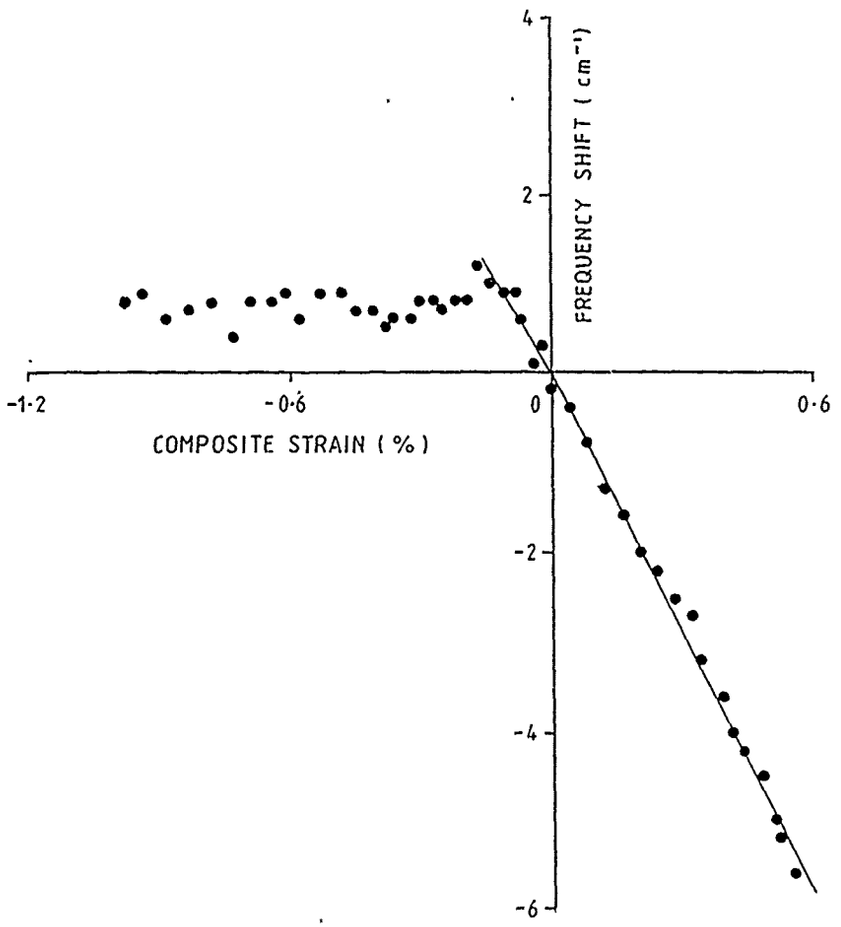

Figure 3.54(b) Raman frequency shift versus composite strain for extension and compression of single HT PBO fibre composite.

ABPBO single fibre composites

Figures 3.55(a) and (b) show the plots of Raman frequency against compressive composite strain for AS and HT ABPBO fibres respectively. The behaviour is similar to PBT and PBO fibres. The intercept and initial slope of the above plots, the ratio of the linear region of the compression curve to tensile curve (R) and the compressive strain at which the compressive failure of the fibre occur ($e_{f,R}$) are all shown in Table 3.8. Again the $e_{f,R}$ for the AS ABPBO fibre is higher than the HT ABPBO fibres (as for PBT and PBO fibres). It is also noticeable that the slope of the linear compressive region for AS ABPBO fibres is about the same as that found in the tensile tests (different from PBT and PBO fibres) but is slightly different for HT ABPBO fibres. The whole picture of the plot of Raman frequency shift against composite strain for extension and compression of AS and HT ABPBO single fibre composite can be seen in Figure 3.56(a) and (b) respectively.

Figure 3.57 shows the plot of Raman frequency against position along fibre scanned at the mid-point of the fibre with an interval of about 20um at two different levels of applied compressive composite strain. It is similar to Figure 3.49(b) for AS PBT fibres. However, although the two plots are on the same scale, the average levels of Raman frequency are quite well separated. This is due to the fact that HT ABPBO fibres have a higher Raman shift factor than AS PBT fibres.

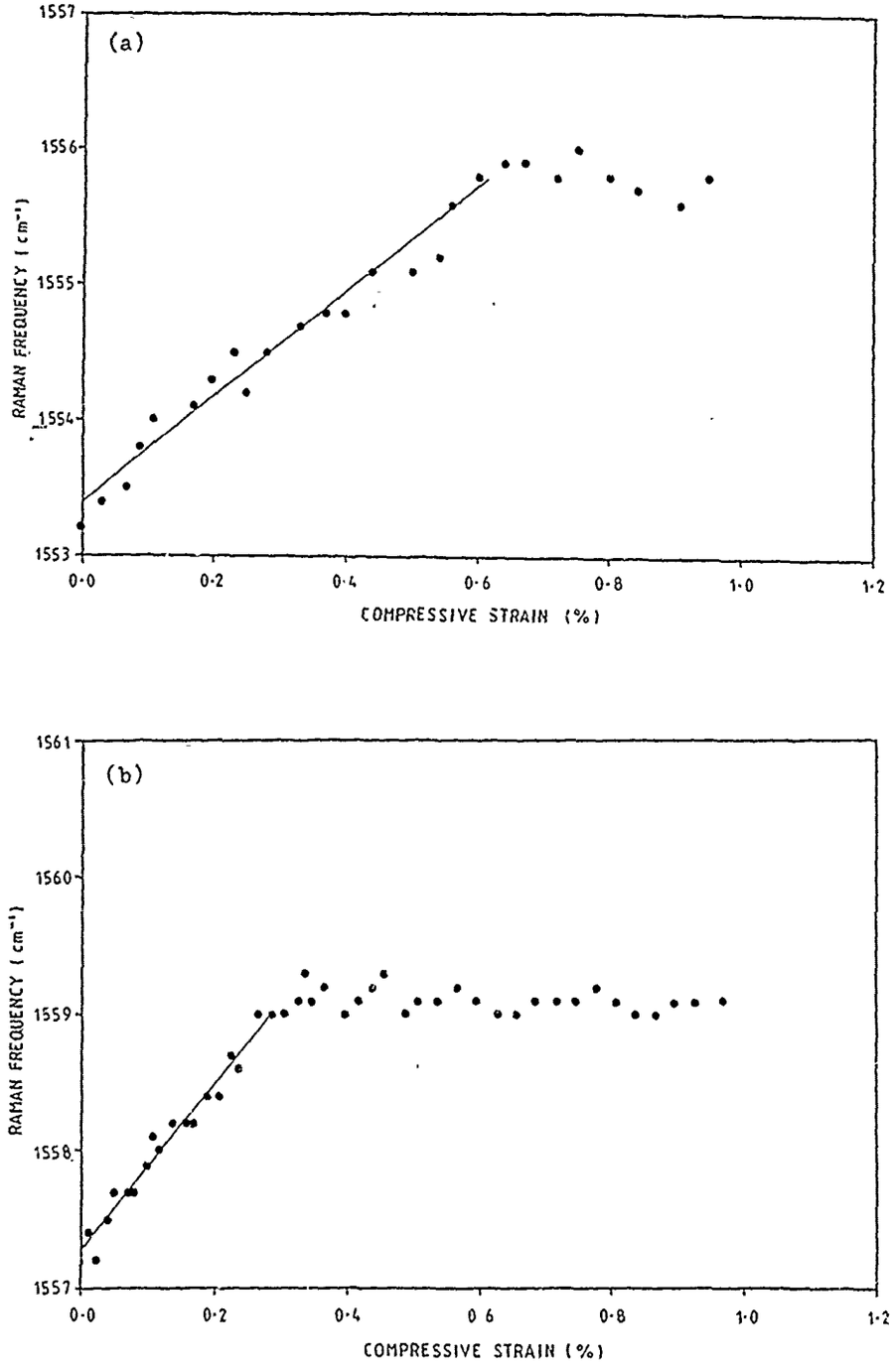

Figure 3.55 Variation of the position 1552 cm^{-1} peak with compressive composite strain for a single ABPBO fibre composite. (a) As-spun; (b) heat treated

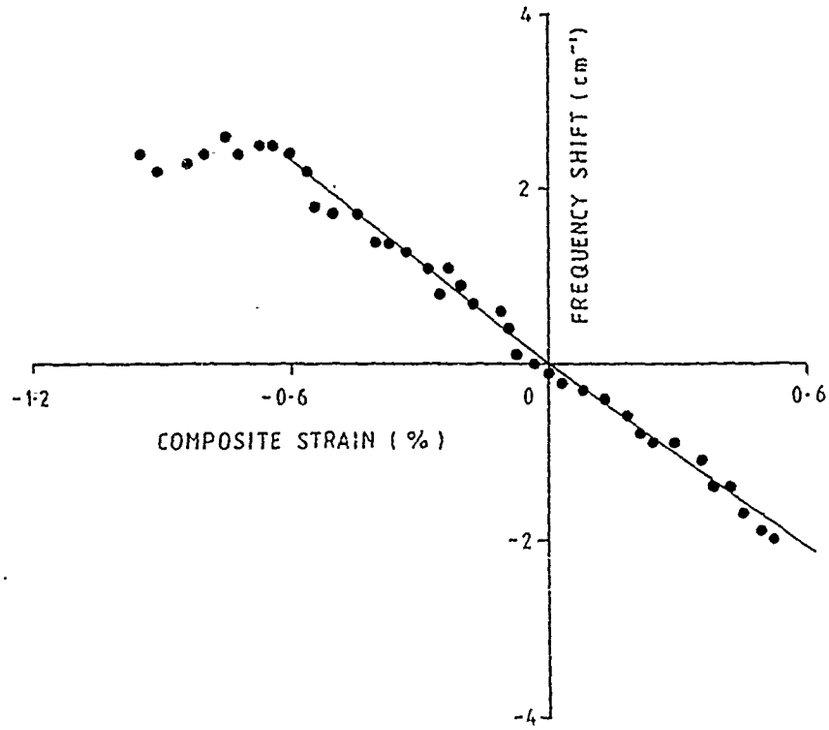

Figure 3.56(a) Raman frequency shift versus composite strain for extension and compression of single AS ABPBO fibre composite.

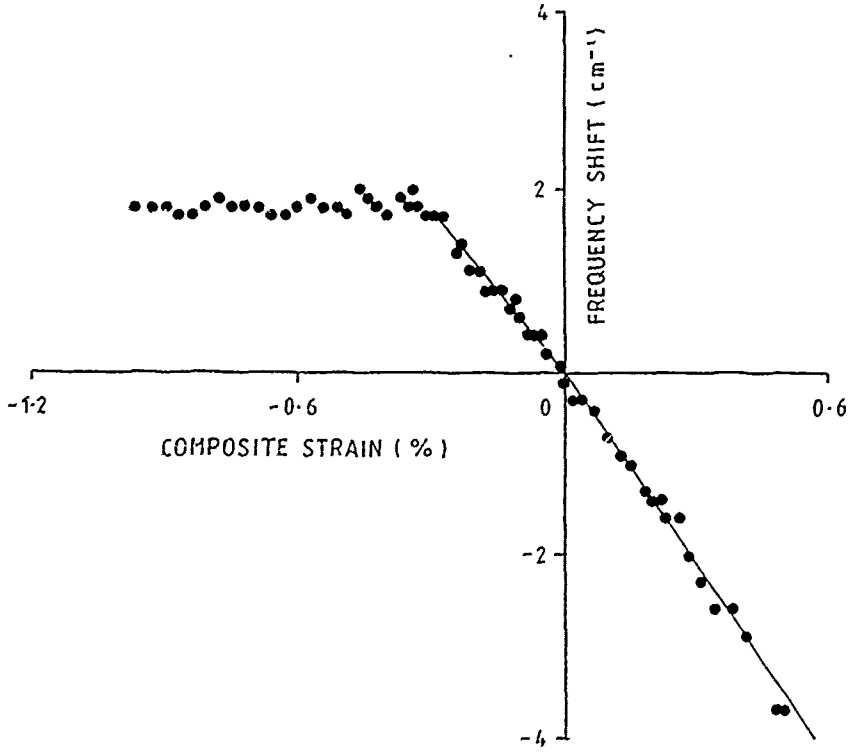

Figure 3.56(b) Raman frequency shift versus composite strain for extension and compression of single HT ABPBO fibre composite.

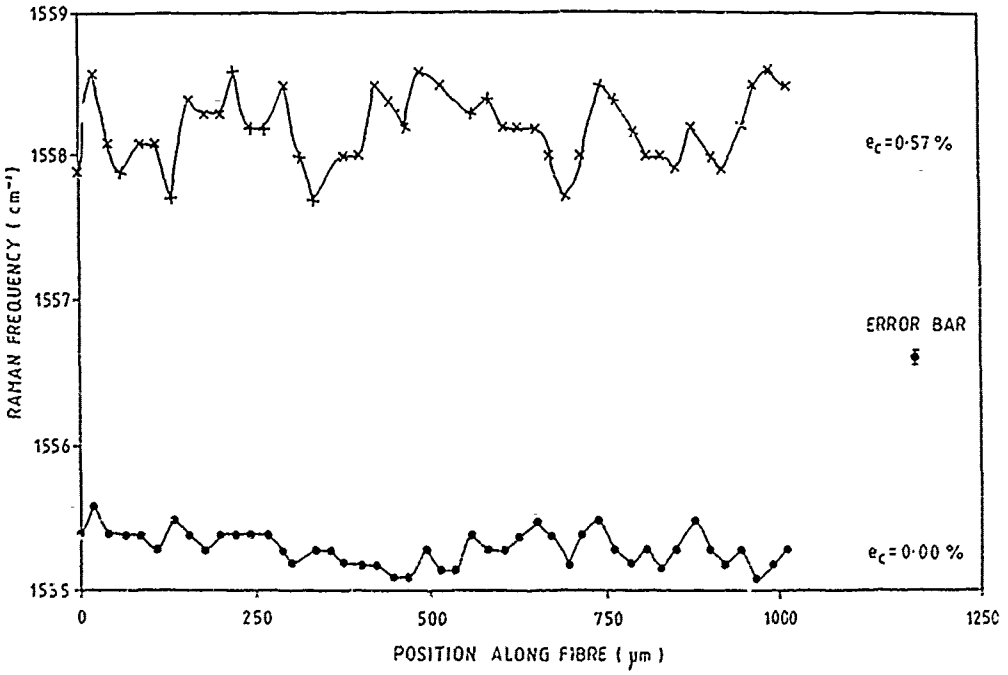

Figure 3.57 Variation of the position 1552 cm^{-1} peak with position along the HT ABPBO fibre for two different levels of applied compressive composite strain (e_c).

3-3 Observations of kinkband formation

PBT single fibre composites

Figures 3.58(a) and (b) show the optical micrographs of the appearance of kinkbands in as-received AS and HT PBT fibres induced by bending in air. As can be observed, the deformed fibres have more and darker kinkbands compared to the undeformed fibres (Figure 3.1). The kinkbands are perpendicular to the fibre direction although HT PBT fibres are more opaque compared to the equivalent as-spun fibres.

Figures 3.59(a) and (b) show the scanning electron micographs of the appearance of kinkbands in as-received AS and HT PBT fibres induced by bending in air. Bulging of the fibre with cracking along the fibre direction can be seen in the kinkbands in the AS PBT fibres. While for HT PBT fibres, there is also fibrillation on the tension side of the bend.

An optical microscope was used to examine the formation of kinkbands in the single fibre mounted in epoxy resin composites using transmitted light. The samples were compressed and micrographs of the fibre were obtained. The number of kinks over a marked length (approx 1mm) were counted from the micrographs at x400 magnification. Figures 3.60(a) and (b) show some of the optical micrographs obtained at different levels of compressive strains for AS and HT PBT fibres respectively. It is noticeable in these that:

(1) The dark lines are the kinkbands, where molecular chains are sharply bent and result in a change in orientation. Consequently all the chains within the kinkband will be sheared with respect to each other and so molecular delamination, including chain rupture, is likely

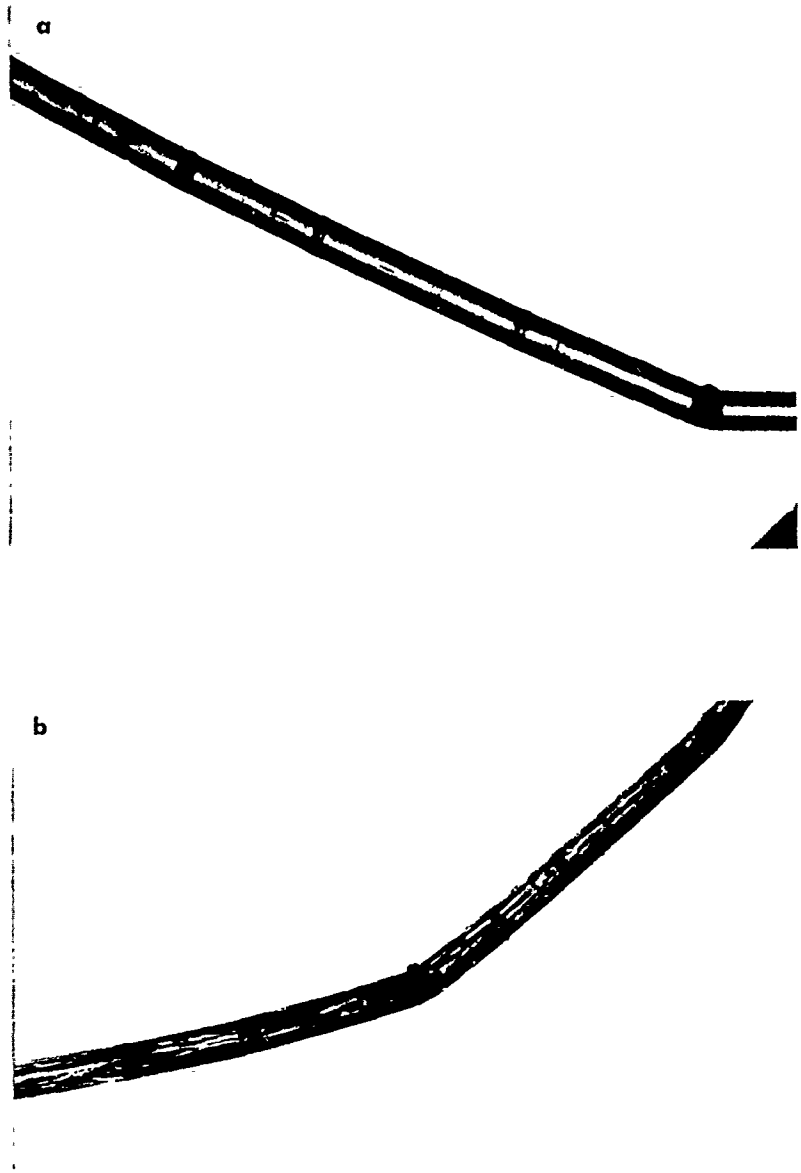

Figure 3.58 Optical micrographs of as-received PBT fibres deformed by bending in air. (a) As-spun; (b) heat treated

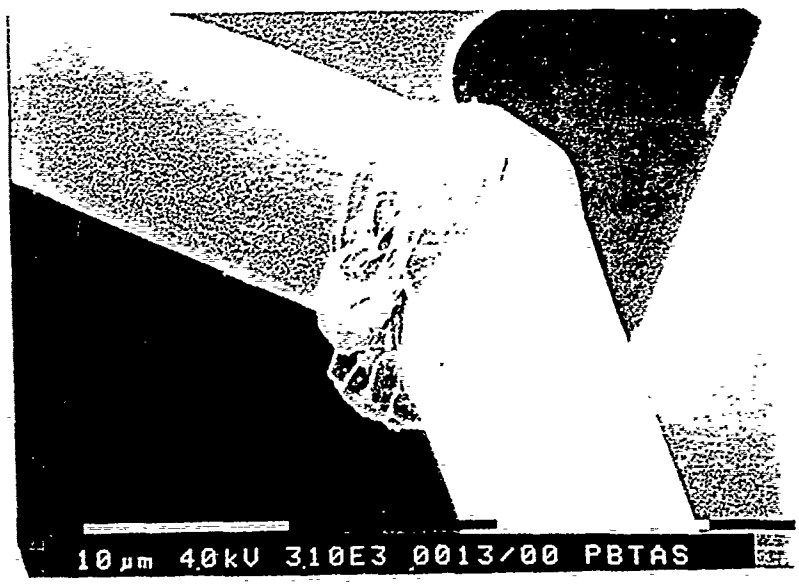

Figure 3.59(a) Kinkbands caused by bending in HS PBT fibre.

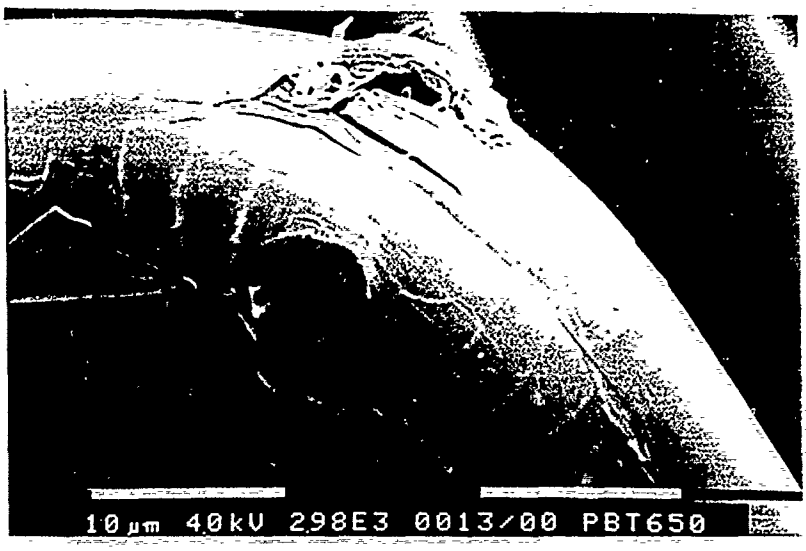

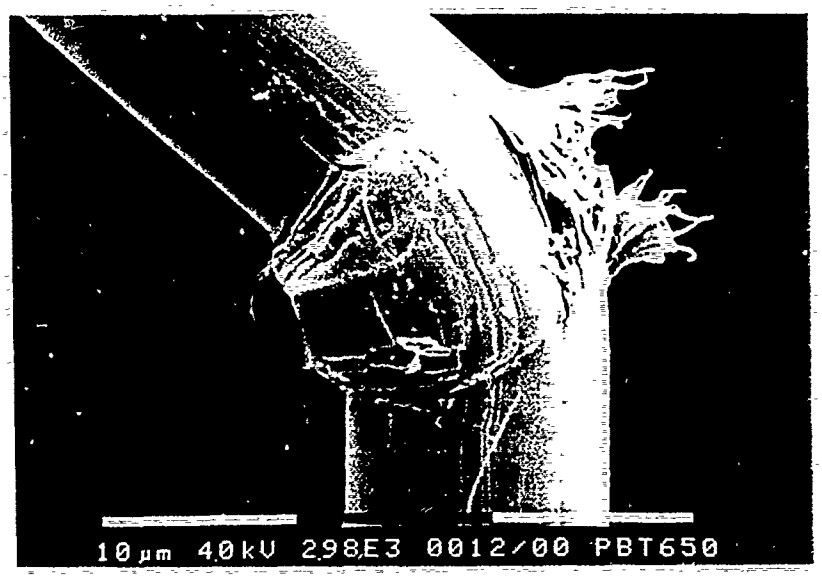

Figure 3.59(b) Kinkbands caused by bending in HT PBT fibre.

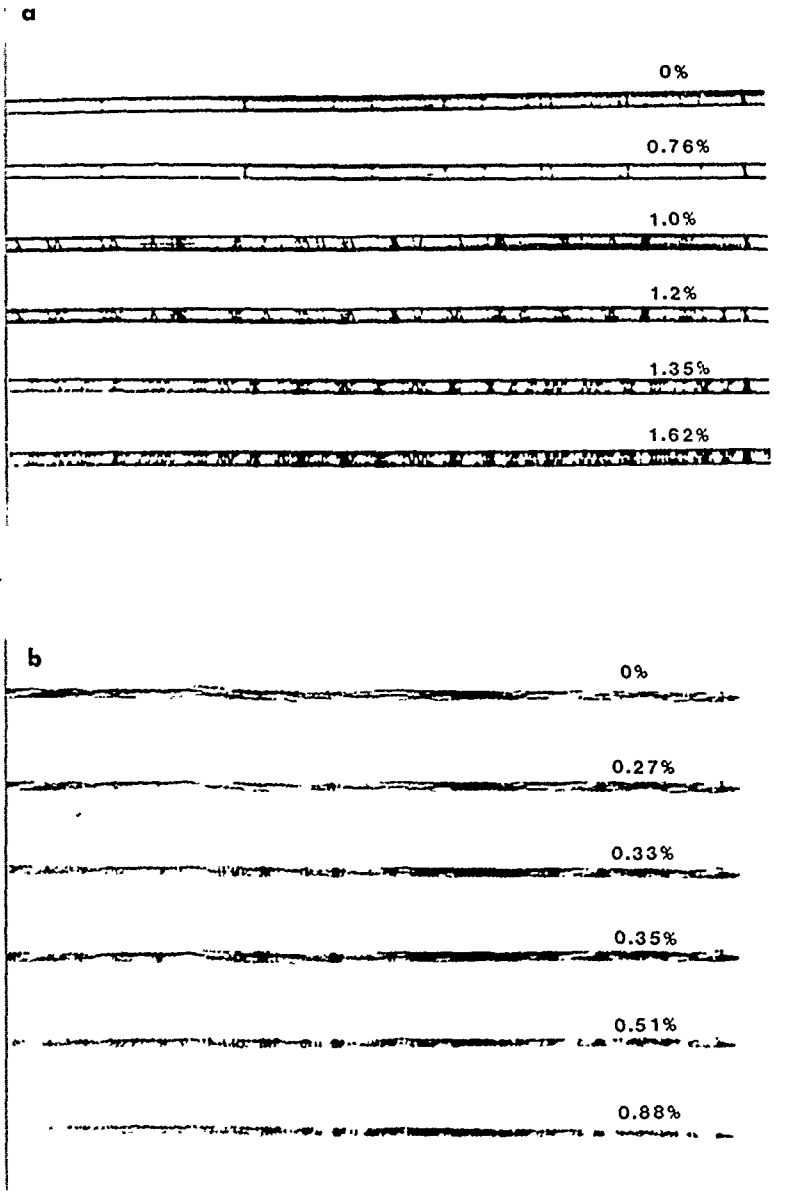

Figure 3.60 A selection of optical micrographs showing the development of kinkbands at different compressive strains in a model composite containing a single PBT fibre. (a) As-spun; (b) heat treated

to occur at the kinkband boundaries.

(2) New kinkbands tend to form close to the position of an existing kinkbands, suggesting that there is a stress concentration near the kinkbands.

(3) An increase in the compressive strain not only creates new kinkbands but existing kinkbands tend to be darker and more pronounced. This suggests that the amount of deformation in a kinkband increases as reported (21) previously in Kevlar fibres. In addition to the generation of new kinkbands and the thickening of each kinkband, the intersection of kinkbands at higher level of compressive composite strain may complicate the appearance of the specimen.

(4) It was also found that the angles of kinkbands remain approximately constant as compressive strain is increased. This is also observed in Kevlar fibres (21). The angles of kinkbands do not appear to be uniform along the fibre, they range from 65° to 90°, this may be due to a variation in kinkband angle or a variation on the viewing angles. The angles of kinkbands for PBT fibres (i.e 65°-90° for AS and 70°-90° for HT) are in agreement with previous reports (i.e approximately 70° (22)). However the angles of kinkbands are higher for the HT PBT fibres compared to AS PBT fibres. As described earlier the kinkbands were found to be approximately perpendicular to the fibre direction for as-received AS PBT fibre but at about 0.85% compressive strain, a helical patterns of kinkband started to appear.

(5) AS and HT PBT fibres (Figure 3.60) show a progressive helical formation of kinkbands around the fibre with increasing load. Helical compressive kinkbands in cylindrically orthotropic materials such as wood and PPTA have been studied by DeTeresa (22). He indicated that the PPTA fibre exhibits cylindrically orthotropic structural symmetry, like

wood, formed by a collection of hypothetical radial sheets. He concluded that the formation of kinkbands in orthotropic materials result from shearing between the planes of easy shear slip. This mechanism might be universal for orthotropic materials which are compressed parallel to the planes of easy shear slip. Helical kinkbands in PPTA and wood result from the cylindrically orthotropic symmetry of these materials. DeTeresa also concluded that helical kinkband formation under axial compression should be exhibited by other cylindrically orthotropic materials which have the same mechanical anisotropy of wood and PPTA fibres. PBT fibres may exhibit the same compressive failure as PPTA fibres since it is a cylindrical orthotropic materials as well. Many workers (22, 23) have reported that kinkbands were close to the surface of the fibre.

(6) It is noted that the orientation of the kinkbands along the PBT fibre embedded in a matrix during compression is slightly different from the as-received fibres in the air. The difference may be due to constraint of fibre embedded in the epoxy resin which is similar to that for a composite. The kinkbands in the as-received AS and HT PBT fibres in the air (Figures 3.1(a) and (b) respectively) appear to be perpendicular to the fibre direction while the kinkbands in AS and HT PBT fibres embedded in a matrix (Figure 3.60) during compression are seen to grow in a helical manner around the fibre. This may be due to the different types of deformation imposed.

(7) It should also be noted that a very fine line revealing voids can be observed in the middle of some AS PBT fibres but were not so obvious in HT PBT fibres and a few disconnections of the void were found in AS PBT fibres (Figure 3.61). It has been reported that a large number of macrovoids were observed in AS PBT fibres (24).

Figure 3.61 Disconnection of line in undeformed AS PBT fibre.

Figure 3.62 shows the number of kinkbands as a function of compressive composite strain of AS and HT PBT fibres. The number of kinkbands was counted in more than one areas on the fibre and the results were found to be almost identical. At first when the samples are compressed the number of kinkbands are virtually constant (at the as-received level) until the strain at which new kinkbands start to form is reached. The number of kinkbands increases rapidly until a point where no new kinkband are formed is reached.

Table 3.9 shows the angles of kinkband and the compressive composite strain at which new kinkbands start to form (e_{kO} from optical microscopy) and compressive composite strain at which compressive failure of fibre occurs (e_{kR} from Raman microscopy) for AS and HT PBT fibres. It can be seen that the e_k values obtained using both techniques for AS PBT fibres are considerably higher than for the HT PBT fibres. It can also be seen that the results obtained from Raman microscopy are slightly different from the results obtained from optical microscopy. Raman results appear to be lower than the values obtained from optical microscopy. It may be deduced that Raman microscopy is detecting the onset of kinkbanbs before they can be visualised. However the results obtained from both techniques may not be exactly comparable since the Raman microscopy only focuses on a spot on the fibre of a few um. Hence it is a localized test method where variation of results can occur from local inhomogeneities. In constrast kinkbands in a region of about 1mm are observed using optical microscope.

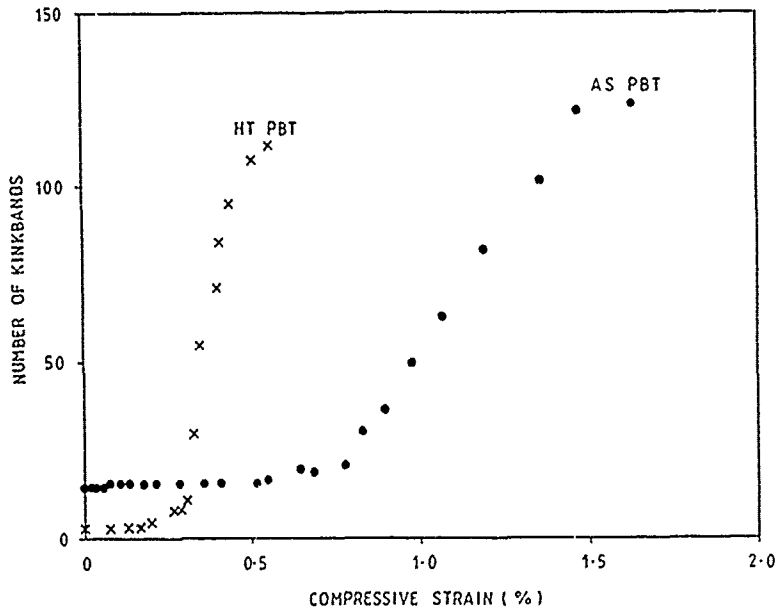

Figure 3.62 Number of kinkbands versus compressive strain for a single fibre composite of AS and HT PBT fibres.

Types of single fibre composite	Angles of kinkband (°)	e_{KO} (%)	e_{KR} (%)
AS PBT	65-90	-0.80	-0.73
HT PBT	70-90	-0.30	-0.23
AS PBO	60-77	-0.86	-0.61
HT PBO	60-90	-0.35	-0.17
AS ABPBO	60-80	-0.87	-0.60
HT ABPBO	70-90	-0.38	-0.25

Table 3.9 Angles of kinkband, compressive strain at which new kinkbands start to form from optical microscopy (e_{KO}) and compressive strain at which compressive failure of fibre occurs from Raman microscopy (e_{KR}) for AS and HT PBT, PBO and ABPBO fibres.

PBO single fibre composites

Figures 3.63(a) and (b) show the optical micrographs of the kinkbands in as-received AS and HT PBO fibres induced by bending in air respectively. As can be observed, the deformed fibres have more and darker kinkbands compared to the undeformed fibres (Figure 3.3). The kinkbands in AS PBO fibres are perpendicular to the fibre direction (similar to PBT fibres) while they are at an angle in HT PBO fibres although HT PBO fibres are more opaque compared to the equivalent as-spun fibres which makes the appearance of the kinkbands less obvious.

Figures 3.64(a) and (b) show scanning electron micrographs of the appearance of kinkbands in as-received AS and HT PBO fibres induced by bending in air respectively. Bulging of the fibres with cracking along the fibre direction near kinkbands can be seen in both types of fibres.

Figures 3.65(a) and (b) show some of the optical micrographs obtained at different levels of compressive strains for AS and HT PBO fibres respectively. It can be seen that:

(1) The angles of kinkbands remain the same as compressive strain increased (similar to PBT fibres). The angles of kinkbands appear not to be uniform along the fibre, they range from 60° to 90°, this may be due to a variation in actual angle or a variation on the viewing angles. However the angles of kinkbands are higher for the HT PBO fibres than for AS PBO fibres (similar to PBT fibres).

(2) The kinkbands in AS and HT PBO fibres appear optically as a few faint and fine black lines grouped together at a particular angle (i.e 60°-90°) to the fibre axis. It is believed that each faint and fine black line represents the buckling of separated microfibrils due to the elastic instability (25). If the compressive strain increases in the

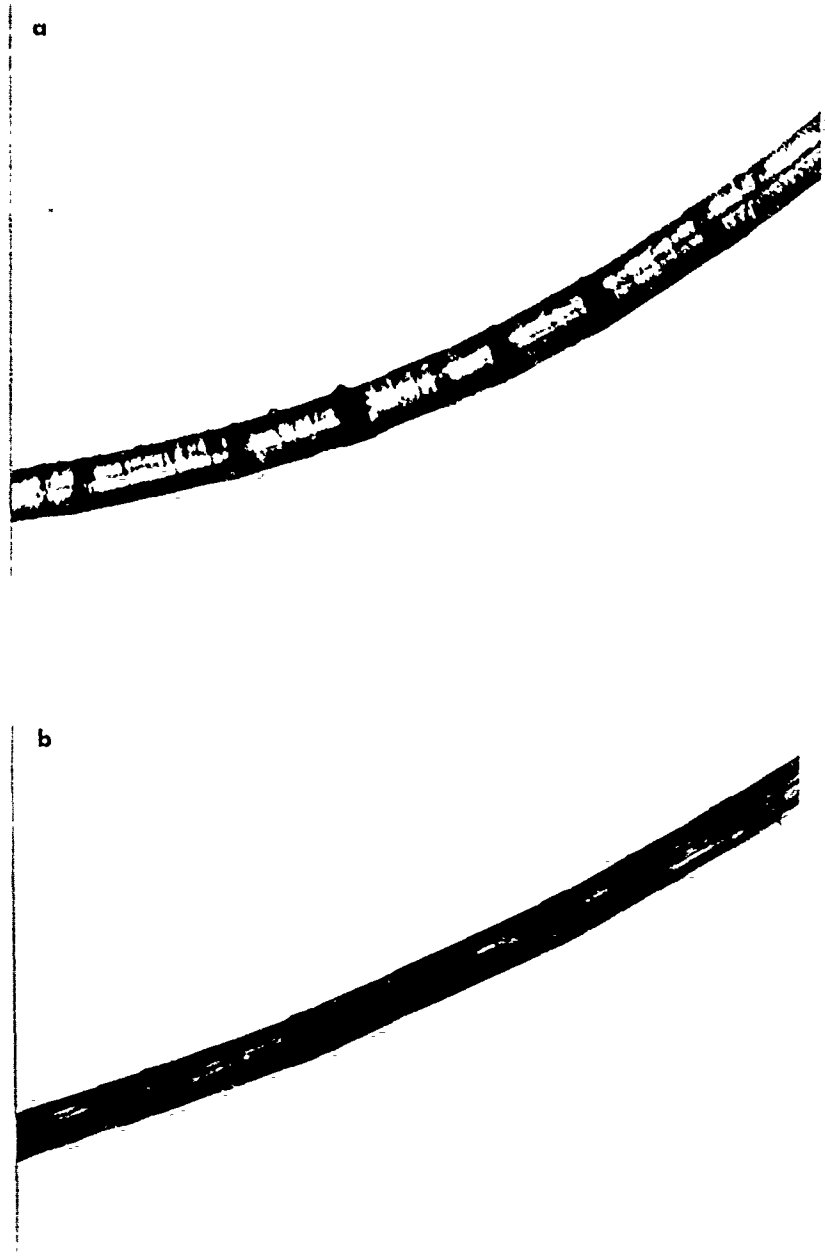

Figure 3.63 Optical micrographs of as-received PBO fibres deformed by bending in air. (a) As-spun; (b) heat treated

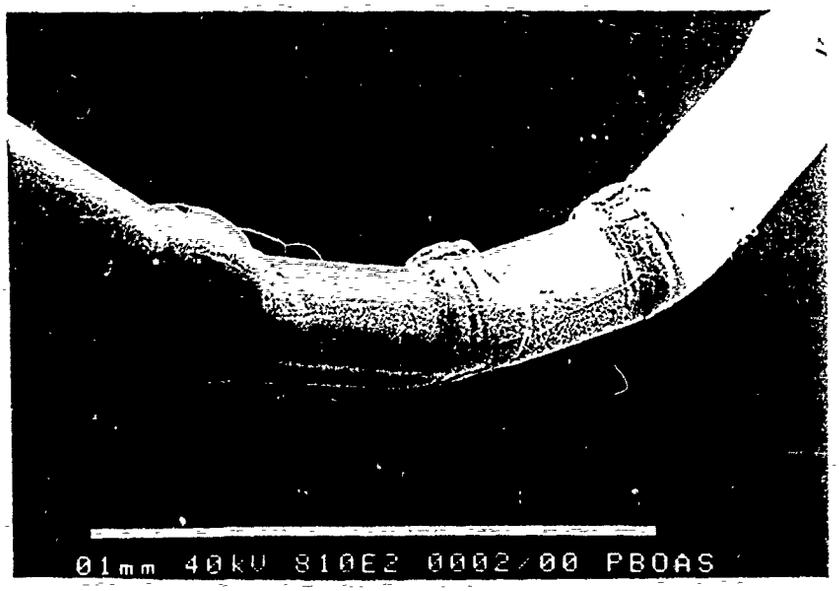

Figure 3.64(a) Kinkbands caused by bending in AS PBO fibre.

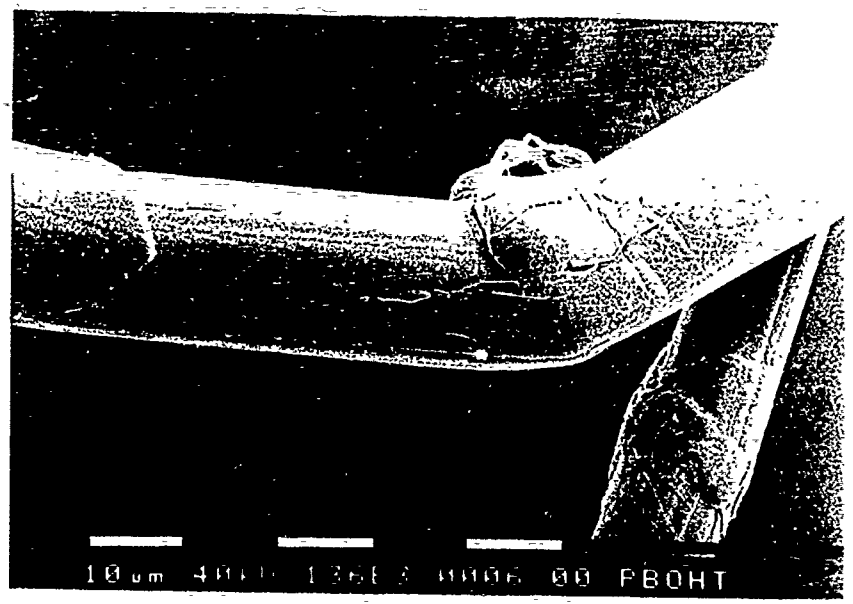

Figure 3.64(b) Kinkbands caused by bending in HT PBO fibre.

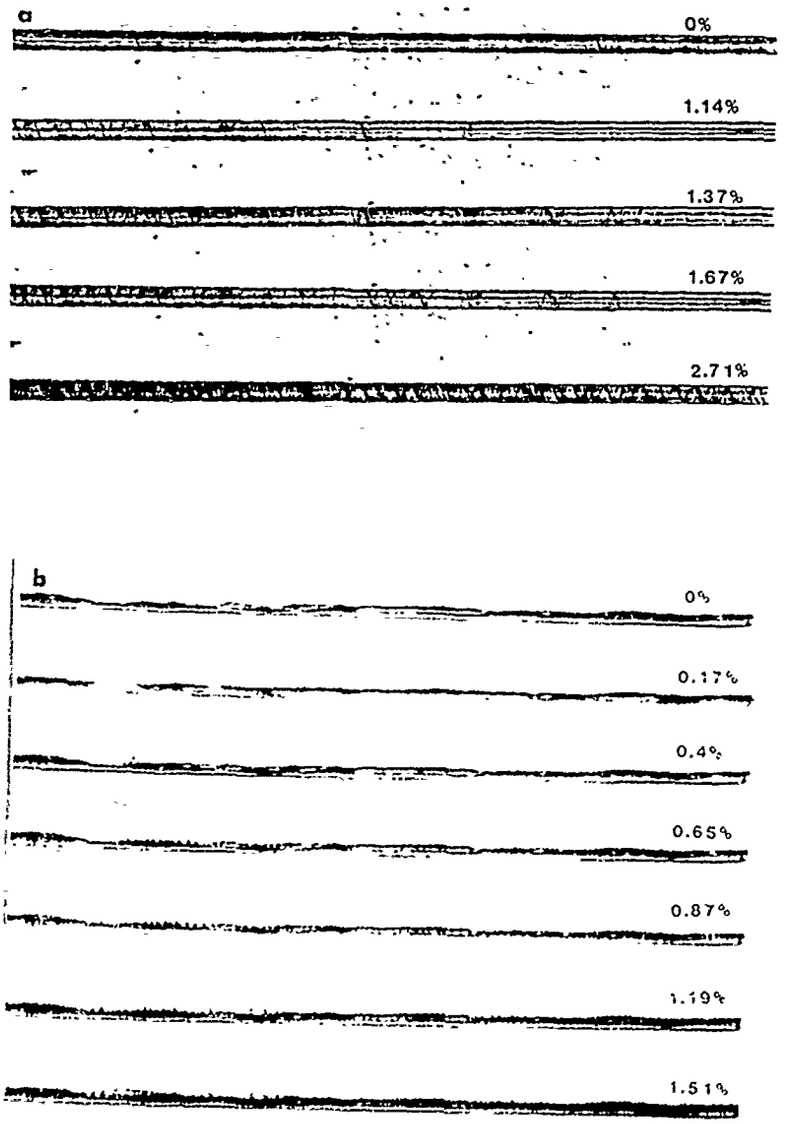

Figure 3.65 A selection of optical micrographs showing the development of kinkbands at different compressive strains in a model composite containing a single PBO fibre. (a) As-spun; (b) heat treated

fibre, the core of the black line group gets darker and many faint and fine black lines are added to the group. It is believed that the darkening of the core means that the separation and buckling of microfibrils progressess through the fibre(25). Careful observation of Figures 3.65 show that the compressive kinkbands for PBO fibres appear as black V-shaped bands.

(3) The kinkbands in the as-received AS and HT PBO in the air (Figure 3.3) appear to be perpendicular for the AS PBO fibres and for the HT PBO fibres at an angle to the fibre direction. The kinkbands of the fibres embedded in a matrix (Figures 3.65(a) and (b)) appear as black V-shaped bands during compression. The difference may be due to constraint of fibre embedded in the epoxy resin which is most appropriate for composite.

(4) A very fine line revealing the voids can be observed in the middle of some AS and HT PBO fibres.

Figure 3.66 shows the number of kinkbands as a function of compressive composite strain of AS and HT PBO. The number of kinkbands was counted in more than one areas on the fibre and the results were found to be almost identical. The behaviour of the curve is similar to PBT fibres.

Table 3.9 shows the angles of kinkband and the compressive composite strain at which new kinkbands start to form (e_{kO} from optical microscopy) and strain at which compressive failure of fibre occurs (e_{kR} from Raman microscopy) for AS and HT PBO fibres. It can be seen that the e_k values for AS PBO fibres are considerably higher than the HT PBO fibres.

Figure 3.67 shows the optical micrographs of an undeformed, loaded (to 2.5% strain, > e_k), unloaded and reloaded single AS PBO

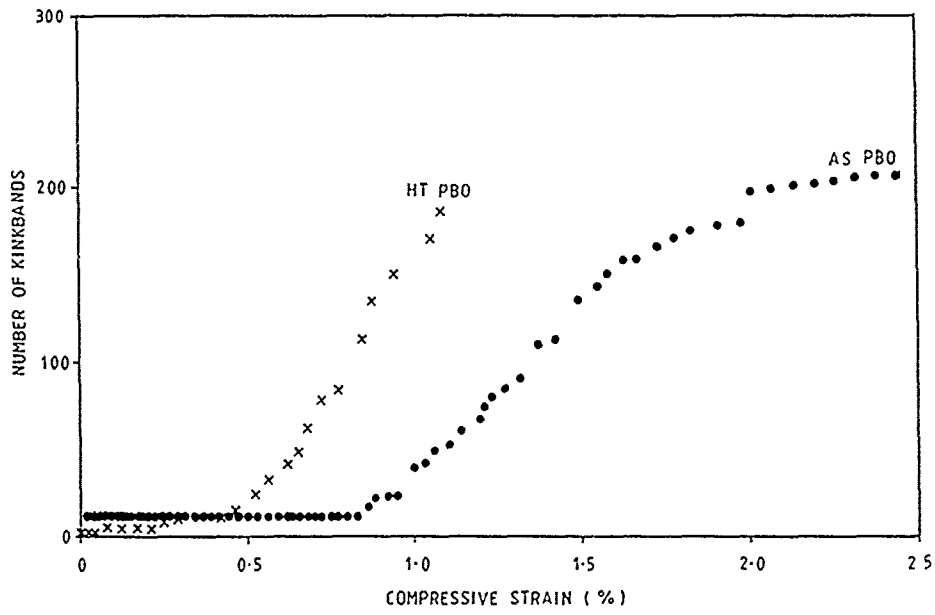

Figure 3.66 Number of kinkbands versus compressive strain for a single fibre composite of AS and HT PBO fibres.

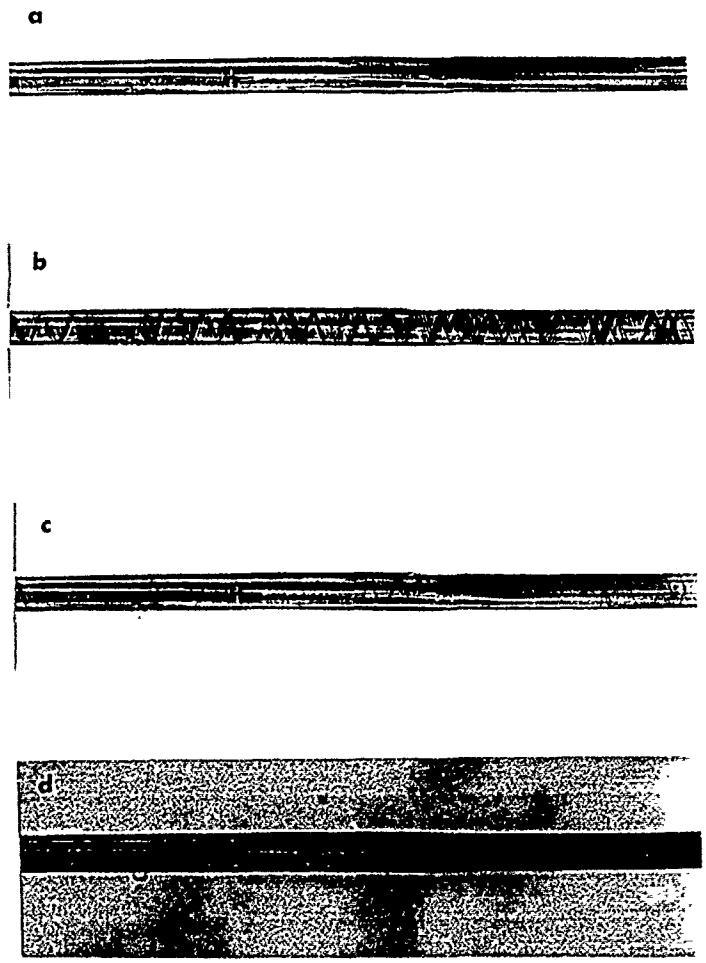

Figure 3.67 Optical micrographs of (a) original (e_c= 0%);
(b) first loading (i.e e_c= 2.5%);
(c) relaxed (i.e back to e_c= 0%) and
(d) secondary loading (i.e e_c= 2.5%) for AS PBO single fibre composite. (e_c= compressive composite strain)

fibre composite. The second loading was applied only after the first loading had relaxed completely. The kinkbands were seen in the fibre after unloading (Figure 3.67c)) indicating that permanent deformation occurs in the fibre at the kink boundary. Similar behavious has been reported in Kevlar 49 fibres (26) and PBO fibres (25). It can also be seen that the formation of kinkbands from the first and second loading is in exactly the same position. This shows that the fibre has undergone permanent plastic deformation after e_k. The detailed mechanism of the deformation has been reported by Dobb et al(27). It would appear that the onset of plastic deformation during compression arises from abrupt localized changes in orientation of the molecular chains to form kinkbands (i.e all the chains within the kinkband will be sheared with respect to each other). Further compression produces a pile-up of kinkbands which result in the appearance of bands of extruded material in the fibre surface.

ABPBO single fibre composites

Figures 3.68 (a) and (b) show the optical micrographs of the appearance of kinkbands in as-received AS and HT ABPBO fibres induced by bending in air. . As can be observed, the deformed fibres have more and darker kinkbands compared to the undeformed fibres (Figure 3.5). The kinkbands in AS ABPBO fibres are at an angle to the fibre direction (similar to HT PBO fibres) while a black V-shape patterns of kinkbands can be seen along the fibre in HT ABPBO fibres.

Figures 3.69(a) and (b) show the scanning electron micrographs of the appearance of kinkbands in AS and HT ABPBO fibres induced by bending in air. Bulging of the fibre with cracking along the fibre direction at the point of kinkbands can be seen in AS ABPBO fibres while for HT ABPBO fibres, the kinkbands are quite different from the rest of the fibres described earlier as no cracks or any bulging of the fibres occur at the point of kinkbands formation. The kinkbands are formed at an angle to the fibre axis.

Figures 3.70(a) and (b) show some of the optical micrographs obtained at different levels of compressive strains for AS and HT ABPBO fibres respectively. It is noticeable in that:

(1) The angles of kinkbands remain the same as compressive strain increased (similar to PBT and PBO fibres). The angles of kinkbands appear not to be uniform along the fibre, they range from 60°-90°, this may be due to a variation in kinkband angle or a variation on the viewing angles. The measured angles are slightly higher for ABPBO fibres (i.e 60°-80° for AS and 70°-90° for HT) compared to previous report (i.e 50°-60° (22)). However the angles of kinkbands are higher for the HT ABPBO fibres than for the AS ABPBO fibres.

(2) It appears that the formation of kinkbands for ABPBO fibres is

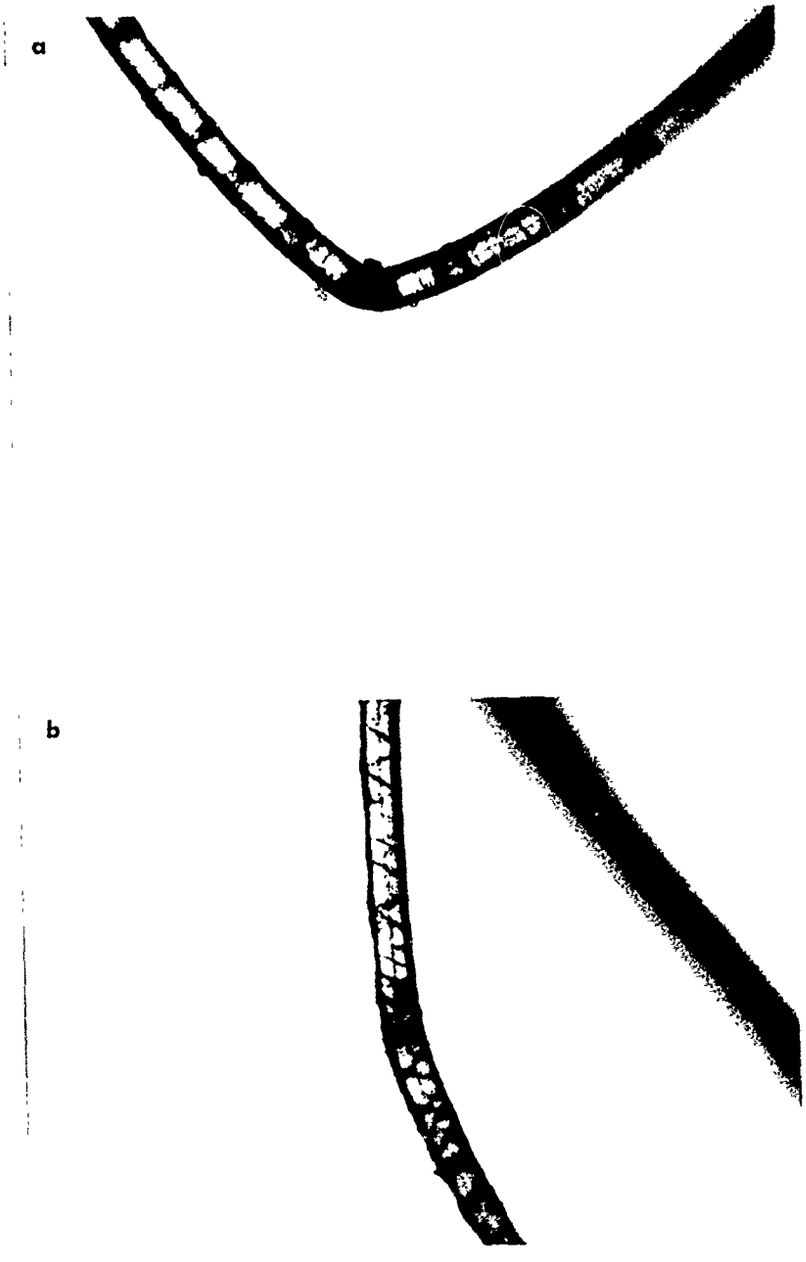

Figure 3.68 Optical micrographs of as-received ABPBO fibres deformed by bending in air. (a) As-spun; (b) heat treated

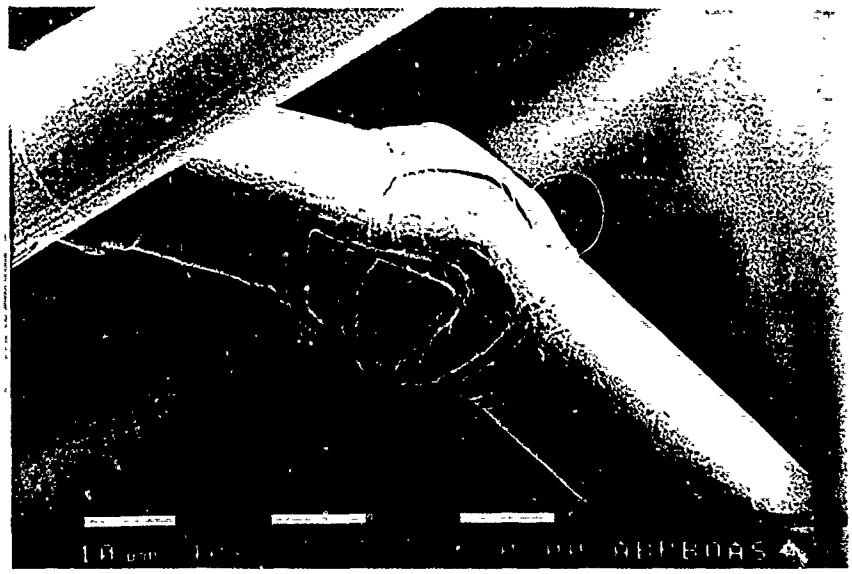

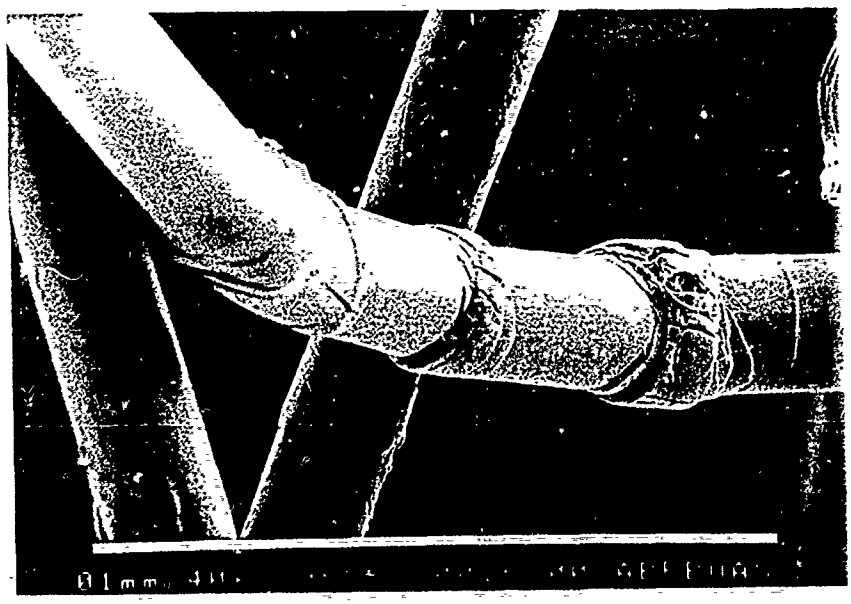

Figure 3.69(a) Kinkbands caused by bending in AS ABPBO fibre.

Figure 3.69(b) Kinkbands caused by binding in HT ABPBO fibre.

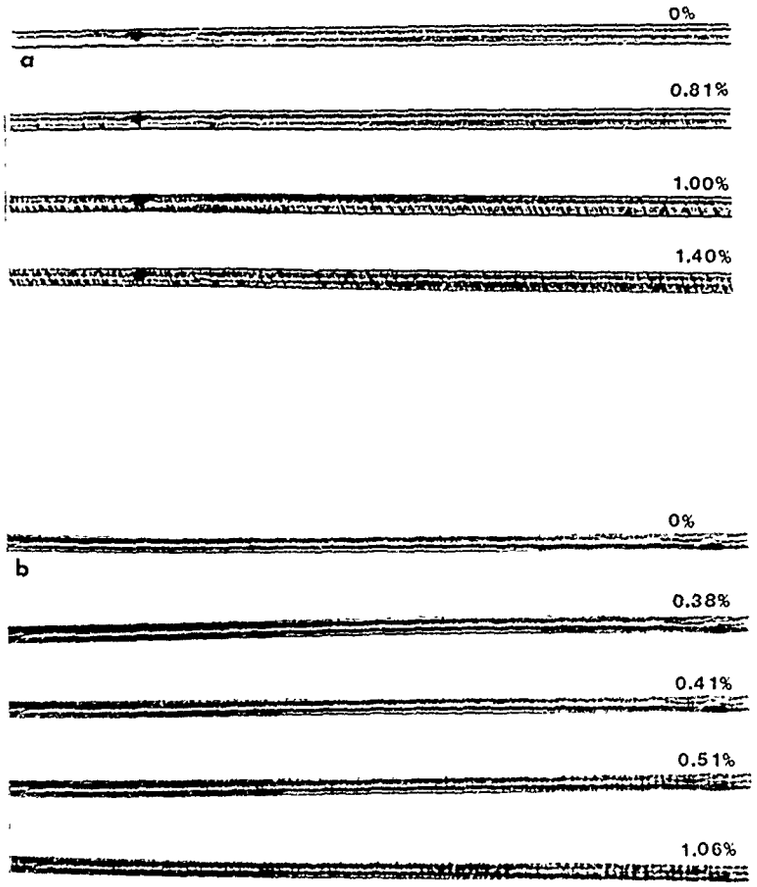

Figure 3.70 A selection of optical micrographs showing the development of kinkbands at different compressive strains in a model composite containing a single ABPBO fibre. (a) As-spun; (b) heat treated

similar to PBO fibres. The kinkbands appear as a few faint and fine black lines grouped together at a particular angle (i.e 60°-90°) to the fibre axis. Careful observation of Figures 3.70 show that the compressive kinkbands are parallel to one another with a few V-shaped bands along the fibre.

(3) The kinkbands in the as-received AS ABPBO fibres (Figure 3.5(a)) are parallel to one another and at an angle to the fibre direction. In constrast the same fibre embedded in a matrix has a formation of kinkbands parallel to one another with some V-shaped bands (Figure 3.70(a)). The kinkbands in the as-received HT ABPBO fibres (Figure 3.5(b)) in air appear as dark V-shaped bands while the same fibre embedded in a matrix has a formation of kinkbands similar to the AS ABPBO fibre during compression.

(4) A very fine line revealing the voids can be observed in the middle of AS and HT ABPBO fibres (similar to PBT and PBO fibres) and a few disconnections of the void were found in HT ABPBO fibres (Figure 3.71).

Figure 3.72 shows the number of kinkbands as a function of compressive composite strain of AS and HT ABPBO fibres. The number of kinkbands was counted in more than one areas on the fibre and the results were found to be almost identical. The behaviour of the curve is similar to PBT and PBO fibres.

Table 3.9 shows the angles of kinkband and the compressive composite strain at which new kinkbands start to form (e_{kO} from optical microscopy) and strain at which compressive failure of fibre occurs (e_{kR} from Raman microscopy) for AS and HT ABPBO fibres. It can be seen that the e_{k} values for AS ABPBO fibres are considerably higher than for the HT ABPBO fibres.

Figure 3.71 Disconnection of line in undeformed HT ABPBO fibre.

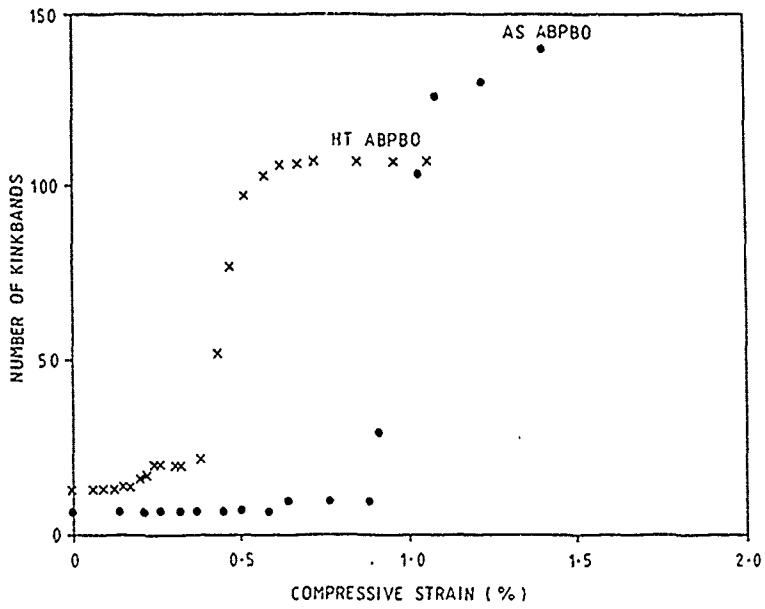

Figure 3.72 Number of kinkbands versus compressive strain for a single fibre composite of AS and HT ABPBO fibres.

4 CONCLUSIONS

A detailed study has been made of the relationship between structure and mechanical properties of both as-spun and heat-treated PBZ fibres deformed in both tension and compression. Three types of fibres have been studied PBT, PBO, ABPBO and their behaviour has been compared in detail. The findings are detailed below:

4-1 Structure

It has been found that for the three types of fibres, heat-treatment improves the structural order within the fibres. It is found that after heat-treatment the crystallites in PBT fibres are not three dimensionally ordered but show only two dimensional order due to axial disorder of the molecules. In the case of the PBO fibres there is evidence of a higher level of axial order than for PBT whereas for ABPBO, heat-treatment leads to the development of a well-defined three-dimensional crystal structure within the crystallites in the fibres.

4-2 Tensile properties

The tensile properties of the different fibres have been examined in detail. It has been found that the three as-spun fibres undergo yielding and plastic deformation whereas the heat-treated fibres show approximately elastic deformation up to fracture. Heat treatment is found to significantly increase fibre modulus with the highest modulus being obtained for HT PBT (267 GPa) The tensile strength is relatively unaffected by heat-treatment and the highest levels of strength of the order of 3 GPa, are found for the PBO fibres. The elongation to break

of the three types of fibres is found to decrease significantly by a factor of about 2 on heat treatment. The highest elongation has been found for AS ABPBO (4.3%).

4-3 Molecular deformation

It has been demonstrated that molecular deformation in the fibres can be followed using Raman microscopy. It is found that for all three types of materials the bands in the Raman spectra shift to lower frequency on the application of an applied tensile stress or strain. This is a direct reflection of the macroscopic deformation of the fibre being translated into deformation of the rigid rod molecules within the fibres. It is found for a particular type of fibre that the rate of shift of the Raman peaks increases with fibre modulus showing that the improvement in mechanical properties is due to the molecules becoming more highly deformed at a given fibre strain following heat treatment. It has also been shown that good spectra can be obtained from all of the fibres within an epoxy resin in a composite enabling in situ [illegible] been found that for some of the fibres the rate of shift of the Raman bands (per unit strain) is less in compression than in tension, indicating that for these fibres the Young's modulus may be lower in compression than in tension. The ratio of compression than in tension modulus is found to be about 0.55 for PBT, 0.8 for PBO and the order of 1 for ABPBO.

4-4 Kinkband formation

The formation of kinkbbands in the fibres has been followed by the axial compression of blocks of epoxy resin containing single fibres. The development of kinkbands has been followed using both direct observation and from strain-induced shifts in the Raman spectra of fibres. It has been found that the critical strain at which kinkbands form can be determined using the two techniques although the values of the critical strain are generally found to be lower using Raman microscopy. This shows that the Raman technique has the ability of detecting molecular kinking before any macroscopic kinkband formation can be observed and is therefore superior to other methods that are employed. The detailed form of the kinkbands in the fibres has been examined using scanning electron microscopy upon kinkbands obtained from fibres deformed in air, although their detailed appearance is different from those obtained within a composite.

4-5 Suggestions for further work

It has been shown that Raman microscopy is a powerful method of following the tensile and compressive deformation of PBZ fibres and there is plenty of scope for extending this work. It would be of considerable interest to look in detail at the relationship between the compressive fibre modulus and kinkband formation. It is likely that a low compressive modulus will lead to relatively easy kinkband formation. The Raman technique could also be extended to look in detail at the micromechanics of the deformation of PBZ fibres in composites. Clearly a large number of variables could be investigated including fibre surface treatment and fibre volume fraction for both tensile and compressive deformation.

It would also be of interest to look in detail at the structure of kinkbands using electron microscopy. High resolution techniques could be used to examine the changes of molecular oritation at kinkband boundaries. It may be possible to relate this to the molecular deformation determined using Raman microscopy and hence help to design fibres with improved compressive behaviour.

5 REFERENCES

(1) Day, R. J., Robinson, I. M. and Young, R. J. Polymer 28 (1987) 1833

(2) Minter, J. R., Shimanwa, K. and Thomas, E. L. J. Mater. Sci. 16 (1981) 3303

(3) Odell, J. A., Keller, A., Atkins, E. D. T. and Miles, M. J. J. Mater. Sci. 16 (1981) 3309

(4) Krause, S. J., Haddock, T. B., Vezie, D. L., Lenhert, P. G., Hwang, W. F., Price, G. E., Helminiak, T. E., O'Brien, J. F. and Adams, W. W. Polymer 29 (1988) 1354

(5) Allen, S. R., Filippov, A. G., Farris, R. J. and Tomas, E. L. in ' Strength and stiffness of Polymers ' (Eds A. E. Zachariades and R. S. Porter), Marcel Dekker, New York, (1983) P.257

(6) Young, R. J., Day, R. J. and Zakikhani. M. J. Mat. Sci. 25 (1990) 127

(7) Allan, S. R. J. Mater. Sci. 22 (1987) 853

(8) Ang, P. P. MSc Dissertation, UMIST (1988)

(9) Venkatesh, G. M., Shen, D. Y. and Hsu, S. L. J. Polymer Sci., Polym. Phys. Edn 19 (1981) 1475

(10) Shen, D. Y., Venkatesh, G. M., Burchell, D. J., Shu, P. H. C. and Hsu, S. L. J. Polym. Sci., Polym. Phys. Edn 20 (1982) 509

(11) Shen, D. Y. and Hsu, S. L. Polymer 23 (1982) 969

(12) Wool, R. I. J. Polym. Sci., Polym. Phys. Edn 13 (1975) 1795

(13) Wool, R. P. and Boyd, R. H. J. Appl. Phys. 51 (1980) 5116

(14) Bretzlaff, R. S. and Wool, R. P. J. Appl. Phys. 52 (1981) 5964

(15) Robinson, I. M., Young, R. J., Galiotis, C. and Batchelder, D. N. J. Mater. Sci. 22 (1987) 3642

(16) Greenwood, J. H. and Rose, P. G. J. Mater. Sci. 9 (1974) 1809

(17) Dobb, M. G., Johnson, D. J. and Saville, B. P. Polymer 22 (1981) 960

(18) Technical report, AFWAL-TR-824154 Part III

(19) Kumar, S. Fibre Producers Conference Proceedings, April 26-28 (1988) Greenville, S. C

(20) Jahankhani, H., Vlattas, C. and Galiotis, C. Interfacial Phenomena in Composite Materials '89 p.125

(21) Takahashi, T., Miura, M. and Sakurai, K. J. of Applied Polym. Sci. 28 (1983) 579-586

(22) Deteresa, S. J. AFWAL-TR-4013, University of Massachusetts (1985)

(23) Drzal, L. T. Final report AFWAL-TR-86-4003, Mat. Lab., AFWAL, WPAFB (1984)

(24) Allen, S. R. PhD Dissertation, University of Massachusetts (1983)

(25) Fidan, S. MSc Thesis, Air Force Institute of Technology (1988)

(26) Deteresa, S. J., Allen, S. R., Farris, R. J.and Porter, R. S. J. of Mat. Sci. 19 (1984) 57 57

(27) Dobb, M. G., Johnson, D. J. and Saville, B. P. Polymer 22 (1981) 960